

Technical Report

TR-19-16

December 2019



Task Force on EBS C-session

Calculation of Benchmarks 1–5

Martin Birgersson

SVENSK KÄRNBRÄNSLEHANTERING AB

SWEDISH NUCLEAR FUEL
AND WASTE MANAGEMENT CO

Box 3091, SE-169 03 Solna
Phone +46 8 459 84 00
skb.se

SVENSK KÄRNBRÄNSLEHANTERING

ISSN 1404-0344

SKB TR-19-16

ID 1872512

December 2019

Task Force on EBS C-session

Calculation of Benchmarks 1–5

Martin Birgersson, Clay Technology AB

This report concerns a study which was conducted for Svensk Kärnbränslehantering AB (SKB). The conclusions and viewpoints presented in the report are those of the author. SKB may draw modified conclusions, based on additional literature sources and/or expert opinions.

A pdf version of this document can be downloaded from [www\(skb.se](http://www(skb.se).

© 2019 Svensk Kärnbränslehantering AB

Summary

The modeling work within the EBS Task Force chemistry session (C-session) has been organized around five collections of results from various experiments performed on bentonite/montmorillonite, referred to as benchmarks. All of these benchmarks concern various aspects of transport of salts in compacted bentonite, but focus is also on various physico-chemical (advective flow, ion exchange) and chemical processes (mineral dissolution, complex formation). The teams involved in the C-session has been free to choose whichever aspects of a specific experiment to model, based e.g. on available tools.

Here is reported the modeling work by Clay Technology (Martin Birgersson) within the C-session. This work has focused on treating montmorillonite interlayer pores adequately, and on developing and applying a model which only takes these pores into account – the homogeneous mixture model.

The results show that many observed effects are naturally accounted for by only considering montmorillonite interlayer pores:

- The variation of the diffusive flux of chloride salts with ionic strength is mainly an effect of the corresponding variation of the difference in electrostatic potential between the source reservoir and the clay (Benchmark 1).
- The tendency for bentonite to take up relatively large amounts of sulfate and selenate is mainly an effect of these ions having very low activity coefficients at high ionic strength (Benchmarks 2 and 5).
- Cation exchange is understood as a combined effect of diffusion and the presence of an electrostatic potential difference between external solutions and the clay. Selectivity can be analyzed in terms of interlayer activity coefficients (Benchmark 3).
- The effects of hyperfiltration (reverse osmosis) and density redistribution under external water pressure gradients are readily analyzed in the homogeneous mixture model (Benchmark 4).

Sammanfattning

Modelleringsarbetet inom "EBS Task Force Kemi" (C-session) har hanterat fem separata sammanställningar av resultat från experiment gjorda på montmorillonit/bentonit. Dessa sammanställningar kallas "Benchmarks". Alla Benchmark-experiment berör aspekter av salttransport i kompakterad bentonit, men fokus ligger också på andra fysikalkemiska (advektiva flöden, jonbyte) och kemiska (mineralupplösning, komplexbildning) processer. Grupperna inom C-sessionen har varit fria att själva välja vilka experimentaspekter att modellera, baserat t ex på vilka numeriska verktyg som man har haft tillgång till.

Här rapporteras Clay Technologies (Martin Birgerssons) modelleringsarbete i C-sessionen. Detta arbete har lagt vikt vid en adekvat beskrivning av interlayer-porer i montmorillonit och har fokuserat på att utveckla och tillämpa en modell vilken tar endast dessa porer i beaktande (homogeneous mixture model).

Resultaten visar att flertalet observerade effekter kan förklaras på ett naturligt sätt genom att endast hantera interlayer-porer i montmorillonit:

- Variationen av kloridsalters diffusiva flöde med jonstyrkan beror huvudsakligen på en motsvarande variation i skillnaden i elektrostatisk potential mellan lera och extern lösning (Benchmark 1).
- Bentonitens benägenhet att ta upp relativt stora mängder sulfat och selenat beror till stor del på att dessa joner har väldigt låga aktivitetskoefficienter vid hög jonstyrka (Benchmark 2 och 5).
- Katjonbytesprocesser förklaras som en kombination av diffusion och den elektrostatiska potentialskillnaden mellan lera och extern lösning. Selektivitet kan analyseras i termer av aktivitetskoefficienter i interlayer-porerna (Benchmark 3).
- Effekter av hyperfiltrering (omvänt osmos) och densitetsomfördelningar under externt pålagda vattentrycksgradienter kan hanteras behändigt i homogeneous mixture model (Benchmark 4).

Contents

1	Introduction	7
2	Benchmark 1	9
2.1	Treated as a pure diffusion process	10
2.1.1	Model fitting	11
2.1.2	Discussion	13
2.2	A homogeneous mixture model	14
2.2.1	Structure of compacted bentonite	14
2.2.2	Model description	15
2.2.3	Results	17
3	Benchmark 2	21
3.1	CaSO ₄ through-diffusion	22
3.1.1	Results	23
3.2	Gypsum dissolution in Ca-montmorillonite	24
3.2.1	Results	25
3.3	Gypsum dissolution in Na-montmorillonite	26
3.3.1	Results	27
4	Benchmark 3	29
4.1	Treatment of experimental data	30
4.2	Treated as a pure diffusion process	31
4.3	Homogeneous mixture model	33
4.3.1	Model details	33
4.3.2	Results	35
5	Benchmark 4	39
5.1	Involved processes	39
5.1.1	Density response	39
5.1.2	Electrostatic response	41
5.1.3	Hyperfiltration	42
5.1.4	Initial salt content	43
5.2	A decoupled homogeneous mixture model	43
5.3	Results	45
6	Benchmark 5	49
6.1	Homogeneous mixture model	50
6.1.1	Selenate	50
6.1.2	Iodide	53
6.1.3	Comparison with selenate	55
6.1.4	Perchlorate	57
6.1.5	Pertechnetate	59
6.1.6	Chloride	61
6.1.7	Summary	63
	References	65

1 Introduction

The modeling work within the “chemistry” session of the SKB Task Force on Engineered Barrier Systems (C-session) has been organized around a set of five collections of results from various experiments performed on bentonite/montmorillonite. Given these so-called benchmark data sets, each involved modeling team have been free to choose whichever aspects of a specific experiment to model, based e.g. on available tools.

Clay Technology’s work within the C-session has mainly been focused on formulating and exploring a consistent model for compacted bentonite based on an adequate treatment of montmorillonite inter-layers, which dominates the pore structure in these systems. Much of this work has been published and presented elsewhere (Birgersson 2017, Birgersson et al. 2017, Birgersson and Karnland 2009, 2010, Glaus et al. 2013, Hedström and Karnland 2012, Hsiao and Hedström 2015). This report focuses on presenting simulations of the benchmark experiments using the developed model.

The five benchmark data sets originate from the following sets of experiments

1. Chloride salt through-diffusion tests in pure homoionic montmorillonite.
These tests were conducted by Clay Technology exclusively for use within the Task Force on Engineered Barrier Systems.
2. Gypsum dissolution and sulfate diffusion in Na- and Ca-montmorillonite.
These tests were conducted by Clay Technology and are reported in Birgersson et al. (2009).
3. Ca/Na ion exchange tests on compacted montmorillonite.
These tests were conducted by Clay Technology and are reported in Karnland et al. (2011).
4. High pressure infiltration of a “MX-80” bentonite sample with artificial, “Äspö”-like, groundwater.
These tests were performed by University of Bern, reported in Fernández et al. (2011).
5. Through-diffusion tests of various salts in “B75” bentonite under tracer-like conditions.
These tests were performed by UJV, Rez, Czech Republic, and distributed with in the C-session.

The rest of the report is organized in separate chapters for each of the benchmark data set experiments.

2 Benchmark 1

The data set of Benchmark 1 consists of results from two sets of through-diffusion tests performed in one sample of Na-montmorillonite and one sample of Ca-montmorillonite. The samples were confined in test cells and contacted from one side (the source side) by salt solutions of various concentrations, and from the other side (the target side) by deionized water. The source solutions were CaCl_2 in case of Ca-montmorillonite, and NaCl in case of Na-montmorillonite. The amount of salt diffusing into the target reservoir was recorded by regularly measuring the concentration in this solution. Thus, at the basic level, the Benchmark 1 data consists of pairs of measured target reservoir concentrations (C_i) and corresponding values for the time of measurement (t_i). Schematics for the experimental set-up is shown in Figure 2-1.

For convenience, when comparing with modeling results, the basic data is converted to an outflux as a function of time by the following transformation

$$j_{exp}(\bar{t}_i) = \frac{V_{target}}{A} \cdot \frac{C_i - C_{i-1}}{t_i - t_{i-1}} \quad (2-1)$$

where A is the cross sectional area of the clay sample, V_{target} is the target reservoir volume, and \bar{t}_i is the average time of the i :th measurement interval, given by

$$\bar{t}_i \equiv \frac{t_i + t_{i-1}}{2} \quad (2-2)$$

The index i , which denotes the order of the measurements, begins at 1 in the above formulas, while the initial time and target concentration are both zero (i.e. $t_0 = 0$, $C_0 = 0$).

Rather than converting the experimental data, the model could of course instead be made to output the time evolution of the target reservoir concentration. However, analyzing the results in terms of the time evolution of the outflux is more natural, as the ultimate purpose of the exercise is to better understand the underlying physical processes.

The strategy adopted for simulating this benchmark is to first assume the simplest process possible – pure diffusion in a homogeneous medium – and not pay attention to specific properties of the clay material (other than that it consists of a certain part water and a certain part solids). In a second step, the results obtained from this approach are explained by invoking ion equilibrium and chemical processes specific to the clay materials.

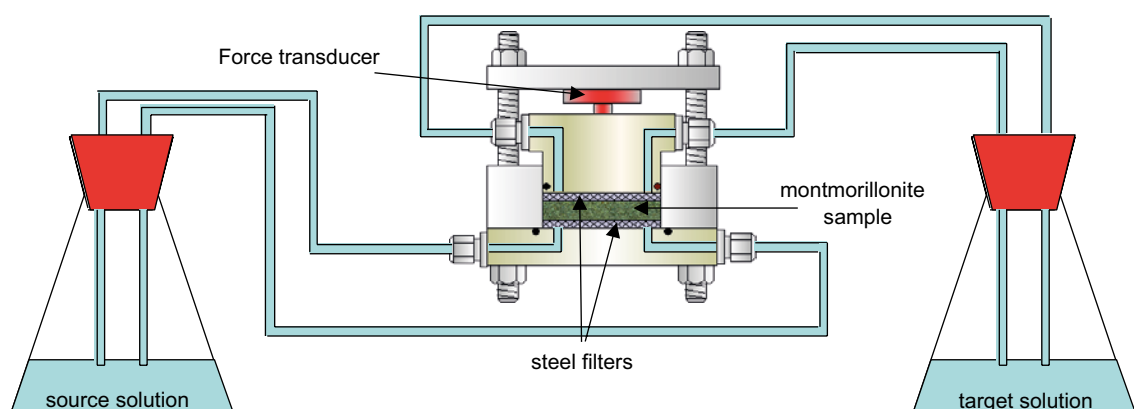


Figure 2-1. Basic test set-up for salt diffusion experiments of Benchmark 1 (Birgersson 2011¹).

¹ Birgersson M, 2011. EBS-TFC: Experimental overview of Benchmarks 1–4. Task Force <https://www.skb.se/taskforceebs/memberpages/data-deliveries/> (Data Deliverable TFC) Internal document.

2.1 Treated as a pure diffusion process

As a first step in analyzing the through-diffusion data, we will thus adopt a pure diffusion model, where the clay sample is assumed a homogeneous porous medium in which the salt diffuses with diffusion coefficient D_c

$$j(x, t) = -\phi \cdot D_c \cdot \frac{\partial C(x, t)}{\partial x} \quad (2-3)$$

Here $j(x, t)$ denotes molar flux, ϕ is the porosity (i.e. the volume fraction of water), and $C(x, t)$ is the salt concentration as a function of position and time (the clay domain is $0 \leq x \leq L$). Note the presence of the physical porosity (ϕ) in this equation. The flux is thus measured in units of mol/(s · m² porous media), while the diffusivity D_c is a so-called pore diffusivity.

As the model assumes no additional processes contributing to altering the concentration (e.g sorption, or pore volume evolution), the resulting governing equation for concentration evolution is the ordinary Fick's second law

$$\frac{\partial C(x, t)}{\partial t} = D_c \cdot \frac{\partial^2 C(x, t)}{\partial x^2} \quad (2-4)$$

This equation is to be solved together with boundary conditions

$$C(0, t) = C_0 \quad C(L, t) = 0 \quad (2-5)$$

and the initial condition

$$C(x, 0) = 0 \quad (2-6)$$

where C_0 is an arbitrary constant (discussed below).

Equations 2-4–2-6 constitutes the present model, which depends on the two parameters D_c and C_0 . Figure 2-2 displays the time evolution of the outflux (i.e. $j(L, t)$) for several models corresponding to different parameter values.

The steady-state concentration profiles is

$$C_{ss}(x) = C_0 \cdot \left(1 - \frac{x}{L}\right) \quad (2-7)$$

with the corresponding steady-state flux

$$j_{ss} = \frac{\phi \cdot D_c \cdot C_0}{L} \quad (2-8)$$

The steady-state flux is consequently determined by the product of D_c and C_0 . The breakthrough time – the time related to when outflux starts to deviate from zero – is on the other hand determined solely by D_c (apart from L)

$$t_{bt} \equiv \frac{L^2}{6 \cdot D_c} \quad (2-9)$$

From these dependencies it follows that a specific parameter pair (D_c, C_0) generates a unique outflux evolution. Conversely, fitting the model to experimental data, produces unique values of D_c and C_0 (within experimental error, of course).

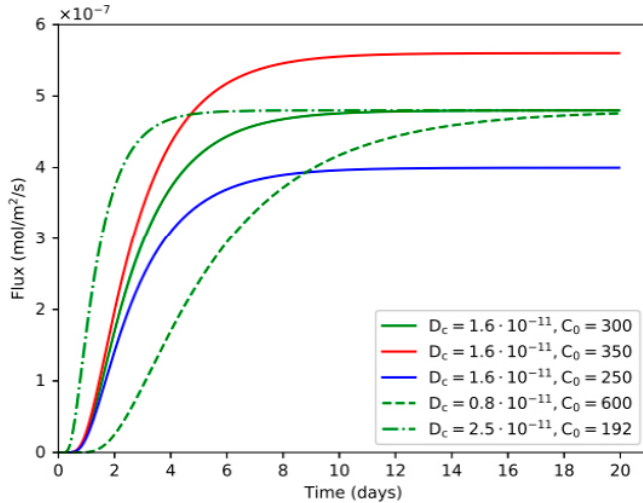


Figure 2-2. Outflow evolution for a set of different pairs of parameters (D_c, C_0). The green curves have the same steady-state flux but different breakthrough times. The fully drawn lines (different color) have the same breakthrough time but different steady-state flux. The model have $L = 5$ mm and $\phi = 0.5$. Concentration unit in the legend is mM.

2.1.1 Model fitting

The models were fitted assuming the same diffusion coefficient in all tests performed on the same sample, while the parameter C_0 was varied for each individual test. The fitted values are found in Table 2-1, and the model results are compared with the experimental data in Figures 2-3 and 2-4. These figures also shows models with slightly varied parameters demonstrating the level of uncertainty; the diffusion coefficient in the Na-montmorillonite sample have an uncertainty roughly in the range 2.1×10^{-11} – 1.7×10^{-11} m²/s and in the Ca-montmorillonite sample the interval is 10×10^{-11} – 8×10^{-11} m²/s. The values of C_0 naturally show a corresponding uncertainty range.

The experimental data reveal a noise level of the outflux of approximately 1×10^{-8} mol/m²/s. Since the steady-state flux increases with source concentration and diffusion coefficient (cf. Equation 2-8), the relative error is thus considerably more pronounced in tests with low values of these parameters. This is especially true for the test with 100 mM NaCl, where the steady-state flux is barely above the noise level. Reasonably, the estimated value for C_0 in this data set is therefore significantly overestimated.

Table 2-1. Parameters for each model fitted to the benchmark data set. Parameter D_c was varied for each of the two samples, parameter C_0 was varied for each individual test. Porosity and sample length was taken from the test specifications.

Test	D_c (m ² /s)	C_0 (mM)	C_0/C_{source}	Porosity	Length (mm)
1.0 M NaCl	1.9×10^{-11}	267	0.267	0.49	5.4
0.4 M NaCl	1.9×10^{-11}	80.5	0.201	0.49	5.4
0.1 M NaCl	1.9×10^{-11}	13.0	0.130	0.49	5.4
CaCl ₂ 0.4 M	9.0×10^{-11}	143	0.358	0.53	7.8
CaCl ₂ 0.1 M	9.0×10^{-11}	33.4	0.334	0.53	7.8
CaCl ₂ 0.025 M	9.0×10^{-11}	6.6	0.264	0.53	7.8

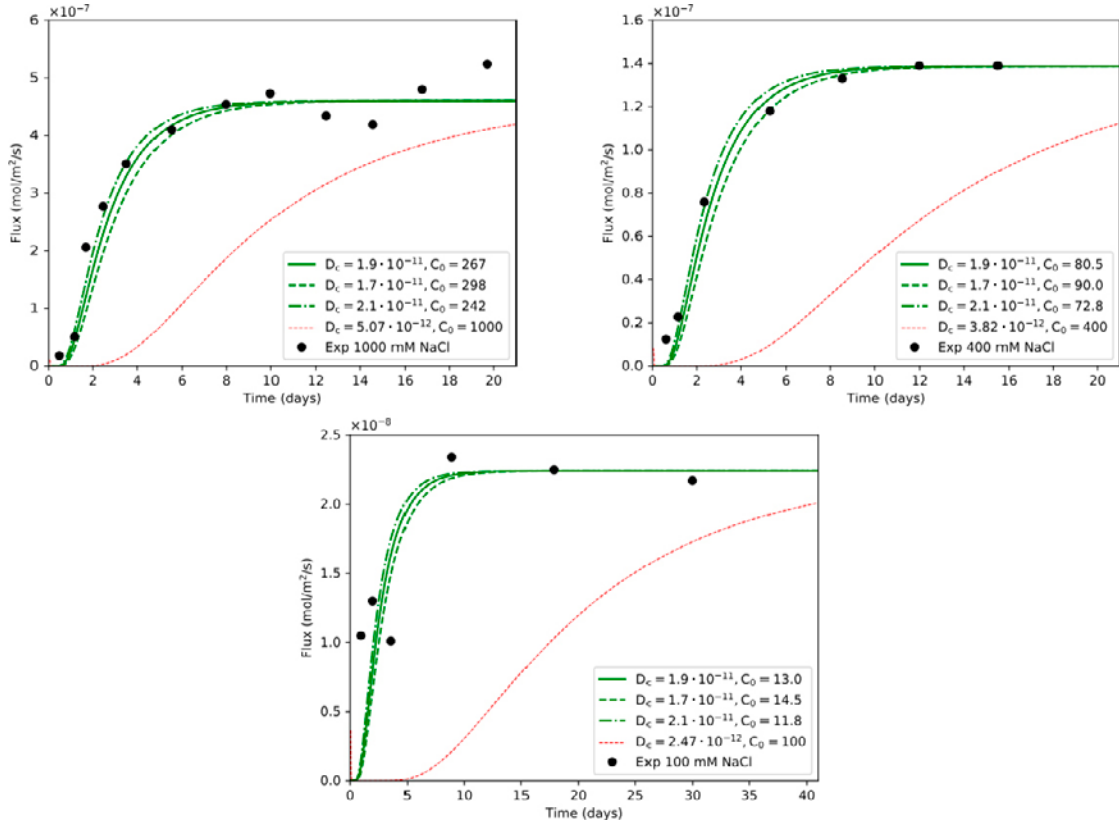


Figure 2-3. Fitted models to NaCl experimental data. The experimental outflux was derived from the measured target concentration evolution using Equation 2-1. The red curves show the flux when C_0 is set equal to C_{source} , while D_c is fitted to the steady state flux.

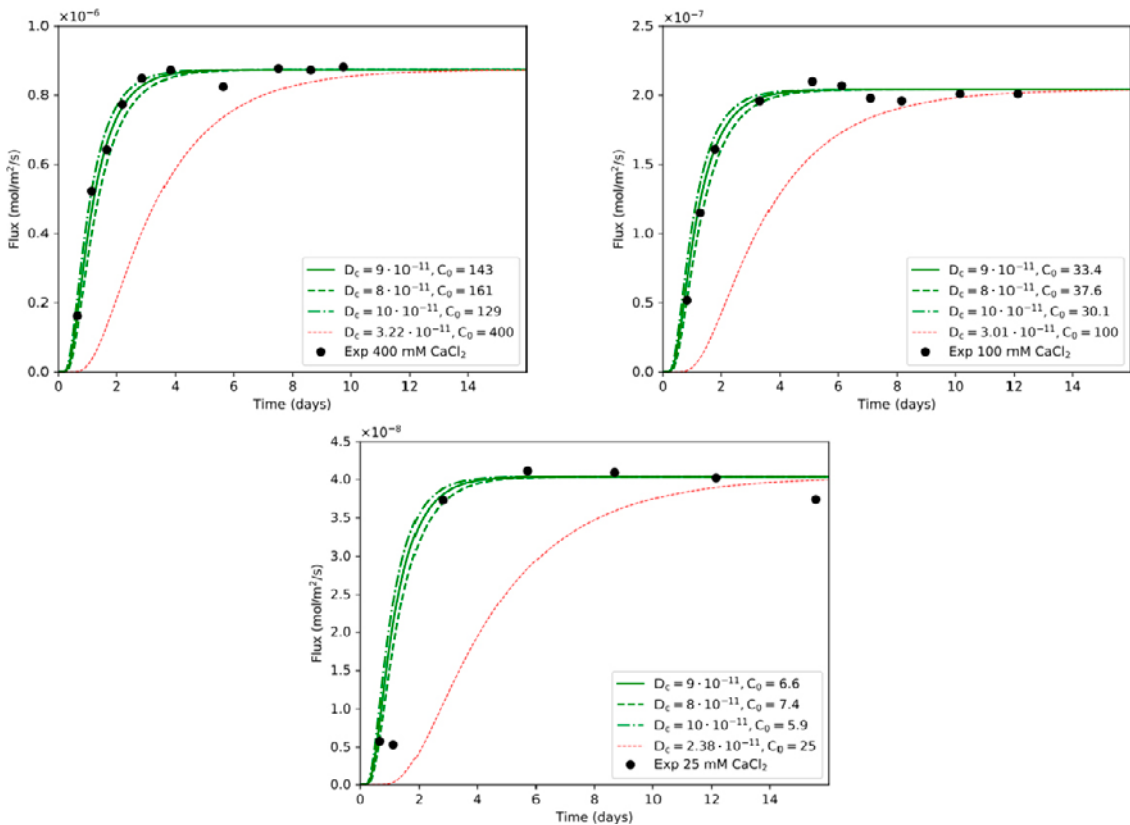


Figure 2-4. Fitted models to CaCl_2 experimental data. The experimental outflux was derived from the measured target concentration evolution using Equation 2-1. The red curves show the flux when C_0 is set equal to C_{source} , while D_c is fitted to the steady state flux.

2.1.2 Discussion

The previous section showed that the experimental results can be reproduced by a simple diffusion model, using the same value of D_c for tests performed on the same sample. This strongly suggests that D_c represents a physical diffusion coefficient, and that diffusion, as described by Equation 2-3, is the only mechanism at play in these tests. Such a simple behavior is quite remarkable, considering that the chemical conditions differ significantly between the tests, and are quite extreme in some cases – in the test with the highest concentration, a concentration difference of 1 000 mM is maintained across a ~5 mm thick clay sample that consists of ~50 vol-% water.

The parameter C_0 , in contrast, takes on values which need further interpretation. First, all C_0 values are considerably lower than the source solution concentration (C_{source}); if the clay behaved as a conventional porous system (Figure 2-5), these quantities should be equal (the resulting flux evolution if C_0 is set equal to C_{source} , while D_c is fitted to the steady state flux is shown in Figures 2-3 and 2-4). Second, the ratio C_0/C_{source} systematically increases with C_{source} in both samples. Finally, the values of C_0/C_{source} are considerably larger in the Ca-montmorillonite as compared to the Na-montmorillonite sample, as shown in Figure 2-6.

It is interesting to compare the present experiments with chloride tracer through-diffusion tests (Glaus et al. 2010, Molera et al. 2003, Muurinen et al. 1988, Van Loon et al. 2007). Tracer tests differ from the ones treated here in that they are performed with an identical “background” electrolyte in the two reservoirs; only a trace amount of a radioactive isotope is added on the source side.

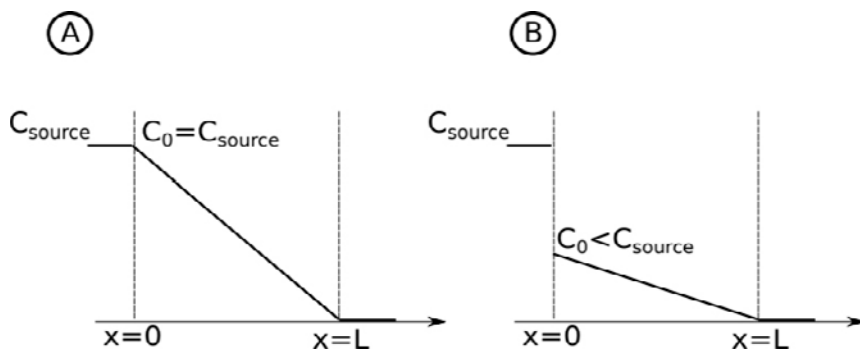


Figure 2-5. A) Steady-state profile of a conventional porous system: The concentration varies continuously (i.e. without disruption) across borders to external solutions. B) Steady-state profile in model successfully fitted to montmorillonite flux data.

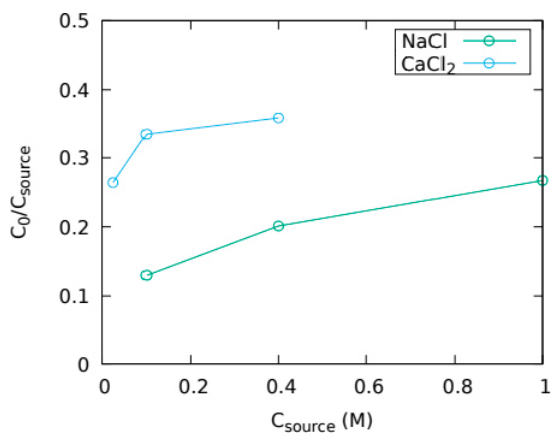


Figure 2-6. Ratio between the fitted parameter C_0 and the source concentration in all performed tests.

Anion tracer tests are almost universally evaluated using a model where the flux is expressed as (cf. Equation 2-3)

$$j(x, t) = -\epsilon \cdot D_c \cdot \frac{\partial C_{\text{bulk}}(x, t)}{\partial x} \quad (2-10)$$

where C_{bulk} is *assumed* to behave as the concentration in a conventional porous system (see e.g. Van Loon et al. 2007, Bourg and Tournassat 2015) (Figure 2-5A). The flux itself, however, is not conventional, because it contains a free parameter ϵ – the *effective porosity* – rather than the physical porosity. The effective porosity description of tracer tests is therefore mathematically equivalent to the model defined here, as seen from the steady-state flux

$$j_{ss} = \frac{\epsilon \cdot D_c \cdot C_{\text{source}}}{L} \quad (2-11)$$

Comparing with Equation 2-8 gives

$$\epsilon = \phi \cdot \frac{C_0}{C_{\text{source}}} \quad (2-12)$$

The free parameters ϵ and C_0 are thus related by a trivial transformation involving two well-defined constants (ϕ and C_{source}). This does not mean that C_0 should be interpreted as an effective porosity (whatever that means), but that physical interpretation of ϵ (or C_0) is arbitrary; a free fitting parameter does not quantify “effective porosity” simply by giving it a name.

ϵ (or ϵ/ϕ) in anion tracer tests behaves in principle identical to C_0/C_{source} evaluated here: ϵ/ϕ is considerably smaller than unity, and increases systematically with the *background* concentration (Bourg and Tournassat 2015). (Whether ϵ differs in Ca- as compared to Na-montmorillonite cannot be stated due to lack of experiments performed on Ca-montmorillonite.)

The similarity between anion tracer and salt diffusion confirms that the diffusive behavior indeed is very simple in compacted bentonite – there is no qualitative difference between chloride diffusing at trace levels in constant chemical background, and diffusion of salt under huge chemical gradients.

Still, C_0 behaves in a non-trivial manner that requires an explanation. The remaining part of the chapter is devoted to give this explanation, and, as a consequence, eliminate the need for a free parameter when fitting models to data. It is worth emphasizing that by invoking enough free parameters, model fitting becomes quite trivial (as e.g. demonstrated here) – the “hard” part of the modeling work lies in exchanging arbitrary fitting parameters for real physical insight, rather than simply giving them catchy names.

2.2 A homogeneous mixture model

2.2.1 Structure of compacted bentonite

Compacted bentonite is used to seal off various sections in waste repositories, e.g. to reduce the mass transfer capacity to and from a KBS-3 canister. In order to have this function the bentonite must be *confined*, i.e. the solid parts must be prevented from crossing boundaries to external water by means of a semi-permeable component. With such a boundary condition the bentonite is pressurized when in equilibrium with the environment. The pressure difference between bentonite and external water – the *swelling pressure* – in combination with the material’s rheological properties is the underlying cause for its sealing ability.

Thus, compacted bentonite is not simply a material in the usual sense of the word, but requires the above described boundary condition to be well-defined; with unrestricted access to water it will swell – in some cases indefinitely – and no longer be compacted (it may be defined as an *isolated* system, but that is of no interest here). In practice, the semi-permeable components are e.g. steel-filters in laboratory test configurations, or the host rocks in field-tests or in actual repositories.

From its definition it is expected that the pore volume of compacted bentonite is dominated by montmorillonite interlayer pores. While this is confirmed experimentally (Holmboe et al. 2012), it may also be anticipated as a direct consequence of swelling pressure; since swelling ultimately is caused

by hydration of interlayer spaces, the presence of swelling pressure proves that compacted bentonite mainly contains interlayer pores, which are “craving” for more water, but which are prohibited from expanding further due to the confinement.

That the pore volume of compacted bentonite is dominated by interlayer pores motivates the use of the so called homogeneous mixture model of bentonite (Birgersson et al. 2017). The defining feature of this model – which will be adopted here – is that it assumes the *entire* pore volume is distributed in a single type of interlayer pores, characterized by the average interlayer distance.

In the modeling presented in this section, the bentonite is thus still assumed to be a homogeneous diffusive domain, but the boundary condition between bentonite and external solutions is now more involved. Since the bentonite domain contains charged entities which are prohibited to move across the semi-permeable components (the montmorillonite particles), it fulfills the criteria for Donnan equilibrium (Birgersson 2017). As a consequence, the concentration profile for any charged species exhibits a discontinuity across the interface between bentonite and external solutions (this is intuitively easy to see for cations, since the interlayers always contain a high concentration of cations compensating structural charge). Note that a concentration discontinuity is a very natural interpretation of the result that $C_0 < C_{\text{source}}$ from the previous section (Figures 2-5 and 2-6). Thus, adopting the homogeneous mixture model does not only comply with the nature of compacted bentonite (which is dominated by interlayer pores), but also comply with the observed diffusional behavior without having to make additional, *ad hoc* assumptions (which is the case for an “effective porosity” interpretation).

2.2.2 Model description

Here we adopt a framework for calculating the chemical equilibrium between bulk solutions and montmorillonite interlayers based on the so-called Donnan approximation (Birgersson 2017, Birgersson and Karnland 2009). This approach assumes that the electrostatic potential within the interlayer pore is everywhere constant; the step in electrostatic potential across a clay/bulk solution interface is referred to as the Donnan potential (labeled ϕ^*).

The Donnan potential depends on the density of the clay as well as on the composition of the bulk solution; generally, its magnitude increases with decreasing ionic strength (for a given salt solution) and with increasing clay density. A lowered electrostatic potential in the clay implies a lower equilibrium concentration of anions – a reduction that can be substantial. For this reason it may be important to consider not only the major anionic species in an external solution, but also other species formed from the ions, which may be of different valency (in the following, species formed from combining ions will be referred to as complexes). For instance, in the case of NaCl diffusion, there is a minor amount of charge neutral NaCl^0 complex present



and in tests with CaCl_2 solutions, the complexes CaCl^+ and CaCl_2^0 should be considered



Thermodynamic data for complex formation is taken from the Lawrence Livermore National Laboratory database, *llnb.dat*, distributed with the Phreeqc software (Parkhurst and Appelo 2013).

The present model is solved using a numerical code specifically developed by Clay Technology within the EBS Task Force for dealing with the combination of diffusion and Donnan equilibrium (referred to as the CT code in the following). Apart from solving Fick’s second law (Equation 2-4) on a one dimensional grid, this code performs Donnan equilibrium calculations at each domain interface at each time step in accordance with the theoretical framework presented in Birgersson (2017). As an illustration of this framework, the equation to be solved for the Donnan potential in the case of a CaCl_2 solution reads

$$2 \cdot f_D^{-2} \cdot \Gamma_{\text{Ca}^{2+}} \cdot C_{\text{Ca}^{2+}} + f_D^{-1} \cdot \Gamma_{\text{CaCl}^+} \cdot C_{\text{CaCl}^+} - f_D \cdot \Gamma_{\text{Cl}^-} \cdot C_{\text{Cl}^-} = c_{IL} \quad (2-16)$$

where f_D is a transformation of the Donnan potential

$$f_D \equiv e^{\frac{F \cdot \phi^*}{RT}} \quad (2-17)$$

and Γ_i denotes an activity coefficient ratio for species i

$$\Gamma_i = \frac{\gamma_i^{\text{ext}}}{\gamma_i^{\text{int}}} \quad (2-18)$$

where γ_i^{ext} and γ_i^{int} respectively denotes activity coefficient in the bulk solution and in the clay at the interface.

c_{IL} is a parameter characterizing the clay and is given by

$$c_{IL} = \frac{\text{CEC} \cdot \rho_w}{w \cdot F} \quad (2-19)$$

where w is the water-to-solid mass ratio, CEC denotes the cation exchange capacity (charge equivalents per mass unit), and F is Faraday's constant (1 eq/mol). Note that charge neutral species (e.g. CaCl_2^0) do not enter the equation for the Donnan potential.

The CT code also performs chemical speciation calculations at each time step (e.g. Equations 2-14–2-15, in the case of CaCl_2 -diffusion).

The CT code requires the specification of activity coefficients for all included species, both in bulk water solutions and in interlayer pores (see e.g Equation 2-18). At present, the code treats these coefficients as constants in each domain. For bulk solutions, the activity coefficients were taken from corresponding batch calculations made using Phreeqc (Parkhurst and Appelo 2013). The Phreeqc calculations were also used to verify the speciation calculations in the CT code.

The activity coefficients in interlayer pores for ions are here calculated using the mean salt method and the approach suggested in Birgersson (2017). For complexes, the activity coefficients are here put equal to unity everywhere. This arbitrary choice is discussed further below.

A schematic figure of the geometry of the implemented model, which also takes into account the filters in the tests, is found in Figure 2-7. Corresponding material parameters are listed in Table 2-2. As diffusion coefficients in the modeling was used the ones inferred from the previous modeling (Section 2.1).

Table 2-2. Material parameters. From Birgersson (2011). Assuming a cation exchange capacity of 0.875 eq/kg.

Filter	Na-montmorillonite	Ca-montmorillonite
D_c (m^2/s)	5×10^{-10}	1.9×10^{-11}
Porosity (-)	0.35	0.49
c_{IL} (mmol/kgw)	0	2500
Length (mm)	2	5.4
		7.8

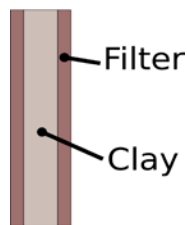


Figure 2-7. Schematics of the model used for simulating through-diffusion of salts.

2.2.3 Results

Table 2-3 shows the speciation of the NaCl solutions in the three different NaCl diffusion tests at the end of the simulations (20 days), i.e. in the steady-state phase. This table also lists the values of the Donnan potential (f_D) and the ion equilibrium coefficient for the total amount of chloride ($\Xi_{\text{CL TOT}}$), defined as the ratio between the total concentration of chloride in the clay and in the bulk solution. For the NaCl-calculation, this quantity is

$$\Xi_{\text{CL TOT}} \equiv \frac{[\text{Cl}^-]_{\text{clay}} + [\text{NaCl}^0]_{\text{clay}}}{[\text{Cl}^-]_{\text{ext}} + [\text{NaCl}^0]_{\text{ext}}} \quad (2-20)$$

The modeled outflux evolution for the three NaCl diffusion tests is shown in Figure 2-8. Table 2-4 and Figure 2-9 show the corresponding results for the modeled CaCl₂ diffusion.

Table 2-3. Speciation in the external solution and the clay at the filter/clay interface in the NaCl system after 20 days simulation.

	0.1 M	0.4 M	1.0 M
External solution			
[Na ⁺]	0.0986	0.3846	0.9225
[Cl ⁻]	0.0986 (99.0 %)	0.3846 (97.0 %)	0.9225 (93.6 %)
[NaCl ⁰]	0.0010 (1.0 %)	0.0119 (3.0 %)	0.0631 (6.4 %)
γ_{Na^+}	0.785	0.723	0.726
γ_{Cl^-}	0.767	0.667	0.612
γ_{NaCl^0}	1.0	1.0	1.0
Clay			
[Na ⁺]	2.5049	2.559	2.779
[Cl ⁻]	0.0049 (83.5 %)	0.059 (83.2 %)	0.279 (81.5 %)
[NaCl ⁰]	0.0010 (16.5 %)	0.012 (16.8 %)	0.063 (18.5 %)
γ_{Na^+}	0.832	0.832	0.859
γ_{Cl^-}	0.568	0.568	0.568
γ_{NaCl^0}	1.0	1.0	1.0
f_D	0.037	0.131	0.281
$\Xi_{\text{CL TOT}}$	0.059	0.179	0.347

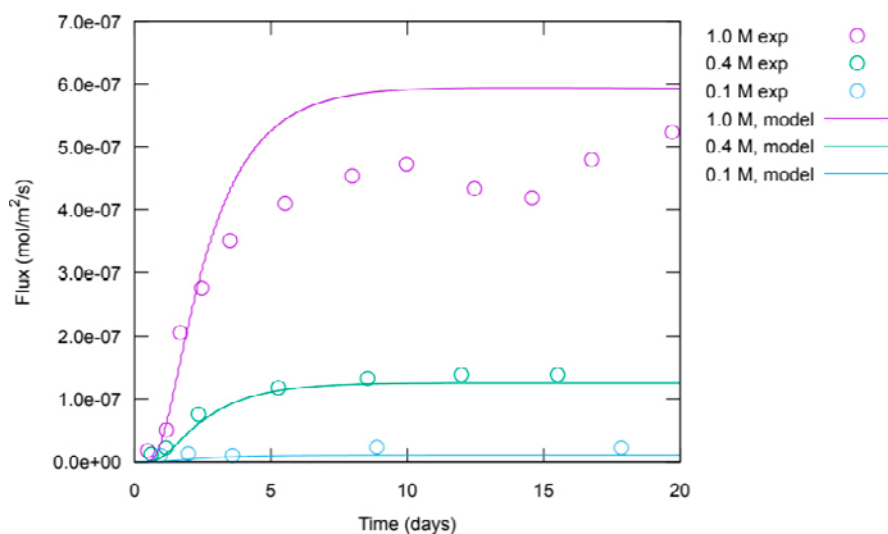


Figure 2-8. Simulated NaCl outflux.

Table 2-4. Speciation in the external solution and the clay at the filter/clay interface in the CaCl_2 system after 16 days simulation.

	0.025 M	0.1 M	0.4 M
External solution			
$[\text{Ca}^{2+}]$	0.0242	0.0954	0.3658
$[\text{Cl}^-]$	0.0486 (99.8 %)	0.1916 (99.5 %)	0.7399 (97.6 %)
$[\text{CaCl}_2^0]$	0.0001 (0.2 %)	0.0007 (0.4 %)	0.0082 (1.1 %)
$[\text{CaCl}_2^0]$	0.0000 (0.0 %)	0.0001 (0.1 %)	0.0050 (1.3 %)
$\gamma_{\text{Ca}^{2+}}$	0.428	0.292	0.249
γ_{Cl^-}	0.789	0.689	0.594
γ_{CaCl^+}	1.0	1.0	1.0
$\gamma_{\text{CaCl}_{20}}$	1.0	1.0	1.0
Clay			
$[\text{Ca}^{2+}]$	1.055	1.077	1.201
$[\text{Cl}^-]$	0.011 (95.0 %)	0.058 (94.7 %)	0.323 (91.5 %)
$[\text{CaCl}_2^0]$	0.001 (4.9 %)	0.003 (4.9 %)	0.020 (5.6 %)
$[\text{CaCl}_2^0]$	0.000 (0.1 %)	0.000 (0.4 %)	0.005 (2.9 %)
$\gamma_{\text{Ca}^{2+}}$	0.427	0.413	0.445
γ_{Cl^-}	0.571	0.571	0.571
γ_{CaCl^+}	1.0	1.0	1.0
$\gamma_{\text{CaCl}_{20}}$	1.0	1.0	1.0
f_D	0.152	0.250	0.413
$\Xi_{\text{CL TOT}}$	0.220	0.317	0.466

Figures 2-8 and 2-9 show that the homogeneous mixture model is able to reproduce the experimental behavior of salt diffusion. Of course, the fits are not perfect, but it must be kept in mind that the performed procedure in this section has been to replace a free fitting parameter (C_0) with a calculation based on physical insight (treating interlayer pores). In doing so, the modeling becomes considerably more involved – both a varying electrostatic potential and interlayer activity coefficients must be taken into account – and is naturally burdened with increased uncertainty regarding specific parameter values.

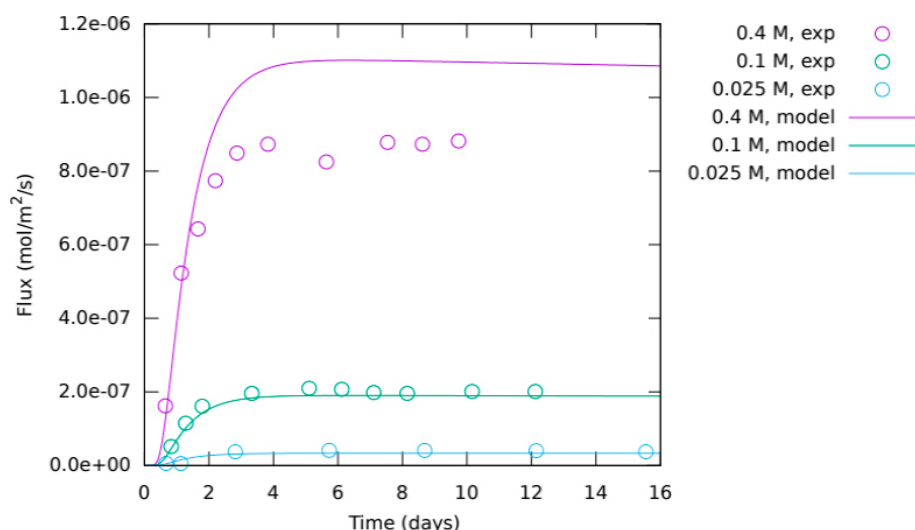


Figure 2-9. Simulated CaCl_2 outflux.

From this perspective, the agreement between experiments and the present modeling is actually quite remarkable, and is a strong indication that the diffusional behavior of salt (and tracers) in compacted montmorillonite is governed by Donnan equilibrium between the external bulk solution and the interlayer pores; not only does the simulations reproduce the non-linear trend of increasing (steady-state) flux with increasing source concentration, they also reproduce the rather different behavior observed in the Ca- and Na-montmorillonite sample respectively. Both of these effects are qualitatively explained by the value of the Donnan potential under the various conditions of the tests; the “Donnan factor”, f_D , depends approximately on the square-root of the external concentration in case of CaCl_2 (Equation 2-16), while this dependence is approximately linear in the case of a NaCl solution (Birgersson 2017). In Figure 2-10 the calculated values of the ion equilibrium coefficient for chloride is compared with the ratio C_0/C_{source} , evaluated in Section 2.1.

It can thus be concluded that interlayer pores constitute the major transport pathway for ions, and that an adequate treatment of these is obviously crucial when modeling compacted montmorillonite systems.

The results furthermore show that the relative amount of complexes is considerably larger in the clay as compared to the external solutions. The relative amount of complexes in the external solution decreases strongly with concentration (Tables 2-3 and 2-4). The relative amount of NaCl^0 and CaCl^+ in the clay, on the other hand, show much weaker dependence on the external concentration. This behavior is explained by how f_D decreases with external concentration in combination with the fact that the concentration of these complexes in the external solution depends approximately on the square on the external concentration. Thus, while the concentration in the clay of the negatively charged (major) species Cl^- is increasingly suppressed with decreasing external concentration (approximately linear in external concentration), the charge neutral species NaCl^0 is not influenced, and the concentration of the positively charged CaCl^+ is increasingly enhanced (approximately as the inverse square-root on the external concentration). As a result, the relative amount of these species in the clay stays approximately constant.

Note that the complex NaCl^0 consequently gives a non-negligible contribution to the chloride inventory of the clay, also when its concentration is very small in the external concentration. This effect is quite subtle and demonstrates the importance of including complexes in the calculations if high accuracy is to be achieved. Figure 2-11 shows the steady-state profiles of chloride species in the case of 0.4 M external concentration. It should be noted that the exact value of the amount of complexes depends directly on the values of the corresponding activity coefficients (Equation 2-18.) Here this issue has not been addressed, and these coefficients were put equal to unity. This choice gives an “ideal” activity coefficient ratio $\Gamma = 1$, and the noted influence of complexes can be said to represent the effect of electrostatics alone. In reality, ions pairs may behave far from “ideal”, and this issue – especially the behavior of (charged) aqueous species in an interlayer environment – needs further investigation. It is a topic which cannot be escaped if adequate chemical calculations in bentonite are desired, and it certainly contributes to the uncertainty in the present modeling results.

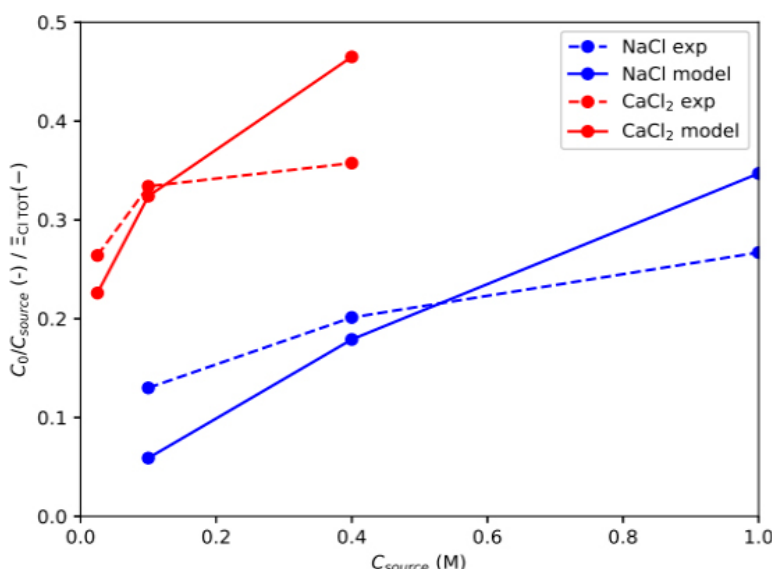


Figure 2-10. Calculated ion equilibrium coefficients ($\Xi_{\text{Cl},\text{TOT}}$) compared with the ratio C_0/C_{source} evaluated in Section 2.1.

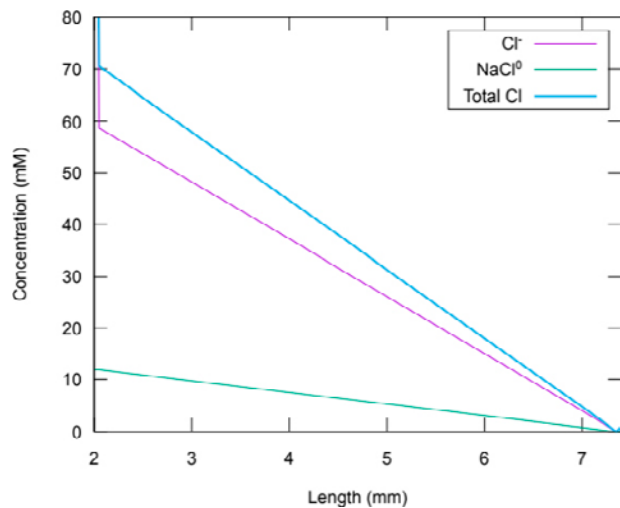


Figure 2-11. Steady-state profiles of chloride species in the clay in the case of 0.4 M NaCl external solution. The complex NaCl^0 constitutes approximately 17% of the chloride present in the clay.

One might be tempted to use the (interlayer) activity coefficients as fitting parameters, as illustrated in Figure 2-12, where the interlayer coefficient for the Cl^- species has been adjusted in order to fit the model basically perfectly in the case of 1.0 M and 0.4 M NaCl solutions. It is of course no surprise that a perfect fit can be achieved, but the interpretation of the corresponding activity coefficients should be made with caution. Firstly, the available data is not enough to give a unique set of fitted parameters. Secondly, the intrinsic uncertainty of the experimental data itself must be evaluated before ascribing significance to these kind of changes in activity coefficients parameters. With that being said, the result presented in Figure 2-12 suggests that the actual interlayer activity coefficient for chloride at high external concentration may be higher than what is predicted by the mean salt method. This type of information should be used in further investigations on interlayer activities.

The issue of interlayer activity coefficients is further addressed when modeling sulfate and selenate diffusion in Chapters 3 and 6.

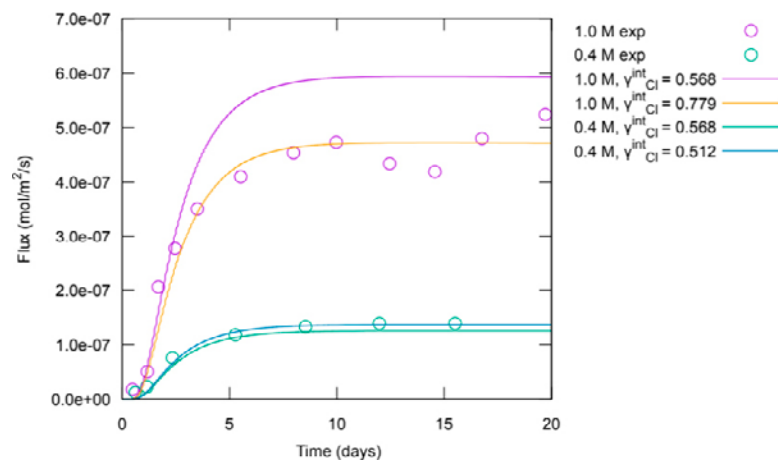


Figure 2-12. Alternative models for 1.0 M and 0.4 M NaCl diffusion where the activity coefficient for Cl^- has been adjusted for better fitting.

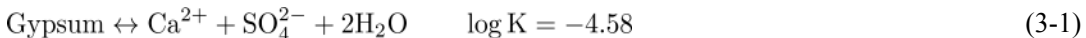
3 Benchmark 2

The data of Benchmark 2 origins from two different types of tests. Firstly, it contains results from a through-diffusion test of the same type as those in Benchmark 1 (Chapter 2). In this case a sample of Ca-montmorillonite was sandwiched between a reservoir of saturated CaSO_4 solution and a second reservoir containing deionized water. The experimental data has been transformed to a set of data points for outflux vs. time, in the same manner as discussed in Chapter 2.

Secondly, Benchmark 2 contains data from tests where a geometrically controlled source of gypsum was placed within a montmorillonite sample, which, in turn, was contacted by reservoirs of deionized water on both sides. Diffusion of ions from the gypsum source into the external water was recorded.

The experimental set-up is basically identical as that for Benchmark 1 (Figure 2-1). A schematic illustration of the samples in the gypsum dissolution tests is shown in Figure 3-1.

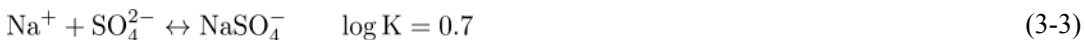
As in the previous section, these tests are here modeled using the CT code, adopting the homogeneous mixture model for the montmorillonite sample, and taking into account Donnan equilibrium at interfaces to external bulk water solutions. Dissolution of gypsum, as well as the aqueous chemistry involving sulfate ions must be treated when modeling all of these tests. The chemical reaction for gypsum dissolution is



The reaction for formation of the neutral species CaSO_4^0 is



and the reaction for forming NaSO_4^- is



The values for the equilibrium constants in these reactions ($\log K$) were taken from the default database of the reactive-transport code Phreeqc (Parkhurst and Appelo 2013).

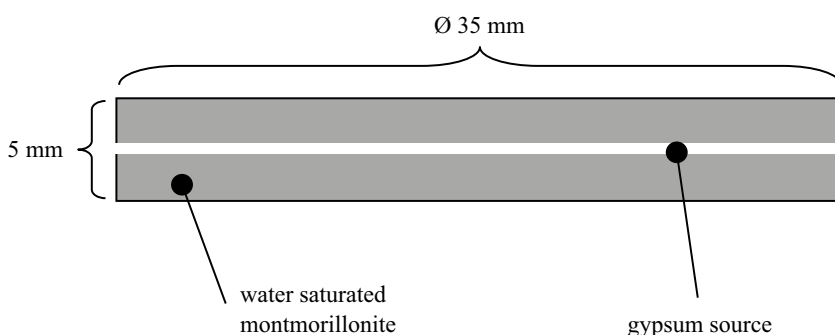


Figure 3-1. Schematic illustration of the clay sample in the gypsum dissolution tests in Benchmark 2. The width of the gypsum source is exaggerated for illustrative purposes (Birgersson 2011¹).

3.1 CaSO₄ through-diffusion

In the source reservoir, the solution is in equilibrium with gypsum (Equation 3-1) which is expressed in terms of the law of mass action as

$$c_{\text{Ca}^{2+}} \cdot c_{\text{SO}_4^{2-}} = 10^{-4.58} \cdot \frac{1}{\gamma_{\text{Ca}^{2+}} \cdot \gamma_{\text{SO}_4^{2-}}} \quad (3-4)$$

The equilibrium with the CaSO₄⁰ complex can similarly be expressed

$$c_{\text{CaSO}_4^0} = c_{\text{Ca}^{2+}} \cdot c_{\text{SO}_4^{2-}} \cdot 10^{2.25} \cdot \frac{\gamma_{\text{Ca}^{2+}} \cdot \gamma_{\text{SO}_4^{2-}}}{\gamma_{\text{CaSO}_4^0}} \quad (3-5)$$

In the source reservoir, this relation reduces to

$$c_{\text{CaSO}_4^0} = 10^{-2.33} \cdot \frac{1}{\gamma_{\text{CaSO}_4^0}} \quad (3-6)$$

Equations 3-4 and 3-6, together with the charge neutrality constraint $c_{\text{Ca}^{2+}} = c_{\text{SO}_4^{2-}}$, give unique values of the source reservoir concentrations for Ca²⁺, SO₄²⁻, and CaSO₄⁰. In the CT code, a total sulfate concentration of 15.05 mM was specified in the source reservoir, rather than performing the actual gypsum dissolution reaction. This value was taken from a batch reaction calculation of the same system using Phreeqc. The activity coefficients for the species in the bulk solution used in the CT code was also taken from this Phreeqc calculation, and are listed in Table 3-1.

Approximately 30 % of the solution in the source reservoir is in the form of complexes ($c_{\text{CaSO}_4^0} \approx 4.6$ mM) – a much larger part as compared with the external NaCl and CaCl₂ solutions of Benchmark 1.

The geometry of the model used for the diffusion modeling is the same as schematically shown in Figure 2-7, and Table 3-2 lists the adopted relevant material parameters.

Equilibrium between Ca²⁺, SO₄²⁻, and CaSO₄⁰ (Equation 3-5) was explicitly calculated in the montmorillonite and filter domains throughout the simulation, assuming constant activity coefficients (Table 3-1).

The adopted modeling strategy was to use the diffusion coefficient and the interlayer activity coefficients for SO₄²⁻ and CaSO₄⁰ as fitting parameters. In addition, two cases with other choices for these activity coefficients were explored, in order to investigate the variability of the results.

Table 3-1. Adopted values of activity coefficients. The values in the source reservoir was taken from a phreeqc simulation.

	Ca ²⁺	SO ₄ ²⁻	CaSO ₄ ⁰
γ source reservoir	0.495	0.485	1.009
γ interlayer, case 1	0.495	0.030	1.413
γ interlayer, case 2	0.495	0.485	2.018
γ interlayer, case 3	0.495	0.020	1.009

Table 3-2. Adopted material parameters in the simulation of the CaSO₄ through diffusion test. Porosity and length were taken from Birgersson (2011). Assuming a cation exchange capacity of 0.875 eq/kg.

	Filter	Clay
D _c (m ² /s)	5×10^{-10}	1.77×10^{-11}
porosity (-)	0.35	0.49
c _{IL} (mmol/kgw)	0	2500
Length (mm)	2	5

3.1.1 Results

Figure 3-2 shows the resulting fluxes for three choices of interlayer activities for SO_4^{2-} and CaSO_4^0 . The fitted value for the diffusion coefficient in the simulations was $D_c = 1.77 \times 10^{-11} \text{ m}^2/\text{s}$.

The interlayer activity coefficient for calcium was put equal to its value in the source reservoir in all cases. This arbitrary choice is motivated by that it is actually the product $\gamma_{\text{Ca}^{2+}} \cdot \gamma_{\text{SO}_4^{2-}}$ which to a large extent determine the ion equilibrium coefficient for sulfate species in this system (Birgersson 2017). Thus, the variation of the activity coefficient for the sulfate ion could in a sense be viewed as a variation of this product. The activity coefficient for CaSO_4^0 , on the other hand, can be viewed as “independent”, since it does not enter the equation for the Donnan potential. Note, however, that a difference in this parameter between the bulk water solution and the interlayer implies a concentration discontinuity at the filter/clay interface also for this species, although it is charge neutral (see e.g. Figure 3-3).

Figure 3-2 demonstrates that a homogeneous mixture model can be satisfactorily fitted to the experimental data also in this case. With the rather large amount of uncertain parameters it is however difficult to draw very specific conclusions from a successful fit. Simulation case 1 was chosen to be in reasonable correspondence with measured mean activity coefficients for relevant bulk solutions at high ionic strength. The interlayer ionic strength – as defined in Birgersson (2017) – is here approximately equal to 3 700 mM. Although experimental data for such high ionic strength is scarce (and cannot be obtained for a pure CaSO_4 system due to precipitation), for e.g. Na_2SO_4 at 1.85 mol/kgw is reported values $\gamma_{\pm} \approx 0.16$ (Bhatnagar and Campbell 1981) and for CuSO_4 in the range 2.5–10 mol/kgw, is reported $\gamma_{\pm} \approx 0.03$ (Jaskula and Hotłos 1992). As the individual ion activity coefficients for a C_pA_q -salt are related to the mean activity coefficient as $\gamma_{\pm} = (\gamma_{\text{C}}^p \gamma_{\text{A}}^q)^{1/(p+q)}$, these values correspond to $\gamma_{\text{SO}_4^{2-}} = 0.06$ (assuming $\gamma_{\text{Na}^{+}} = 0.8$) and $\gamma_{\text{SO}_4^{2-}} = 0.02$ (assuming $\gamma_{\text{Cu}^{2+}} = 0.49$) respectively. Although very crude, these estimates indicate that the sulfate activity coefficient is very low at high ionic strength.

Case 2 represents a parameter choice giving a “minimum” amount of sulfate in the clay: the interlayer activity coefficient for sulfate was put equal to its external value (giving a ratio, $\Gamma_{\text{SO}_4^{2-}} = 1$), while a large value was chosen for $\gamma_{\text{CaSO}_4^0}^{\text{int}}$ (corresponding to $\Gamma_{\text{CaSO}_4^0} = 2$). This value is what is given by Phreeqc’s activity model in a simulation of a 1.25 M CaCl_2 bulk solution.

In case 3, the interlayer activity coefficient for $\gamma_{\text{CaSO}_4^0}$ parameters was chosen as to fit to the steady-state flux. Note that a value as low as $\gamma_{\text{SO}_4^{2-}} = 0.02$ had to be chosen in order to fit the data, which indicates that sulfate seems to behave similarly in an interlayer environment as in a corresponding high ionic strength bulk solution.

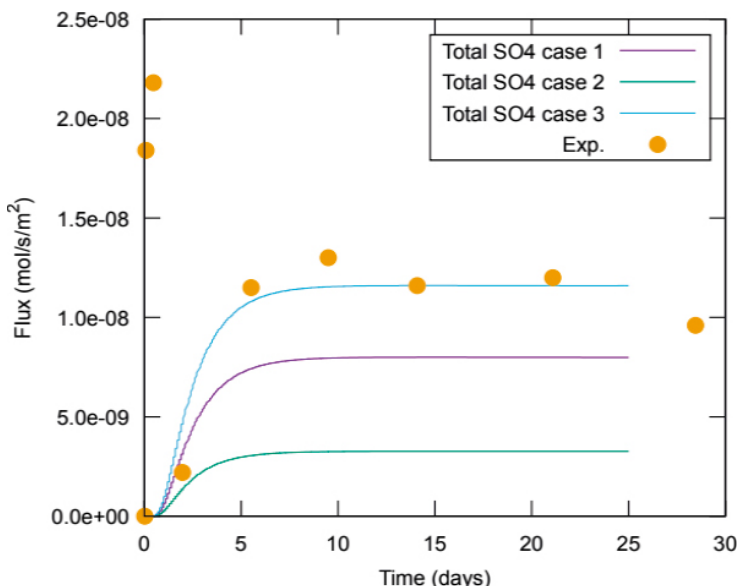


Figure 3-2. Resulting fluxes over the filter/reservoir interface in the modeled through-diffusion of CaSO_4 diffusion in Ca-montmorillonite using three different choices of activity coefficients for the species SO_4^{2-} , and CaSO_4^0 .

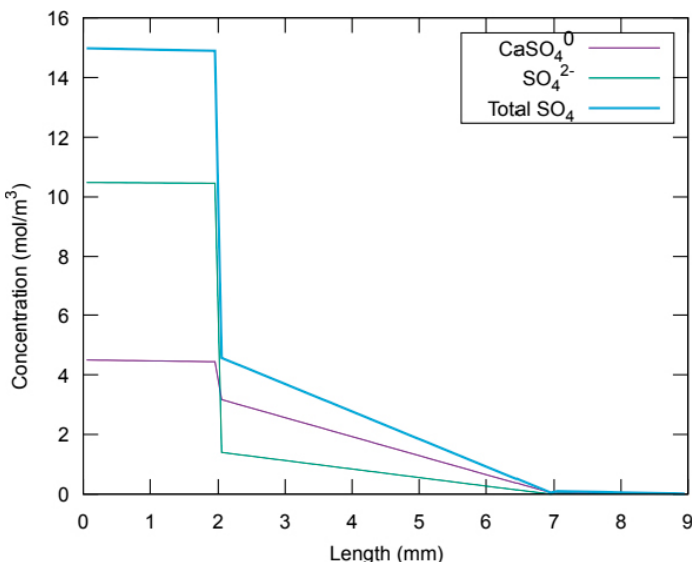


Figure 3-3. Steady-state concentration profile in modeling case I.

The diffusion coefficient for the transport of CaSO_4 through Ca-montmorillonite appears to be considerably lower than diffusion of CaCl_2 in a similar system. Comparing with the result from Chapter 2, the diffusion coefficient evaluated here is approximately only 20 % of the value for CaCl_2 . This is quite different from the difference in diffusion coefficients between Cl^- and SO_4^{2-} in bulk solution at infinite dilution, where chloride is approximately only twice as fast as sulfate.

Figure 3-3 shows the steady state profiles for the sulfate species in simulation case 1. Note that SO_4^{2-} is the dominating species outside the clay, while the complex CaSO_4^0 dominates internally. This is the case for a large set of choices of internal activity coefficients. It is thus plausible that sulfate is mainly transported through the clay in the form of the charge neutral CaSO_4^0 species in this system. It is obviously crucial to include the complex when performing this type of simulation in order to get relevant results.

As the complex dominates internally, this particular experiment alone is not especially suited for verifying the value of the interlayer activity coefficient for SO_4^{2-} (E.g., the entire sulfate inventory may be accounted for by CaSO_4^0 by choosing $\gamma_{\text{CaSO}_4^0} \approx 0.71$ and a large value for $\gamma_{\text{SO}_4^{2-}}$). More information on the value of $\gamma_{\text{SO}_4^{2-}}$ in the interlayer is, however, given when modeling gypsum dissolution in a Na-montmorillonite matrix (Section 3.3).

3.2 Gypsum dissolution in Ca-montmorillonite

The test where gypsum dissolves and diffuses in Ca-montmorillonite was modeled using the same activity coefficients for the involved species as fitted for the through-diffusion test treated in the previous section (i.e. case 3, see Table 3-1). The diffusion coefficient was adjusted for the model to fit the steady state flux.

In this case, the dissolution of gypsum had to be included explicitly in the model, whose geometry is schematically pictured in Figure 3-4. The adopted material parameters are listed in Table 3-3.

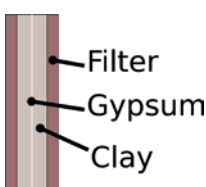


Figure 3-4. Schematics of the model used for simulating gypsum dissolution in Ca-montmorillonite. Material parameters are listed in Table 3-3.

Table 3-3. Adopted material parameters in the simulation of gypsum dissolution in Ca-montmorillonite. Porosity and length were taken from Birgersson (2011). Assuming a cation exchange capacity of 0.875 eq/kg.

	Filter	Clay
D _c (m ² /s)	5 × 10 ⁻¹⁰	1.67 × 10 ⁻¹¹
Porosity (-)	0.35	0.51
c _{IL} (mmol/kgw)	0	2300
Length (mm)	2	5

Gypsum dissolution was performed in the mid cell of the model in each time-step by solving

$$(c_{\text{Ca}} + (\Delta x - \Delta y)) \cdot (c_{\text{SO}_4} + (\Delta x - \Delta y)) = \frac{10^{-4.58}}{\gamma_{\text{Ca}^{2+}} \cdot \gamma_{\text{SO}_4^{2-}}} \quad (3-7)$$

and

$$(c_{\text{CaSO}_4^0} + \Delta y) = \frac{10^{-2.33}}{\gamma_{\text{CaSO}_4^0}} \quad (3-8)$$

where Δy denotes the amount of CaSO_4^0 formed in the present time step, and Δx denotes the amount of gypsum dissolved in the same time step.

In the other cells of the model, the complex equilibrium (Equation 3-5) was still maintained at each time step but gypsum equilibrium was not (i.e. gypsum is only present in one cell in the model).

3.2.1 Results

The resulting outflux (in two directions, labeled “top” and “bottom”) is displayed in Figure 3-5. It can be noted that the modeled steady-state flux agrees with experiment using a diffusion coefficient very similar to the value of the through-diffusion test. Since the clay material is almost identical in the two tests (Ca-montmorillonite of very similar density), this agreement strongly indicates that the same type of processes are active in these two tests.

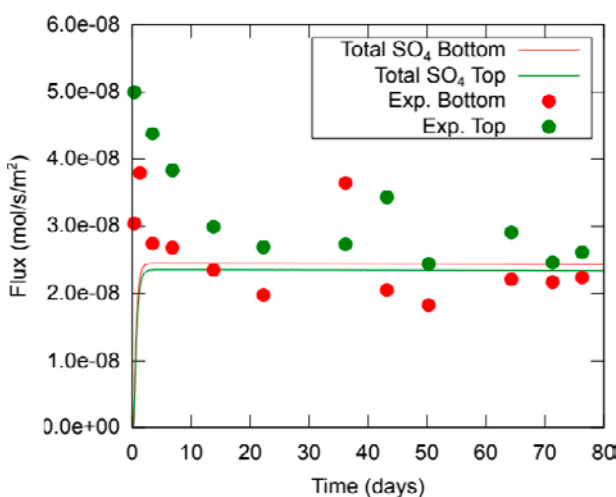


Figure 3-5. Flux in the model for gypsum dissolution in Ca-montmorillonite. The small difference seen for the modeled outfluxes in top and bottom is because the clay domain consists of an even number of cells. The “mid” cell (containing the gypsum) is thus one cell closer to the bottom side.

This similarity is from one point of view not very surprising, but it should be kept in mind that here the gypsum source is embedded within the clay, while in the previous test the source is external to the clay. In the previous test, Donnan equilibrium across the clay/filter interface at the source side controlled the diffusive flow, while here Donnan equilibrium does not play a significant role – it still prevails across the clay/filter interfaces, but it does not influence the flow since the external reservoirs are kept at insignificant concentration levels. In the present test, the flux is completely controlled by the solubility of gypsum *in the interlayer pores*. What is demonstrated in these two tests is basically the zeroth law of thermodynamics: as the source reservoir in the through-diffusion test is in equilibrium both with gypsum and the clay (at the interface), gypsum and the clay must also be in equilibrium, which is seen explicitly in the present test.

As the diffusion distance in the current test is only ~ 2.5 mm (from the middle of the clay sample to the edge), it reaches steady-state quickly – approximately four times faster than the through-diffusion test.

3.3 Gypsum dissolution in Na-montmorillonite

In the test where gypsum dissolves in (initially pure) Na-montmorillonite, also the NaSO_4^- complex must be considered (Equation 3-3). The law of mass action for this reaction reads

$$c_{\text{NaSO}_4^-} = 10^{0.7} \cdot \frac{\gamma_{\text{Na}^+} \cdot \gamma_{\text{SO}_4^{2-}}}{\gamma_{\text{NaSO}_4^-}} \cdot c_{\text{Na}^+} \cdot c_{\text{SO}_4^{2-}} \quad (3-9)$$

In the dissolution process an additional equation must be solved (cf. Equations 3-7 and 3-8)

$$(c_{\text{NaSO}_4^-} + \Delta z) = 10^{0.7} \cdot \frac{\gamma_{\text{Na}^+} \cdot \gamma_{\text{SO}_4^{2-}}}{\gamma_{\text{NaSO}_4^-}} (c_{\text{Na}^+} - \Delta z) \cdot (c_{\text{SO}_4^{2-}} + (\Delta x - \Delta y - \Delta z)) \quad (3-10)$$

where Δz denotes the amount of NaSO_4^- formed in the gypsum cell in each time step. Furthermore, Equation 3-7 is modified to

$$(c_{\text{Ca}^{2+}} + (\Delta x - \Delta y)) \cdot (c_{\text{SO}_4^{2-}} + (\Delta x - \Delta y - \Delta z)) = \frac{10^{-4.58}}{\gamma_{\text{Ca}^{2+}} \cdot \gamma_{\text{SO}_4^{2-}}} \quad (3-11)$$

while Equation 3-8 remains unaltered.

The adopted strategy in this simulation was to use the same interlayer activity coefficients for the species involved in the previous calculations, while fitting the interlayer activity coefficient for NaSO_4^- and the diffusion coefficient to the data. The activity coefficient for Na^+ was set to 0.86, which corresponds roughly to the mean salt value for the initial interlayer ionic strength (2750 mM).

The geometry is similar to the previous model (Figure 3-4). The adopted material parameters of this simulation are listed in Table 3-5.

Table 3-4. Adopted values of activity coefficients in the simulation of gypsum dissolution in (initial) Na-montmorillonite.

	Ca^{2+}	SO_4^{2-}	CaSO_4^0	Na^+	NaSO_4^-
γ interlayer, case 1	0.495	0.020	1.009	0.86	0.10
γ interlayer, case 2	0.495	0.485	0.4	0.86	0.86

Table 3-5. Adopted material parameters in the simulation of gypsum dissolution in Na-montmorillonite. Porosity and length were taken from Birgersson (2011). Assuming a cation exchange capacity of 0.875 eq/kg.

	Filter	Clay
D_c (m/s ²)	5×10^{-10}	8.0×10^{-12}
Porosity (-)	0.35	0.47
c_{IL} (mmol/kgw)	0	2750
Length (mm)	2	5

3.3.1 Results

The resulting flux of sulfate is displayed in Figure 3-6. It can be noted that the flux in this case is much larger as compared to the case of dissolution in Ca-montmorillonite – the maximum flux in this case is an order of magnitude larger than the steady-state flux in Ca-montmorillonite. The flux also shows a more dynamic behavior, with a quickly rising peak up to day 5, after which the flux falls off in a monotonic fashion. The system has not reached steady-state even after 35 days. The more dynamic development of the flux allows for a more robust fit of the diffusion coefficient in this case, as compared to the pure Ca-montmorillonite. Although the flux is larger in this case, it should be noted that the fitted diffusion coefficient is considerably smaller as compared to the Ca-montmorillonite case. A smaller diffusion coefficient may be expected in this case because of a somewhat higher density. However, a comparison between different types of materials should be made with caution.

As the diffusion coefficient is not larger in this case as compared to the previous cases, the higher flux must stem from steeper gradients, i.e. higher concentrations of sulfate. Figure 3-7 shows the concentration of the sulfate species after 0.1 and 40 days in the simulation. Indeed, after 0.1 days the total sulfate concentration in the cell where gypsum dissolves (located at 4.5 mm in this diagram) is almost 100 mM, which should be compared with 4.6 mM in the case of pure Ca-montmorillonite (Figure 3-3). After 40 days the total concentration in the dissolving cell is still as high as 34 mM. The speciation furthermore shows that the dominating species in this case is the NaSO_4^- complex. That this complex dominates is a consequence of the low activity coefficient fitted for this species. In Figure 3-6 is also plotted a simulation case which considerably larger interlayer activity coefficients both for SO_4^{2-} and NaSO_4^- . As the flux is much smaller as compared with experiment, it can be concluded that these interlayer activities are small in the montmorillonite environment. The detailed partitioning between SO_4^{2-} and NaSO_4^- is however difficult to assess from this single experiment.

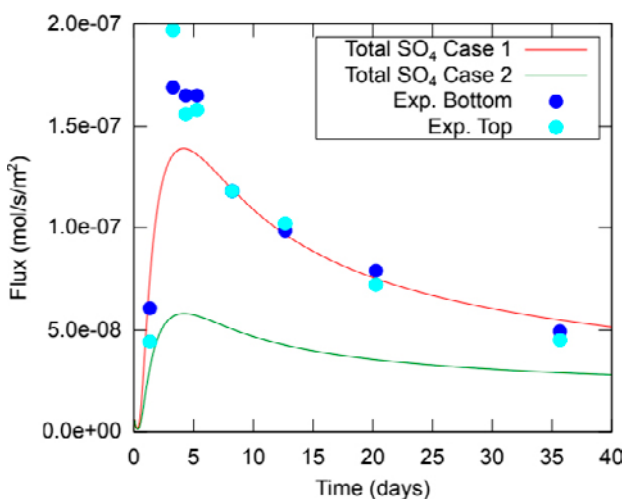


Figure 3-6. Total (out)flux of sulfate in the simulation of gypsum dissolution in (initial) Na-montmorillonite. The sulfate is fully compensated by sodium (Birgersson et al. 2009), as expected at low ionic strength.

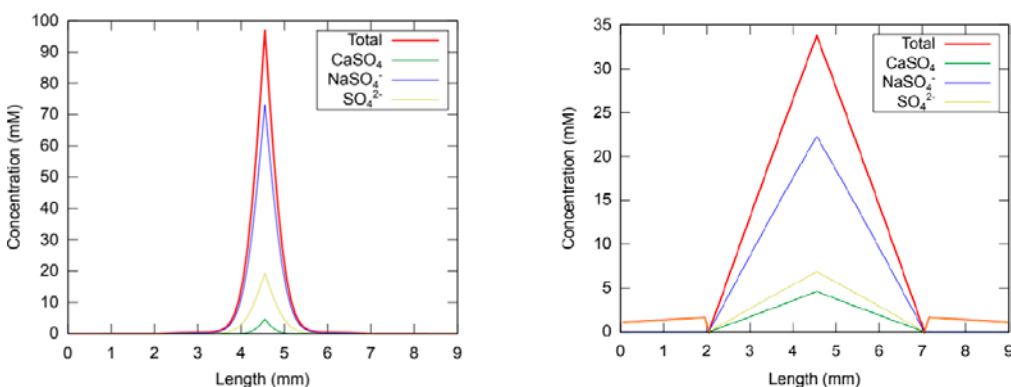


Figure 3-7. Sulfate concentration profiles after 0.1 days (left) and 40 days (right).

Disregarding the details of the $\text{SO}_4^{2-}/\text{NaSO}_4^-$ partitioning, it should be noted that the simulated flux fits very well to the complicated flux evolution. This is indeed a huge indication that chemical processes in the interlayer are both active and relevant. Furthermore, it is again demonstrated that complex formation is crucial to consider in these types of simulations.

The results of the presented simulations indicate that gypsum solubility is a function of the initial amount of calcium in the clay. Figure 3-8 shows the solubility as a function of initial calcium concentration as calculated from Equations 3-4, 3-5, and 3-9 assuming $c_{IL} = 2750 \text{ mol/kgw}$ and the activity coefficients of case 1 (Table 3-4).

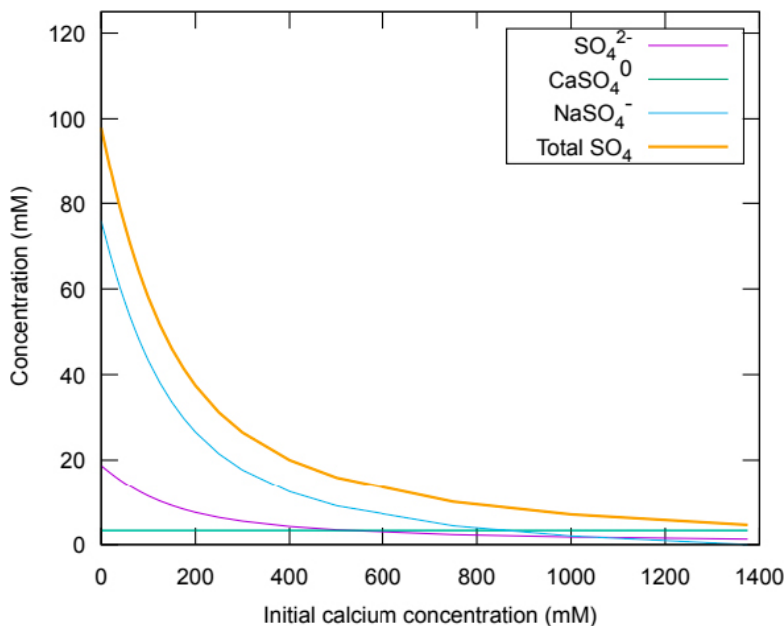


Figure 3-8. Gypsum solubility in Na/Ca-montmorillonite as a function of initial calcium concentration as calculated from Equations 3-4, 3-5, and 3-9 assuming $c_{IL} = 2750 \text{ mol/kgw}$. $\gamma^{int}_{\text{CaSO}_4^0} = 1.413$, $\gamma^{int}_{\text{NaSO}_4^-} = 0.07$, $\gamma_{\text{Ca}}^{int} = 0.495$, $\gamma_{\text{Na}}^{int} = 0.704$, $\gamma^{int}_{\text{SO}_4} = 0.03$.

4 Benchmark 3

The third set of benchmark data originates from a set of Ca/Na ion exchange experiments performed on pure montmorillonite samples (Karnland et al. 2011). Samples of pure Na-montmorillonite and Ca-montmorillonite were prepared in constant volume test cells, in basically the same way as the samples used for the diffusion tests of Benchmark 1 (Chapter 2).

Once water saturated, the samples were exposed to specific chloride solutions; the Na-montmorillonites were contacted with pure CaCl_2 solutions, and the Ca-montmorillonites were contacted with pure NaCl solutions. The total amount of cations in each solution was adjusted to correspond to 25 % of the charge needed to compensate all montmorillonite surface charge (which translates to a specific concentration, given the solution volume of 100 ml).

Once the samples were contacted with the salt solutions, an ion exchange process was initiated, where cations in the solution diffused into the clay, while cations initially located in the clay diffused out in the external solution. This process was continued until equilibrium was reached. At this stage a new amount of salt was added to the external compartment (CaCl_2 in the case of Na-montmorillonite, and NaCl in the case of Ca-montmorillonite). This amount of salt was adjusted so that the total amount of added excess cations corresponded to 50 % of the total montmorillonite charge. Again, the system was allowed to equilibrate. A final stage was then initiated by adding even more salt to the external solutions, this time adjusted so that the total amount of added excess salt corresponded to 100 % of the montmorillonite charge. During the course of the tests, the ion content of the external solutions was regularly measured using ion selective electrodes. Also the swelling pressure response was recorded by continuously sample the force exerted by clay samples, in the same way as was made in the diffusion tests of Benchmark 1. Figure 4-1 shows the schematics of the set-up.

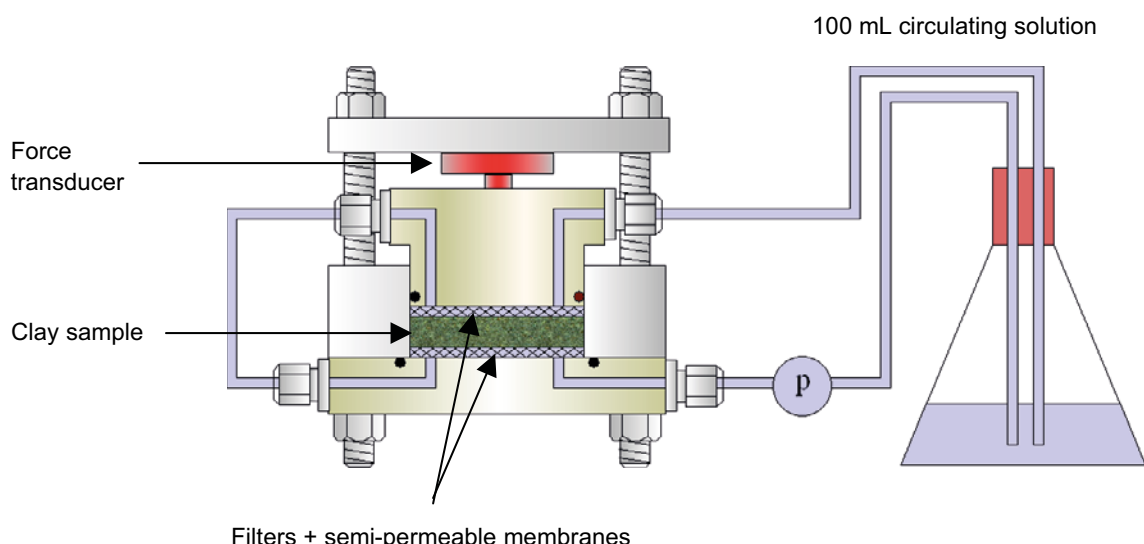


Figure 4-1. Schematics of the experimental set-up of Benchmark 3.

4.1 Treatment of experimental data

Since the total concentration of the external solution at all times is rather small (the largest chloride concentration is < 80 mM), it is expected that only a negligible amount of chloride enters the clay samples (see Chapter 2). Thus, to be consistent, the total amount of calcium and sodium charge measured in the external solution should basically remain constant (except when new solution is introduced).

Figure 4-2 shows the evolution of cation charge – as measured by the selective electrodes – during the first stage of all six tests. It is clear that this measured charge does not remain constant, which indicates that there is an error in measurements using ion selective electrodes. Looking at the samples where the initial solution is pure CaCl_2 (WyNa01, WyNa02, and WyNa03), the initially measured amount of charge resembles quite well the nominal value (i.e. the prepared concentration). On the other hand, in the samples with initial pure NaCl solution, the measured charge is significantly lower as compared to the nominal value. From this observation we conclude that the main error stems from measuring sodium using ion selective electrode. Therefore, in order to have consistent experimental data, we discard the measured sodium concentration values, and instead infer them from the calcium concentration (C_{Ca}) values using the formula

$$C_{\text{Na}}^* = C_{\text{nominal}} - 2 \cdot C_{\text{Ca}} \quad (4-1)$$

where C_{nominal} denotes the (constant) amount of charge expressed in terms of a monovalent cation concentration.

The evolution of the modified sodium concentrations (C_{Na}^*) are shown in Figure 4-3. It should be emphasized that this way of modifying the experimental data represent only one of an infinite set of modifications in order to make the data consistent from the view of charge conservation; the choice made here assumes that the full error is in the measurement of sodium, something which most probably is not completely true. That the calcium concentration measurements also have errors is evident at the beginning of the third stage, where the external calcium concentration is much larger than the nominal value, resulting in negative values for the corresponding modified sodium concentrations. For the most part, however, the calcium concentrations are typically rather small (below 1 mM). It is therefore reasonable to assume that the error in the experimental data is mostly due to measurement problems with the sodium selective electrode.

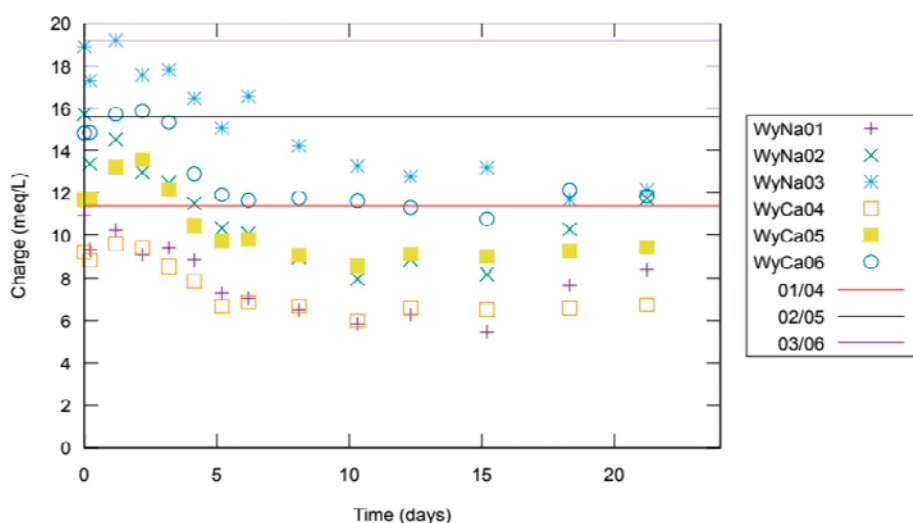


Figure 4-2. Evolution of cation charge during the first stage in all six tests. The lines show the nominal amount of external cation charge in each experiment.

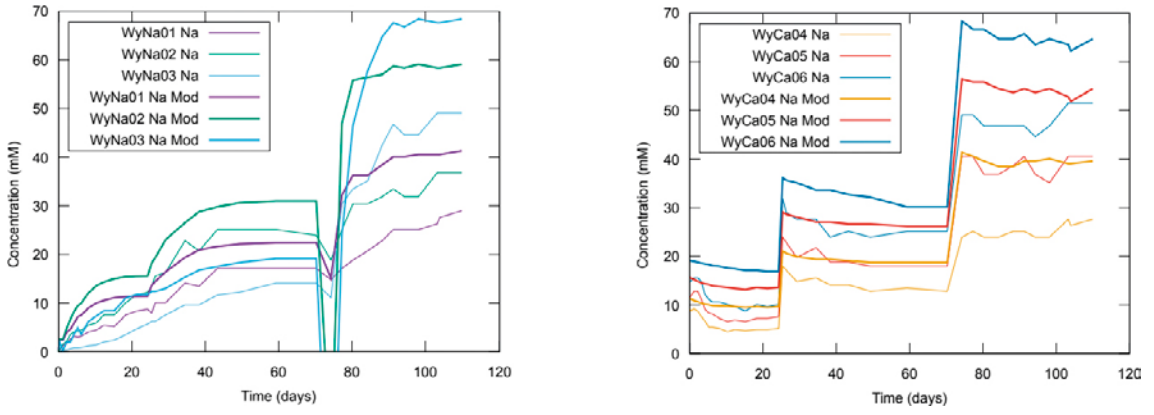


Figure 4-3. Evolution of sodium concentration in all tests. The thick lines show the modified Na concentration, obtained from Equation 4-1.

4.2 Treated as a pure diffusion process

Analogous to the treatment of Benchmark 1, we start by considering a pure diffusion process, assuming that the montmorillonite sample is a homogeneous domain with diffusion coefficient D_c . In this case the boundary condition becomes more complicated to handle, as the amount of ions in the external solution is comparable to the amount of ions in the clay. The boundary concentrations can thus not be treated as constant and the condition is rather written as

$$\frac{dC(0)}{dt} = -A \cdot \phi \cdot D_c V_{sol} \frac{dC(0)}{dx} \quad (4-2)$$

Where $C(0)$ denotes the concentration in the clay domain at the interface to the external solution, A is the cross section area for the sample, ϕ the sample porosity, and V_{sol} the volume of the external solution. This equation simply states the conservation of mass at the boundary (a change in concentration of the reservoir is caused only by diffusion in or out of it).

The time evolution of the total amount of ions which has entered the domain ($M(t)$) can be expressed in analytic form (Crank 1975).

$$\frac{M(t)}{M(\infty)} = 1 - \sum_{n=1}^{\infty} \frac{2\alpha(1+\alpha)}{1+\alpha+\alpha^2 q_n^2} e^{-D_c t / l^2 \cdot q_n^2} \quad (4-3)$$

with

$$\alpha = \frac{V_{sol}}{V_{clay} \cdot \phi \cdot K} \quad (4-4)$$

where V_{clay} is the volume of the clay sample, $M(\infty)$ is the amount of ions which has entered the domain at equilibrium, q_n are solutions to the equation $\tan q_n = -\alpha q_n$, and K relates the concentration in the domain at the interface to the concentration in the external solution as

$$C_{ext} = K \cdot C(0) \quad (4-5)$$

The parameter K thus allows for a concentration discontinuity at the interface. Further, $M(\infty)$ can be shown to be

$$M(\infty) = M_{tot} \frac{1}{1 + \alpha} \quad (4-6)$$

where M_{tot} is the total amount of ions initially in the external solution.

Comparing the results of this pure diffusion model with the experimental observations, several insights can be made. Equation 4-6 show, for example, that if the clay simply functioned as a passive container for the in-diffusion ions (implying concentration continuity at the interface between solution and clay, i.e $K=1$), the equilibrium concentration in the external solution would differ only slightly from its initial value, because its volume is much larger than the total pore volume of the clay. For the present tests, $V_{sol} = 100 \text{ ml}$, $V_{clay} = 4.8 \text{ ml}$, and $\phi \approx 0.5$, which gives $\alpha \approx 40$, and $M(\infty)/M_{tot} \approx 0.025$, if $K=1$. The fact that the equilibrium concentration is much smaller than initial concentration – especially in the case of exposing a Na-montmorillonite to CaCl_2 solutions – thus tells us that the clay functions in a more complicated manner than simply as a passive vessel. Differently put, if the behavior should be explained as a pure diffusion process requires the parameter K to be much larger than unity.

Equation 4-6 can be used to determine α experimentally from measured concentrations

$$\alpha = \frac{M(tot)}{M(\infty)} - 1 = \frac{C_{ext}(0) \cdot V_{sol}}{(C_{ext}(0) - C_{ext}(\infty)) \cdot V_{sol}} - 1 = \frac{C_{ext}(\infty)}{C_{ext}(0) - C_{ext}(\infty)} \quad (4-7)$$

where $C_{ext}(0)$ and $C_{ext}(\infty)$ respectively denotes the initial and equilibrium concentration in the external solution. Combining the empirically estimated α -values with Equation 4-4, gives an empirical estimation of the values of K . Using the calcium concentration data in the first stage of tests on samples WyNa01, WyNa02, and WyNa03, gives $K=17\,726$, $K=26\,741$, and $K=34\,576$, respectively.

Next, it is interesting to look at the expected time scale of the equilibration process described by the present model. Figure 4-4 shows Equation 4-3 plotted using $\alpha = 0.1111$ (corresponding to K in the range 300–400). It is noted that the equilibration process is expected to be finished very quickly, using a reasonable value of the diffusion coefficient (the diffusion coefficient is estimated to be in the range $10^{-11}\text{--}10^{-10} \text{ m}^2/\text{s}$, as inferred in Chapters 2 and 3). This is in contrast to the experimental results which reveal equilibration times of 10–40 days.

Evidently, something is not accounted for in the model which is influential for the observed processes. A strong candidate is the filters which are sandwiching the montmorillonite sample; if their transport resistance is non-negligible, the equilibration process will be prolonged. Indeed, since we concluded from the equilibrium states that the values of K are very large, it is expected that the filters will limit the overall transport capacity, since they are required to maintain the very large concentration discontinuity at the clay interface.

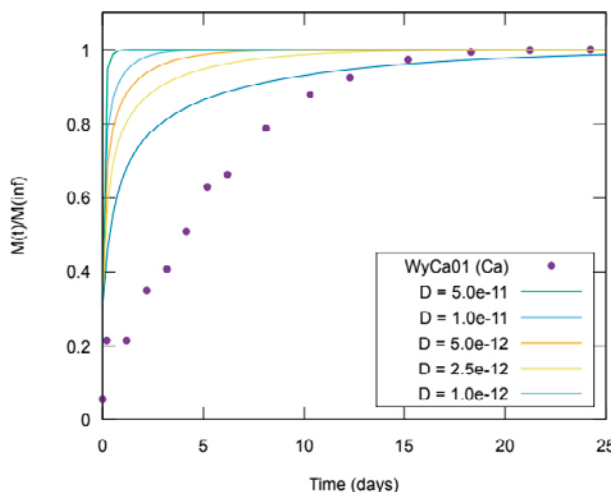


Figure 4-4. $M(t)/M(\infty)$ using the three first terms in Equation 4-3, and $\alpha = 0.1111$ for various values of the diffusion coefficient. The dots show actual experimental data.

4.3 Homogeneous mixture model

It should come as no surprise that there appears to be a huge discontinuity in the ion concentration profiles, across the interface between clay and external solution. This is expected due to the presence of an electrostatic potential difference between a bulk solution and interlayer pores. In contrast to excess salt (which is controlled by the anion, see Chapters 2 and 3), cation concentrations are enhanced in the interlayers since the electrostatic potential is lowered in comparison to the bulk solution, as shown in Figure 4-5 (as a matter of fact, also the CaCl^+ species (Equation 2-14) shows this behavior)

In this section, Benchmark 3 is modeled using the CT code, treating the clay as a single diffusive interlayer domain, and accounting for ion equilibrium at interfaces to external solutions, in the same fashion as for Benchmarks 1 and 2 (Chapters 2 and 3). Since the behavior of these tests is completely governed by the (major) cations, no speciation calculations are performed, and the only aqueous species included are Na^+ , Ca^{2+} , and Cl^- .

4.3.1 Model details

The schematics of the model are the same as for Benchmark 1, as illustrated in Figure 4-6. In this case it is critical to include the filters, since these are expected to limit the mass transfer between the reservoir and the clay. Furthermore, due to the more elaborate boundary conditions it is important to include the correct volume of the external solutions in this case. Note that although the experiment only has a single external solution (100 ml) which is circulated over both filters, the model has two separate solutions (of half the volume, i.e. 50 ml).

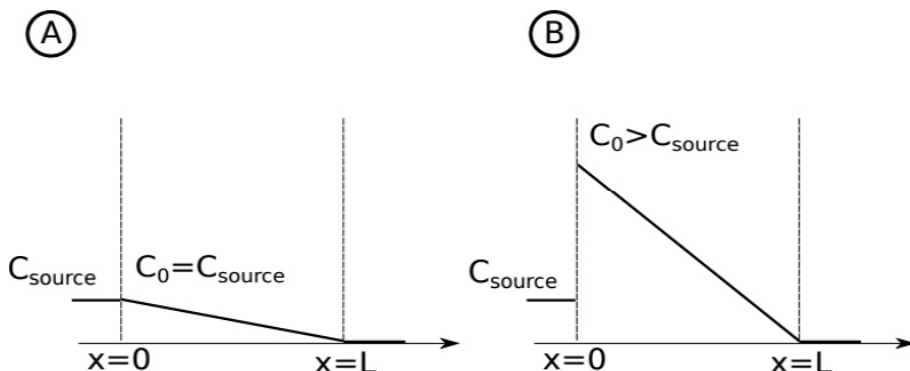


Figure 4-5. A) Steady-state profile of a conventional porous system: The concentration varies continuously (i.e without disruption) across borders to external solutions. B) Steady-state profile in the homogeneous mixture model for a cationic species. Cf. Figure 2-5.

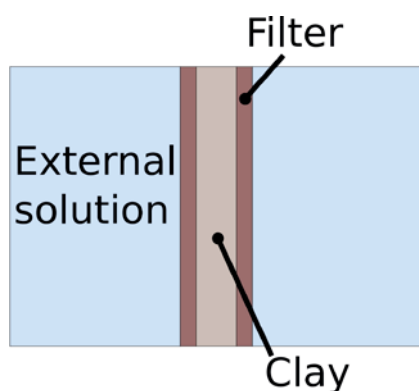


Figure 4-6. Schematics of the implemented model.

The current limitation of the CT code of treating interlayer activity coefficients as constants pose a problem in this case, because the interlayer ionic strength is expected to vary quite substantially during the course of the tests, at least when exposing initially pure Na-montmorillonite samples to CaCl₂ solutions. In these systems the clay evolves from having only sodium in the interlayers to a state strongly dominated by calcium. Due to the higher valency of the calcium ion, the interlayer ionic strength varies accordingly. For a Ca/Na-system at low external concentration, the interlayer ionic strength is given by (see further Birgersson 2017)

$$I_{IL} = c_{IL} \left(1 + \frac{X}{2} \right) \quad (4-8)$$

where X is the calcium charge fraction.

The strategy followed here is to use as constant activity coefficients the values obtained by the mean salt method for the interlayer ionic strength of the final state of all the tests. In all cases, the final states correspond roughly to having ~ 80 % calcium in the interlayers (X ≈ 0.8), thus giving a final interlayer ionic strength of

$$I_{IL} = 1.4 \cdot c_{IL} \quad (4-9)$$

The corresponding mean salt interlayer activity coefficients for sodium and calcium used in all the simulations are listed in Table 4-1 together with other material parameters.

The choice for activity coefficients for chloride in these tests have basically no influence on the result and is here put equal to 0.811 in external solutions and 0.573 in interlayer solutions, respectively, in all simulations.

The homogeneous mixture model gives a direct relationship between ion exchange selectivity coefficients and the corresponding interlayer activity coefficients for the involved cations, as thoroughly discussed in Birgersson (2017). In the case of Ca/Na exchange the relation valid at low external concentration reads

$$K_{GT} = 2 \cdot c_{IL} \cdot \frac{(\gamma_{Na}^{int})^2}{\gamma_{Ca}^{int}} \quad (4-10)$$

The chosen values of interlayer activity coefficients for sodium and calcium thus directly give a corresponding value of the selectivity coefficients. These are also listed in Table 4-1.

The diffusion coefficient of the clay domain was put equal to 5 × 10⁻¹¹ m²/s in all samples, since the experiments gives very little information on this quantity since the time evolution of the process is completely controlled by the filter diffusivity, as discovered in Section 4.2. The filter diffusion coefficient was fitted in each simulation, with the values listed in Table 4-1 (the same value was used for both filters in the set-up).

The filter length is 2 mm in all simulations, and the length of the clay sample is 5 mm.

Table 4-1. Adopted material parameters in the simulation of the Benchmark 3 tests. Porosity and length were taken from Birgersson (2011). Assuming a cation exchange capacity of 0.875 eq/kg. Unit for c_{IL} is mol/kgw, unit for γ is kgw/mol, and unit for D_f is m²/s.

Sample	c _{IL}	ϕ _c	γ _{Ca} ^{int}	γ _{Na} ^{int}	γ _{Ca} ^{ext}	γ _{Na} ^{ext}	K _{GT}	D _f
WyNa01	1 386	0.649	0.281	0.774	0.485	0.820	5.9	7 × 10 ⁻¹⁰
WyNa02	2 148	0.544	0.377	0.897	0.446	0.800	9.2	7 × 10 ⁻¹⁰
WyNa03	3 217	0.440	0.656	1.169	0.423	0.787	13.4	2 × 10 ⁻¹⁰
WyCa04	1 604	0.617	0.300	0.800	0.486	0.820	6.8	4 × 10 ⁻¹⁰
WyCa05	2 304	0.529	0.401	0.934	0.448	0.802	9.8	3 × 10 ⁻¹⁰
WyCa06	3 242	0.440	0.656	1.169	0.426	0.789	13.5	1 × 10 ⁻¹⁰

4.3.2 Results

Figure 4-7 compares the modeled evolution of the external calcium and sodium concentrations with the experimental results for all six tests. Note that in sample WyNa03, only one switch of solutions was performed, adding directly an amount of CaCl_2 so that the total amount added corresponds to 100 % of the montmorillonite charge.

Figure 4-7 shows that the homogeneous mixture model is capable of reproducing the Benchmark 3 results. In all three cases, the final calcium concentrations in the simulations are higher than the corresponding measurements (with the opposite trend for sodium). This difference indicates that the selectivity coefficients of the simulations are too low. Note, however, that the selectivity coefficients in the simulations are quite large as compared to some values often used in reactive transport calculations. The often cited reference of Bradbury and Baeyens (2002), for instance, reports $K_{\text{GT}} = 2.6$ for “MX-80” bentonite, while here the largest value is 13.5 (for WyCa06, see Table 4-1). Thus, although the current experiments suffer from some inconsistencies regarding the measured ion concentrations (Section 4.1), they certainly indicate that often cited values of selectivity coefficients may be quite far from representing “true” values. The issue of treating the ion exchange processes adequately in these types of simulations is of course very important and can only be resolved by performing more detailed and systematic experiments.

Note that the selectivity coefficients in these simulations were derived using Equation 4-10 and mean salt values for activity coefficients. Alternatively, the activity coefficients could have been adjusted to fit the model better to the experimental data. Apart from demonstrating that the model can reproduce the experimental behavior, such a procedure would however not give more useful information, both because the model anyway suffers from treating the activity coefficients as constants, and because of the evident uncertainty in the experimental results.

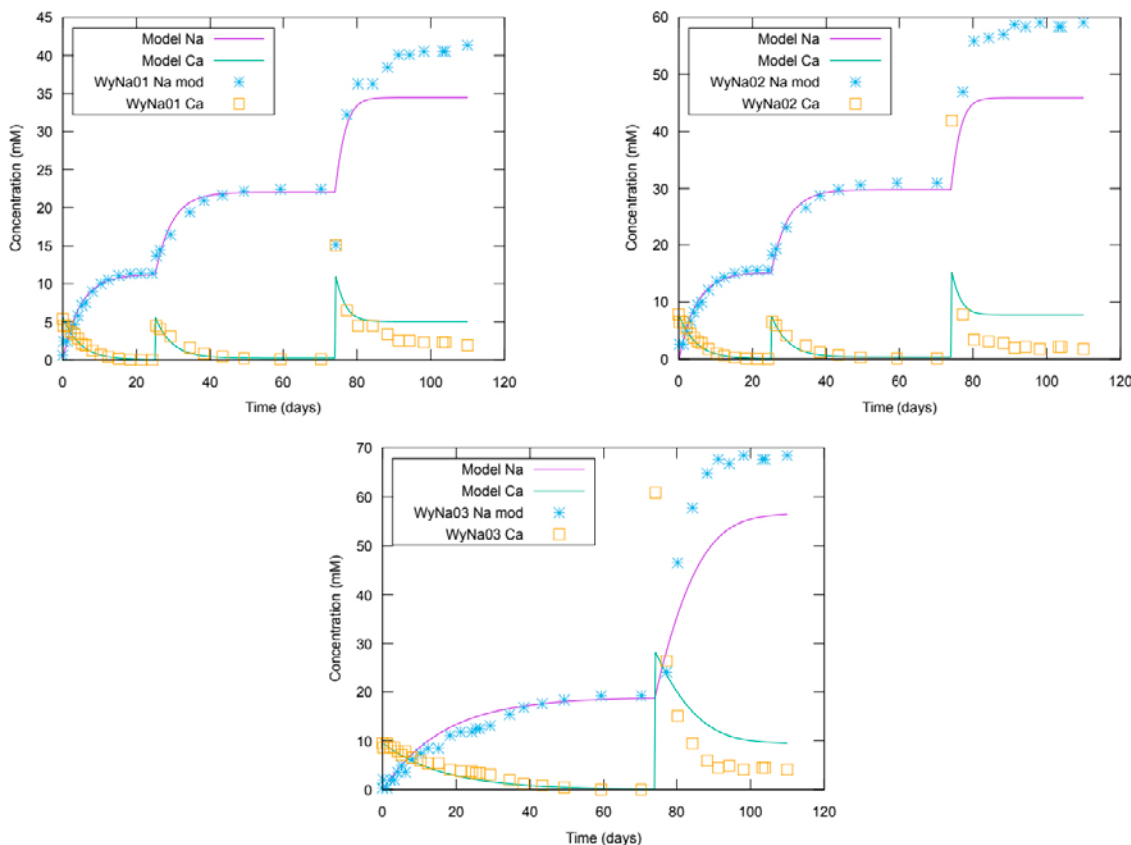


Figure 4-7. Results of modeling the systems where initially pure Na-montmorillonite was contacted with CaCl_2 solutions.

Figure 4-8 shows the results of the model for test WyNa01 when varying the filter porosity variable for the filters. It is evident that the results are highly sensitive to changes in this parameter. This result confirms what was concluded in Section 4.2: the exchange process in these tests is fully controlled by the transport capacity in the filters.

This conclusion is further confirmed in Figure 4-9, which shows the results of the model for test WyNa01 when varying the diffusion coefficient of the clay component. Basically no difference is seen when increasing the base case value by an order of magnitude, which indicates that the clay has basically infinite transport capacity as compared to the filters. Note that the clay *diffusivity* is nevertheless lower than the filter diffusivity; the large transport capacity is due to the enhanced cation concentration in the clay (Figure 4-5). This behavior is completely analogous to what is observed in many cation tracer through-diffusion tests performed at low background concentration (Glaus et al. 2007, Tachi and Yotsuji 2014), as further discussed in Birgersson and Karnland (2009).

Lowering the diffusion coefficient by an order of magnitude gives a small change in behavior, while larger deviations are only observed if the diffusion coefficient is made as small as $5 \times 10^{-13} \text{ m}^2/\text{s}$.

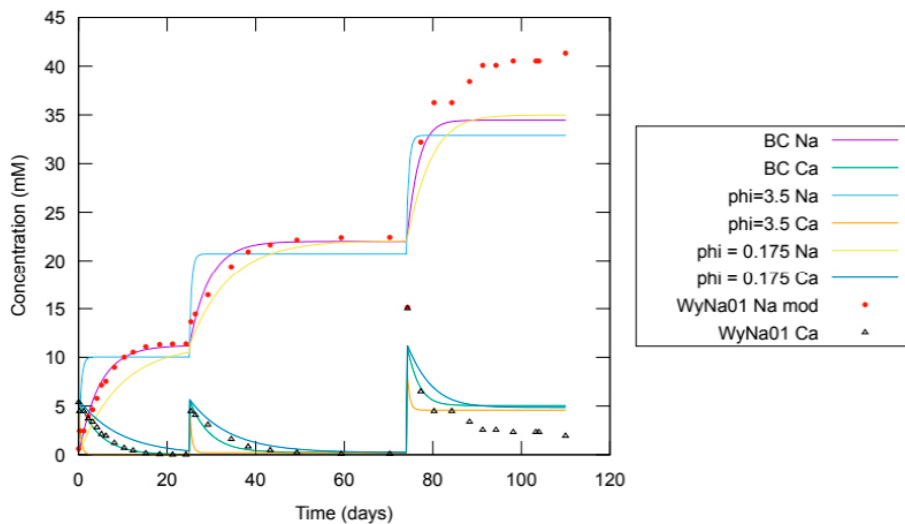


Figure 4-8. Simulations of system WyNa01 with different transport capacity of the filters. For numerical reasons, the filter transport capacity was altered by varying its porosity. In the base case (BC) the porosity is 0.3, in the other two simulations it is put equal to 0.175 (i.e. halved) and 3.5 (i.e increased by more than an order of magnitude). Although a porosity of 3.5 is physically impossible, there is no restriction in the code for using such a value.

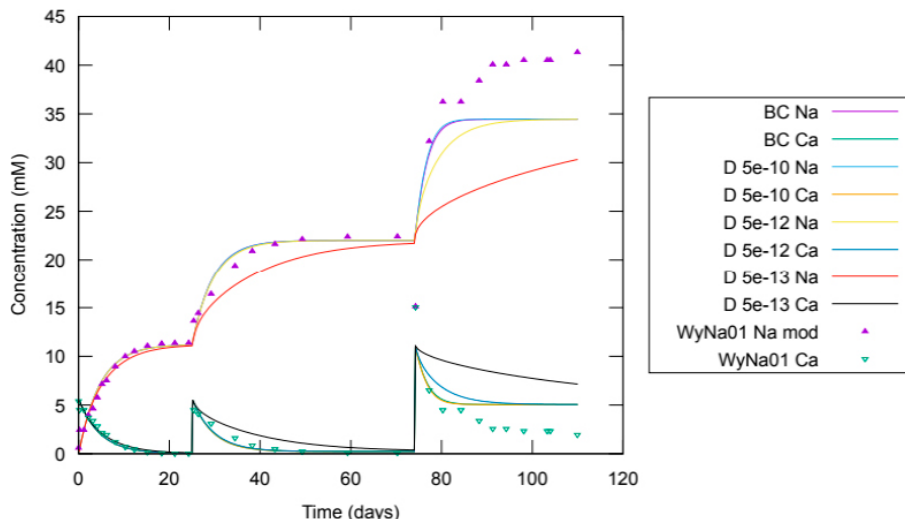


Figure 4-9. Simulations of system WyNa01 with different diffusion coefficients in the clay domain (D).

Figure 4-10 shows the results of the simulations of the systems where initially pure Ca-montmorillonite is contacted with NaCl solutions. As in the previous case, the modeled calcium concentrations are generally larger than the measured values, indicating a too low selectivity coefficient.

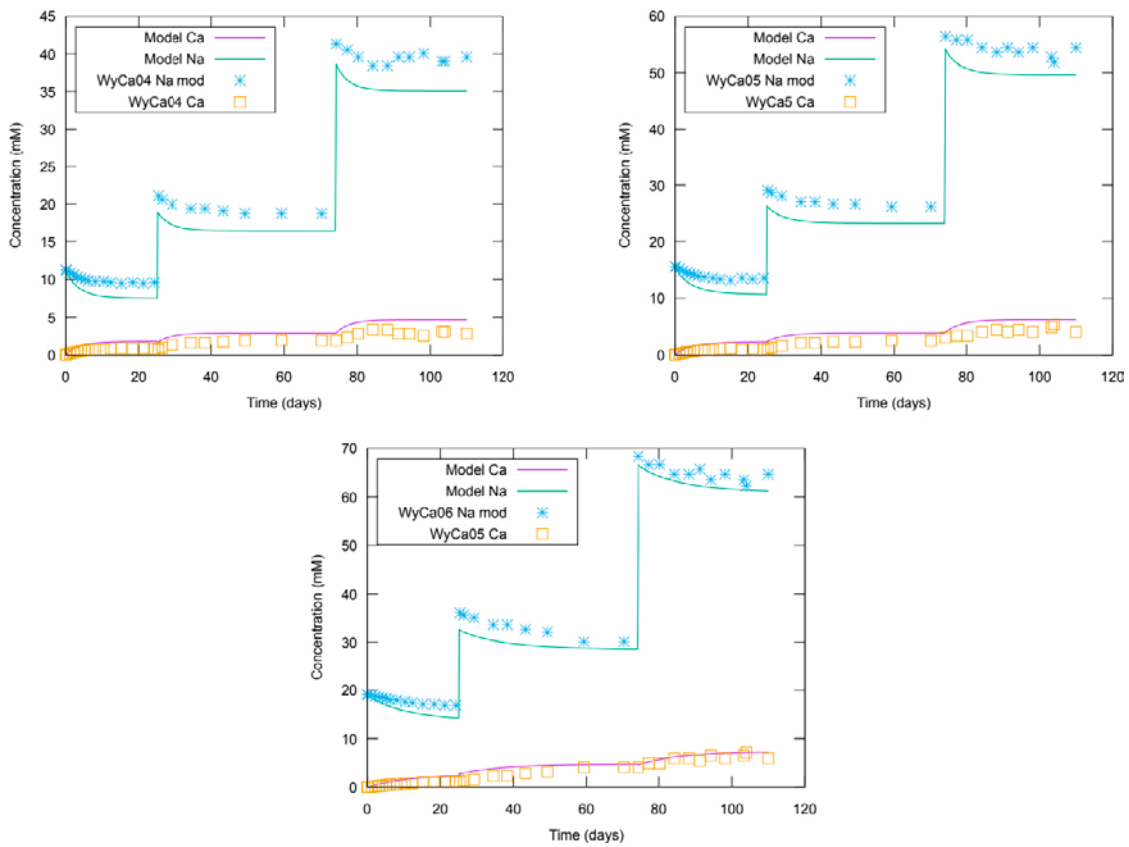


Figure 4-10. Results of modeling the systems where initially pure Ca-montmorillonite is contacted with NaCl solutions.

5 Benchmark 4

Benchmark 4 concerns data from a core infiltration test performed by University of Bern (Fernández et al. 2011). By applying an external pressure difference, a solution of artificial ground water was pushed through a cylindrical “MX-80” bentonite plug of diameter 50 mm and height 50 mm, confined at constant pressure (8 MPa). Samples of expelled water were collected in sequence and analyzed. The external pressure was kept in the range 5–6 MPa on the injection side, while the outflow side was non-pressurized (atmospheric absolute pressure).

The bentonite sample was prepared from material previously installed in the field test LOT A2 in Äspö Hard Rock Laboratory (Karnland et al. 2009). This means, in particular, that the material was water saturated by groundwater at the Äspö site. The solution in the infiltration test was for this reason, presumably, prepared to be similar to Äspö groundwater.

The basic data consists of simultaneously measured values of time and concentrations of a rather large set of aqueous species. Moreover, the data also comprises pressure measurements (confining pressure and injection pressure), and the volume of the solution samples.

5.1 Involved processes

5.1.1 Density response

As bentonite is a swelling material, the sample is expected to respond to the imposed pressurization by redistributing its mass, as well as changing shape and volume. The anticipated steady state configuration is schematically pictured in Figure 5-1, and can be obtained by considering the water chemical potential.

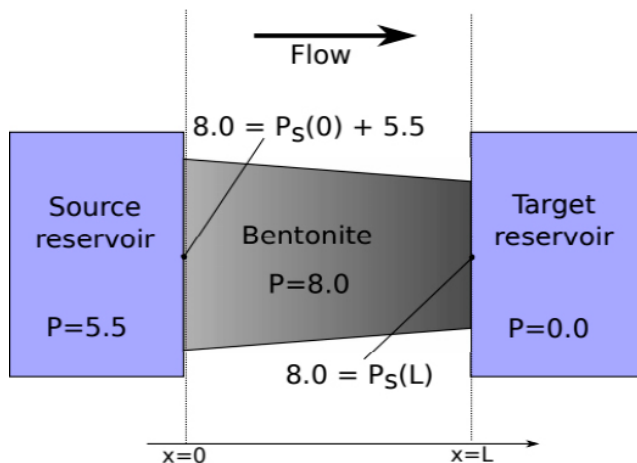


Figure 5-1. Schematics of the configuration of the bentonite plug after adjusting to the imposed pressurization. The clay body is confined at 8 MPa, while the external pressurization on the source side is (on average) 5.5 MPa. The target reservoir is non-pressurized (atmospheric absolute pressure). At the source reservoir, the boundary condition becomes $P_s(0) = 2.5$ MPa, and at the target reservoir $P_s(L) = 8.0$ MPa. Since the sample is confined at a fixed length, the sample adjusts radially; increasing its radius where P_s corresponds to a density lower than the initial density, and decreasing its radius where P_s corresponds to a higher density. The shape of the bentonite sample has been exaggerated for illustrative purposes. Note also that the volume of the target “reservoir” in the real test consists of very little water.

The water chemical potential within the clay depends on both pressure and density and can be written in terms of a function P_s (Birgersson et al. 2008)

$$\mu = \mu_0 + (P - P_s(w)) \cdot v \quad (5-1)$$

where μ_0 is a reference potential corresponding in this case to the infiltrating bulk solution at atmospheric pressure, and v denotes molar volume of water. The function $P_s(w)$ – here expressed in terms of the water-to-solid mass ratio, w – quantifies the water retention properties of the bentonite material, and can be obtained e.g. from vapor pressure measurements of unconfined bentonite, or from separate (swelling) pressure measurements. The water chemical potential in the external compartments (separated from the clay by filters) is $\mu = \mu_0 + P_{ext} \cdot v$, where P_{ext} is the applied external water pressure. The requirement that the chemical potential varies continuously across interfaces to the clay thus gives

$$P_s(w_{interface}) = P - P_{ext} \quad (5-2)$$

In the present case, the confining pressure is $P = 8.0$ MPa, the average external pressure on the inflow side is $P_{ext} = 5.5$ MPa (varying between 6 and 5 MPa), while $P_{ext} = 0.0$ MPa on the outflow side. Equation 5-2 thus directly gives the values for P_s at the two interfaces (indicated by indices “in” and “out”, respectively)

$$P_s(w_{in}) = 2.5 \text{ MPa} \quad (5-3)$$

and

$$P_s(w_{out}) = 8 \text{ MPa} \quad (5-4)$$

Luckily, almost exactly these pressures were measured in the LOT A2 material using the same type of external water (Karnland et al. 2009, Table 7-1). The expected interface densities in the present test can therefore be directly inferred from those results: $w_{in} = 0.285$ (swelling pressure 8.1 MPa) and $w_{out} = 0.359$ (swelling pressure 2.6 MPa). Assuming a linear w -profile across the sample, the corresponding steady-state dry density is shown in Figure 5-2.

Note that the pressure is 8 MPa everywhere in the present case, as a constant pressure boundary condition is imposed. However, also systems confined to constant volume redistribute their mass in an external water pressure difference to such a degree that the internal pressure is basically evened out (Birgersson and Karnland 2015).

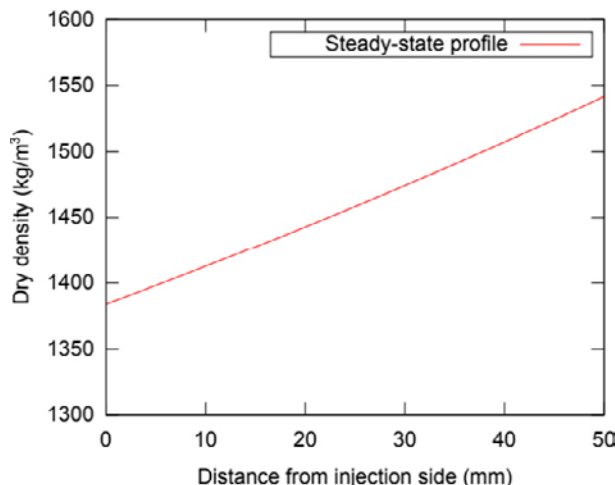


Figure 5-2. The steady-state density profile, achieved by requiring continuous variation of the water chemical potential across the clay interfaces, and assuming an injection pressure of 5.5 MPa, a confining pressure of 8.0 MPa, and a non-pressurized outlet.

An interesting question is on which time scale steady-state is established in the present experiment (or, rather, quasi-steady-state, since the injection pressure is varying slightly throughout the test). An indication is given by the response in hydraulic conductivity (Figure 5-3) during the first three weeks of the experiment, as the pressurization was increased in steps. Thus, the time it takes for the conductivity to stabilize after a pressure step gives a good indication of the times scale for establishing the steady state density profile. As is evident from Figure 5-3, this stabilization is quite quick: within a few days after the pressure changes, the effective hydraulic conductivity is stable. It can thus be assured that the system is mainly in a (quasi-)steady-state concerning density redistribution during the course of the test (which was conducted for almost a whole year).

5.1.2 Electrostatic response

The presence of a density profile implies couplings between several physical properties and mass transfer mechanisms. In particular, it implies the presence of an electrical field across the bentonite sample during the course of the test.

The easiest way to see that a density difference in a bentonite sample is necessarily accompanied by an electric field, is to consider a pure system, containing only montmorillonite particles and counter-ions. A density difference in such a system corresponds directly to a difference in counter ion concentration, which, in turn, implies diffusion of ions from high density regions to low density regions. But such type of diffusion immediately creates charge separation, and a corresponding electric field. This electric field drives an ion current in the direction opposite to the diffusive flux. In equilibrium (steady-state), the diffusive flux and the field driven flux cancel, giving zero current in the sample. Thus, in order to have vanishing electrical currents in an inhomogeneous sample, a non-zero electric field must be present.

Note that the above argumentation is completely general: External water pressure differences over a bentonite sample always induce density differences – and corresponding electrical fields – within the sample. At a most fundamental level, mechanical, hydraulic and electrical phenomena are always coupled in compacted bentonite systems. This coupling is basically never treated in chemical models of bentonite, or in so-called “THM”-models. As a consequence, many parameters in such models necessarily represent “effective” behavior, compensating for neglecting e.g. the electrostatic coupling. In particular, such a basic quantity as the hydraulic conductivity can never be fundamentally understood without taking the electrostatic coupling into account. Note, for instance, that the interlayer pressure in the present experiment is basically 8 MPa everywhere. It is thus clear that liquid transport in compacted bentonite cannot be driven primarily by pressure gradients (it is also an experimental fact that interlayer pressure gradients are basically absent in constant volume systems, see Birgersson and Karnland (2015)). This conclusion is independent of whether or not bulk water exists in compacted bentonite – interlayer water always dominates in any system of interest, and must be adequately handled.

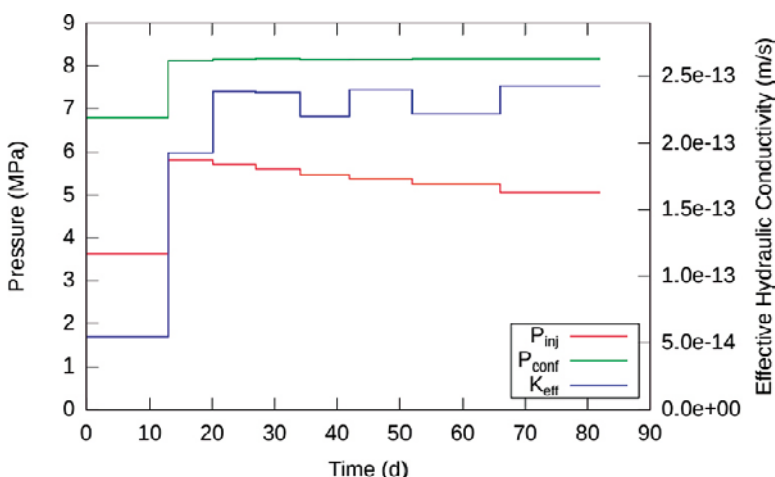


Figure 5-3. Evolution of injection (P_{inj}) and confining pressure (P_{conf}) at the beginning of the test. Also plotted is the effective hydraulic conductivity (K_{eff}), obtained by dividing the corresponding outflow with the maintained pressure difference during a given time interval. Note the slight fall-off of injection pressure, which is a consequence of how pressurization was achieved in the experiment.

In the present system, the electrostatic potential difference across the sample can be approximately calculated by considering the Boltzmann distribution, and assuming that the system contains only mono-valent cations (sodium, say). The steady-state concentration then reads

$$c(x) = c_0 \cdot e^{-F \cdot \phi(x)/RT} \quad (5-5)$$

where $\phi(x)$ is the electrostatic potential, and c_0 is a reference concentration corresponding to zero potential. As the counter-ion concentration in this case is $c(x) = \text{CEC} \cdot \rho_w/(F \cdot w(x))$ (see Equation 2-19), the potential difference over the sample can thus be estimated as

$$\Delta\phi = \frac{RT}{F} \ln \frac{c(0)}{c(L)} = \frac{RT}{F} \ln \frac{w_{out}}{w_{in}} \quad (5-6)$$

Note that the expression for the exact potential difference is more complex since it must account for that the system contains several types of counter-ions, as well as excess ions. Yet, since “MX-80” bentonite is dominated by sodium, Equation 5-6 should be a valid approximation. Inserting the values for w_{out} and w_{in} evaluated above gives $\Delta\phi = -0.23 \cdot RT/F$, i.e. approximately -6 mV at room temperature. This is an order of magnitude smaller than typical Donnan potential steps encountered in the previous modeling exercises (a Donnan potential of -60 mV corresponds roughly to a f_D -value of 0.1).

Figure 5-4 shows the full electrostatic potential profile in a model of a pure mono-valent system with the same density profile as pictured in Figure 5-2 and with external concentration 200 mM on both sides.

5.1.3 Hyperfiltration

Although the parameters used for producing Figure 5-4 have been taken to correspond with the present experiment, there is a crucial effect missing. Salt is transported by advection in the inlet channel from the source reservoir towards the bentonite interface (i.e. the inlet filter). At this interface, on the other hand, transport properties change discontinuously: as just discussed, transport within the bentonite is not simple advection governed by a pressure gradient, and, as discussed throughout this report, the ion concentrations experience a discontinuity at bulk water/bentonite interfaces. As a consequence, salt concentration build-up is expected in the filter connected on the injection side. This is a well known phenomena called hyperfiltration or reverse osmosis, and has been long studied using compacted montmorillonite as “membranes” (see e.g. Fritz 1986). At steady-state it is thus expected that the composition in the injection filter is different from the composition of the source reservoir. In particular, it is expected that the ion concentrations are elevated, and therefore that the water chemical potential is lowered in comparison to the reference (μ_0). Hyperfiltration will hence influence both the ion equilibrium at the injection side (altering the size of the Donnan potential step) as well as the mechanical equilibrium (altering the steady state density profile).

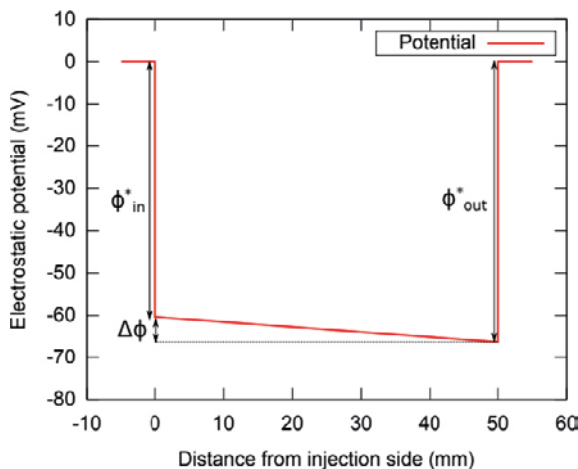


Figure 5-4. The steady-state electrostatic potential profile, in a pure mono-valent model with external concentration $C_0 = 200 \text{ mM}$ and with the same density profile as shown in Figure 5-2. The Donnan potentials at each interface are indicated (see Section 2.2.2), as well as the potential step across the sample, as given by Equation 5-6. $\phi_{in}^* = -60.3 \text{ mV}$ and $\phi_{out}^* = -66.2 \text{ mV}$.

5.1.4 Initial salt content

The LOT A2 test has been quite extensively investigated chemically, and at termination the chloride content was found to be approximately 100 mM uniformly in the parcel. The presence of this chloride is easily understood as a consequence of how the experiment was water saturated: at the start of the test all voids in the test hole (outer and inner slots, interfaces between blocks, etc.) was filled with Äspö groundwater (Karnland et al. 2009). Looking at the analysis of exchangeable cations it is revealed that the parcel only had minor interaction with external water during the test. Since the Äspö water is dominated by calcium, it would be expected that the bentonite also would be dominated by calcium if considerable exchange occurred during the course of the test. Instead, basically all sodium which was present initially in the “MX-80” bentonite was found to remain in the clay. Thus, the LOT A2 parcel basically behaved as an isolated system during the course of the test, and the chloride which was added to it initially remained there at the end of the test. From these considerations it also follows that the chloride content of the parcel at termination most probably *does not* represent an equilibrium value for the corresponding level of chloride in the Äspö groundwater.

The many issues discussed in this section, show that Benchmark 4 represents a formidable modeling task, if it should be done adequately. Moreover, it is noticed that although the experimental data is quite vast, it does not provide tests for several of the involved processes – no information is provided on e.g. density redistribution, hyperfiltration, or on possible electrostatic potential differences.

5.2 A decoupled homogeneous mixture model

The evolution of the ion concentrations on the outflow side was modeled using the CT code. Due to the considerably higher complexity of the present test as compared to the others treated in this report, and due to the limitations of this prototype code, only certain aspects of the involved processes have been included. Therefore, no mechanical couplings were treated, and the sample was assumed to have uniform density, taken to be the average of the distribution derived in the previous section, i.e. a water-to-solid mass ratio $w = 0.322$, corresponding to a dry density $\rho = 1.458 \text{ g/cm}^3$.

Moreover, with a uniform density, the electrostatic potential is uniform within the sample, and all transport is assumed to be uncoupled diffusion within the bentonite (advection in the external compartment is discussed below), where the flux of each species is simply driven by its individual concentration gradient (as a further consequence of decoupling, the diffusion coefficient is taken to be equal for all species). Due to the rather intricate pressure/potential configuration in the present experiment, it can thus be expected that the diffusion coefficient evaluated from the model represents an effective value, “compensating” for the lack of coupling.

However, as in the previous benchmark models, the electrostatic problem is treated adequately at the interfaces between external solutions and bentonite. As in the previous calculations, the bentonite is treated as a homogeneous mixture of water and montmorillonite, and the Donnan equilibrium is calculated at the interfaces (see Section 2.2.2). The schematics of the model are shown in Figure 5-5, and adopted material parameters are listed in Table 5-1.

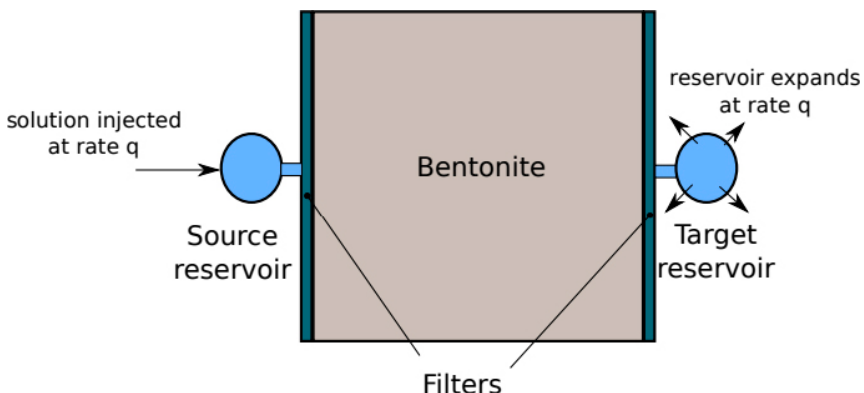


Figure 5-5. Model schematics.

Table 5-1. Material parameters.

	Filter	“MX-80” bentonite	Reservoirs
D_c (m/s ²)	7.5×10^{-10}	3.5×10^{-10}	-
Porosity (-)	0.25	0.47	1.0
c_{IL} (mmol/kgw)	0	2430	0
Length (mm)	3	50	-
Volume (cm ³)	5.9	98.2	0.491*

* The target reservoir was treated as having variable volume, corresponding to the fill-up of liquid as water flows through the system (see Figure 5-5). After each sampling event, this reservoir was reset to the volume 0.491 cm³. For the first time interval, a very low initial value was used, in order to simulate a “dry” initial reservoir.

In order to keep the computation minimal, a reduced set of aqueous species was included, listed in Table 5-2 together with adopted activity coefficients for external solutions and within the bentonite. These values were chosen by considering parameters used in the previous modeling exercises, and the species Na⁺, NaSO₄⁻, Ca²⁺, and CaSO₄⁰ are related as described by Equations 3-5 and 3-9.

In the present case, it should be noted that the external concentrations vary extensively during the course of the test, which weakens the approximation of keeping the (external) activity coefficients constant. These simulations would thus benefit from improving the code to be able handle variable activity coefficients.

Table 5-2. Included aqueous species, and adopted activity coefficients.

Species	γ^{ext}	γ^{int}
Na ⁺	0.723	0.832
Ca ²⁺	0.249	0.445
Cl ⁻	0.557	0.571
SO ₄ ²⁻	0.485	0.02
NaSO ₄ ⁻	0.723	0.1
CaSO ₄ ⁰	1.0	1.009
D ₂ O	1.0	1.0

The advective character of the boundary conditions is taken into account in the model, as shown schematically in Figure 5-5: During each time step, the source reservoir is “replenished” with injection solution at a specified rate q (m³/s). At the same time the volume of the target reservoir is changing by the rate q. By using these boundary conditions, the effect of advection on boundary concentrations, as well as the way sampling was performed in the experiment, are taken into account although explicit water transport is not considered. The specification of the injection solution was taken from the description of the experiment and is given in Table 5-3, which also shows the initial concentrations in the bentonite.

Table 5-3. Ion content of the injection solution and the bentonite in the model. Unit is mM. The specification of the injection solution was taken from Fernández et al. (2011).

Ion	Injection solution	Initial content in bentonite
Na	96.54	1 681.26
Ca	58.3	435.77
Cl	209	120.0
SO ₄	2.07	1.4**
D ₂ O	1.0*	0.0

* The D₂O concentration does not correspond to what was used in the experiment. Since this species functions as a completely inert tracer, its absolute concentration value is however of no concern.

** This value is not very relevant, since the model contains gypsum. The sulfate concentration is therefore quickly adjusted to a value corresponding to equilibrium with this mineral.

The model was executed in 18 time intervals, corresponding to each time a sampling was made in the experiment. At the beginning of a time interval, the target reservoir volume is reduced to its initial value (0.491 ml). This treatment simulates the sampling procedure quite adequately, as substantial amounts of solution are removed from the system in discrete steps. Note that this way of performing the sampling influences the result, in the sense that the chemical interface equilibrium evolves differently from e.g. the case where the entire percolated water volume is kept in contact with the clay sample during the entire test. The end times of the 18 time intervals are days 13, 20, 27, 34, 42, 52, 66, 82, 97, 110, 120, 151, 185, 224, 241, 264, 305, and 315. In all time intervals except for the first, the flow rate is kept at $q = 4.12 \times 10^{-12} \text{ m}^3/\text{s}$. The first interval instead uses $q = 0.88 \times 10^{-12} \text{ m}^3/\text{s}$.

Gypsum is initially present in the model and allowed to dissolve in accordance with the description given in Chapter 3. The gypsum was assumed initially uniformly distributed within the sample, at the level 1 % of dry mass.

5.3 Results

Figure 5-6 shows the resulting evolution of sodium, chloride and deuterium, and compares it with the experimental measurements. Given the crude state of the model, the agreement is quite astonishing. Although far from perfect, some of the breakthrough behavior of D_2O is captured by the model. It should be kept in mind that no advective processes have been accounted for in the model. This resemblance suggests that transport processes in compacted bentonite to a large extent behave “diffusion-like” even when the external conditions are highly advective (the flow velocity in the inlet tube is approximately 0.8 m/day). A similar observation was made in the modeling of Benchmark 1, where it was noted that salt diffuses with basically the same diffusion coefficient although very different external conditions are imposed (see Section 2.1.2).

Even more rewarding is the resemblance in behavior between model and experiment for chloride and sodium. Although the absolute concentration level of sodium is a bit higher than what is given by the model, quite a lot of the qualitative behavior is satisfactorily captured. In particular, the model reproduces the initial peak seen for these two species. And while chloride quite quickly reaches a steady-state, the sodium concentration keeps on declining during the course of the test.

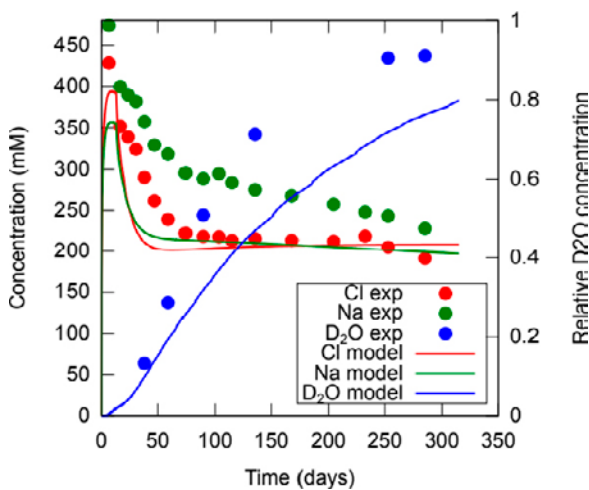


Figure 5-6. Modeled outflow concentrations of sodium, chloride and D_2O (lines) compared with the experimental results.

The initial NaCl peak is easily understood in terms of ion equilibrium: Since the sample contains a substantial amount of chloride initially, this chloride (together with mainly sodium) quickly establishes ion equilibrium across the outlet interface as soon as it gets an opportunity. This equilibrium is such that the initial internal (sodium)chloride concentration is in equilibrium with an external concentration of approximately 400–450 mM. Note that this concentration is considerably higher than the chloride concentration in the Äspö groundwater (~200 mM). It is thus confirmed that the chloride in the A2 parcel had not equilibrated during the course of the LOT field test. This type of behavior basically comes out automatically in a model based on ion equilibrium, while some rather contrived mechanism must be suggested if it should be explained using concepts such as e.g. “effective porosity”.

Figure 5-7 shows the simulated chloride concentration profiles through the system at the end of some of the time intervals. This picture clearly demonstrates the ion equilibrium mechanism at play at the outlet. Initially a high chloride concentration appears on the external side, but this concentration drops as the initial chloride is flushed out of the sample and the internal concentration level lowers. At the same time hyperfiltration occurs at the inlet interface. Here the external concentration continues to rise as salt accumulates in the inlet filter, since bentonite poses a hindrance for the salt transport. This concentration build-up leads to the establishment of an internal concentration gradient which is what drives the steady-state diffusive flux. It is very satisfying that the present model captures the mechanism of hyperfiltration – although there are no measurements to support that the effect occurs in the present test, it is expected based on earlier knowledge (Fritz 1986).

The evolution of calcium and sulfate at the outlet is shown in Figure 5-8, and compared with experimental data. Note that the model has excluded magnesium, and treats all di-valent ions as calcium. For this reason, the model is compared with the sum of experimentally measured concentrations for calcium and magnesium. Although the absolute levels of both calcium and sulfate concentrations are lower than measured, the quantitative behavior of the concentration evolution is reproduced for both ions. The peak seen for calcium/magnesium complies well with the interpretation made earlier: these are cations accompanying chloride which is being flushed out of the sample. The main cation accompanying chloride is of course sodium (the sodium level is roughly an order of magnitude higher than the calcium level), but depending on the details of the chemical environment, a certain amount of di-valent ions should be present. The details of this sodium/calcium ratio depend e.g. on the exact amount of each ion initially present in the system (which is a bit uncertain here), as well as on the relation between the interlayer activity coefficients for these ions (i.e. basically the selectivity coefficient for the Ca/Na, see Chapter 4).

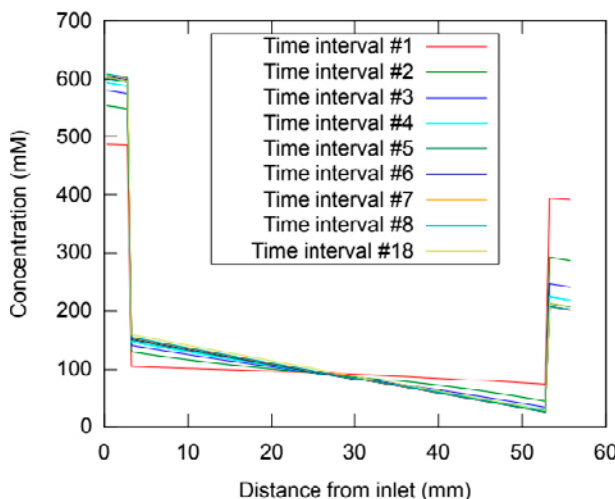


Figure 5-7. Chloride concentration profiles across the system (filters and clay) at various times in the simulation.

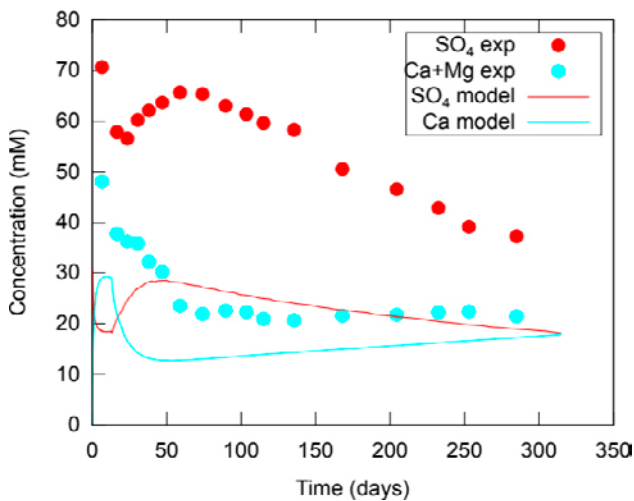


Figure 5-8. Modeled outflow concentrations of sulfate and calcium (lines) compared with the experimental results.

Note how the slope of the model curve agrees well with the slope of the increasing calcium concentration during the latter part of the test. The calcium concentration in the injection solution is approximately 60 mM, showing that calcium is far from steady-state also at the end of the test (this is also true for sodium). What is happening during this stage is a slow conversion of the bentonite plug from a sodium dominated (“MX-80”) to a more calcium dominated clay. Judging from the slope of the calcium concentration curve, such a process would take several years to complete.

The absolute level of the modeled sulfate concentration is considerably lower than what is measured. This mismatch certainly reflects details on how gypsum dissolves within the clay body (see also Chapter 3), e.g. the value of several interlayer activity coefficients as well as on the detailed concentration level of calcium within the clay. However, it is very interesting that the modeled evolution displays the same kind of “wiggle” as is seen in the experimental data. Based on the knowledge on the chloride evolution, this “wiggle” is now easily explained: it occurs because as chloride is flushed out, the ionic strength – and hence, the Donnan factor – decreases in the initial stage of the test. This means that *more* sulfate is distributed in the external compartment, giving a temporary rise before it continues to drop again. Note that, without such an ion equilibrium effect one would expect the sulfate concentration to decrease monotonically, since gypsum is systematically depleted farther and farther away from the interface. Actually, it is difficult to even come up with a suggestion of what could cause this kind of “wiggle” if it is not an effect of a changing Donnan potential.

The evolution of the sulfate concentration profile in the clay is shown in Figure 5-9. Here the ion equilibrium effect on the external concentration on the outlet side is nicely illustrated: the internal concentration of sulfate declines monotonically, both because gypsum is being depleted (seen as a kink in the otherwise very flat profile), and because solubility is slowly decreasing due to the conversion towards a more calcium dominated clay. On the outside, however, the concentration first lowers but then increases because the chemical conditions are changing here (chloride is lost). When the chemical conditions become more stable, the sulfate level again begins to slowly decline on the outside. Note that the present model predicts depletion of gypsum in approximately the first centimeter of the sample at the end of the test.

Figure 5-10 shows the evolution of the calcium content in the system. Not surprisingly, the profiles are rather flat. The slow conversion of the clay plug to a calcium dominated system thus occurs rather uniformly.

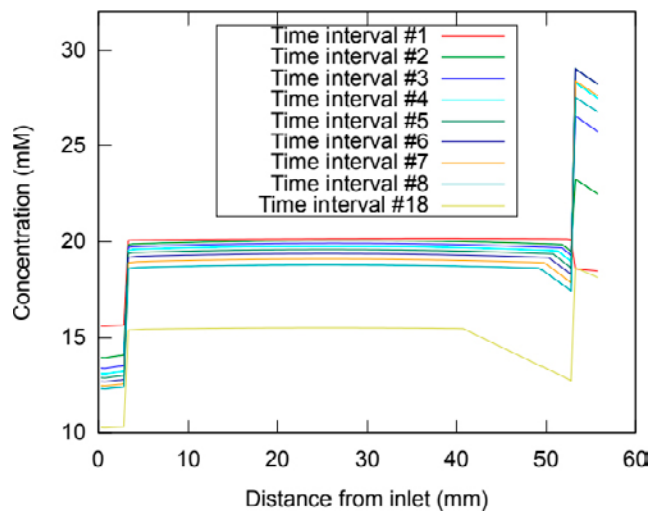


Figure 5-9. Sulfate ($\text{CaSO}_4^0 + \text{NaSO}_4^- + \text{SO}_4^{2-}$) concentration profiles across the system (filters and clay) at various times in the simulation.

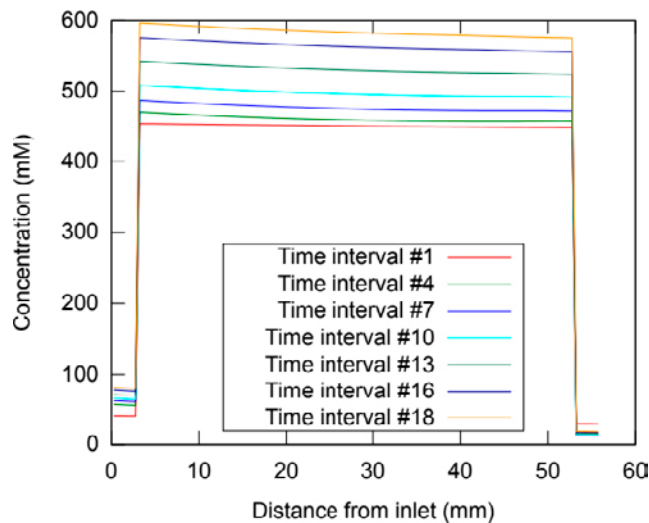


Figure 5-10. Calcium concentration profiles across the system (filters and clay) at various times in the simulation.

6 Benchmark 5

The data of Benchmark 5 origins from a large set of through-diffusion experiments performed on “B75” bentonite (Hofmanová and Cervinka, 2014²). “B75” is a commercial product produced by “partial” sodium activation of raw calcium/magnesium bentonite from the Rokle deposit in Czech Republic.

The experimental set-up is similar to the experiments treated in Chapter 2 in this report (Benchmark 1). In contrast to those experiments, however, the Benchmark 5 tests were conducted in a background electrolyte of either 0.1 M NaCl or 0.1 M NaNO₃ (depending on which salt was considered for diffusion). Several tests were conducted by adding to the source reservoir 0.01 M of a second sodium salt, considered for diffusion. Thus, although these tests have a small difference in concentration between source and target, the chemical conditions resemble more those of a tracer diffusion test than those of Benchmark 1 (in a sense, these *are* tracer tests). In addition, in the cases of chloride and pertechnetate diffusion, the experiments were actually carried out using radioactive tracers (³⁶Cl⁻ and ⁹⁹TcO₄⁻). Thus, for chloride and pertechnetate diffusion, the concentration was strictly the same in both reservoirs.

While the source and target reservoir concentrations are basically the same in all the conducted tests, the density of the clay samples was systematically varied (with nominal values 1300, 1450, 1600 and 1750 kg/m³ of dry density). The sample length was approximately 15 mm in all tests. The following salts were considered for diffusion:

- Na₂SeO₄ (in NaCl background)
- NaI (in NaCl background)
- NaClO₄ (in NaNO₃ background)
- Na⁹⁹TcO₄ (in NaCl background)
- Na³⁶Cl (in NaNO₃ background)

As for Benchmark 1, the present data set contains pairs of values of target concentrations and measurement times. In addition, the present data set also contains information on the concentration profile in the clay at test termination, in form of pairs of values of position (x_i) and “total” concentration (C_{tot,i}). By “total” concentration is here meant the total amount of species distributed in the total volume of the clay section (water and solids).

The “raw” benchmark data was converted to flux vs. time data in the same way as for Benchmark 1 (Chapter 2). The data for the profile at termination was converted to a concentration based on the total amount of water in each clay section (C_{pw,i}) by dividing by the porosity: C_{pw,i} = C_{tot,i}/ϕ.

Being a “natural” bentonite, the “B75” material is considerably more complex than the pure homionic montmorillonite treated in Benchmark 1; not only does it contain substantial amounts of accessory minerals, it also contains at least three different types of exchangeable cations: Mg²⁺, Ca²⁺, and Na⁺. A full chemical modeling of the systems in Benchmark 5 would thus require the inclusion of at least five major species (Mg²⁺, Ca²⁺, Na⁺, and the two anions of the source solution), which in turn may involve a quite substantial number of ion complexes.

The Benchmark 5 tests have here been modeled using the CT code, treating the clay domain as a homogeneous diffusive domain, and treating the ion equilibrium at interfaces between clay and external solutions. Due to the limitations of the CT code concerning speciation calculations, the modelings have been performed using a reduced set of involved ions.

² Hofmanová E, Cervinka R, 2014. Benchmark 5 – Diffusion of selected anions through compacted bentonite. [https://www\(skb.se/taskforceebs/memberpages/data-deliveries/](https://www(skb.se/taskforceebs/memberpages/data-deliveries/) (Data Deliverable TFC) Internal document.

6.1 Homogeneous mixture model

In order to reduce the number of species, calcium and magnesium have been treated as a single species, calcium. The relative amount of calcium and sodium in the model was taken to be 50/50 (chargewise). This choice was made simply because the clay is described as “partially” sodium activated, rather than on measurements of the actual cation population of the samples. The uncertainties in fitted parameter values, inherited from this model choice, are discussed below.

Moreover, due to lack of thermodynamic data, selenate is here treated as behaving identical to sulfate, and the thermodynamics for complex formation for sulfate in Chapter 3 is used without modification for the species NaSeO_4^- and CaSeO_4^0 .

No complexes involving chloride have been included in the simulations. Again, the main reason for this is to reduce the total number of species, but it can also be motivated by the way these experiments are conducted. Since the Donnan potential is set mainly by the background solution, the concentration reduction for the diffusing salt is not as pronounced as if it was the only substance present. The amount of complexes, on the other hand, is directly dependent on the concentration of the diffusing salt. The effect of having a relatively large amount of chloride complexes, which was noted in the tests of Benchmark 1 (Chapter 2), is therefore not expected here. The amount of chloride complexes is here estimated to be only a few percent of the total and may be neglected.

Below follows the results and specific comments for simulating diffusion of each of the specified salts.

6.1.1 Selenate

This data consists of results from four tests made at dry densities 1299, 1450, 1602, and 1746 kg/m³. Each test was run for 21 days.

With the simplifications discussed above, these experiments were modeled using six aqueous species: Na^+ , Ca^{2+} , Cl^- , SeO_4^{2-} , NaSeO_4^- , and CaSeO_4^0 . The modeling strategy was to fit a model to data by adjusting the diffusion coefficient and the interlayer activity coefficient for SeO_4^{2-} . The interlayer activity coefficients for Na^+ , Ca^{2+} , and Cl^- were chosen as the values obtained from the mean salt method (this approach was successful in modeling chloride diffusion in pure montmorillonite, see Chapter 2). The activity coefficients for CaSeO_4^0 and NaSeO_4^- were somewhat arbitrarily set equal to 1.0 and 0.07, respectively. These choices are, however, roughly motivated by that the activity coefficient for a neutral species is not expected to be especially low (it may actually be larger than unity), and by the behavior of NaSO_4^- as explored in Benchmark 2 (Section 3.3).

The source solution reservoir – of volume 60 ml – was in the experiments exchanged once a week in order to keep the boundary condition strictly at constant concentration. For numerical reasons, however, the model instead used source and target reservoirs of three times the size (180 ml), which were not exchanged. The difference in behavior from choosing this boundary condition is negligible.

The modeled outflux is compared with experiment in Figure 6-1, showing that the model can be fitted to the data. It may be noted that the experiments performed in the samples of higher density had not reached steady-state at the time of termination of the tests.

Figure 6-2 compares modeled and experimental concentration profiles at termination. The non-linear profiles in the samples of highest density confirm that these tests were not in steady-state when terminated. The information contained in the concentration profile allows for the models to be satisfactorily fitted to the data even if they have not reached steady-state at termination. This could be compared to Benchmark 1 which do not have information on the distribution within the clay and instead requires the steady-state part of the outflux evolution in order to be uniquely fitted to a two-parameter diffusion model (Section 2.1). Thus, recording the concentration profile at termination may be a way to speed up through-diffusion tests (in many systems, reaching steady-state may take quite a long time). Under any circumstance, recording the concentration profile at termination is valuable since it gives relevant information, also for systems in steady-state.

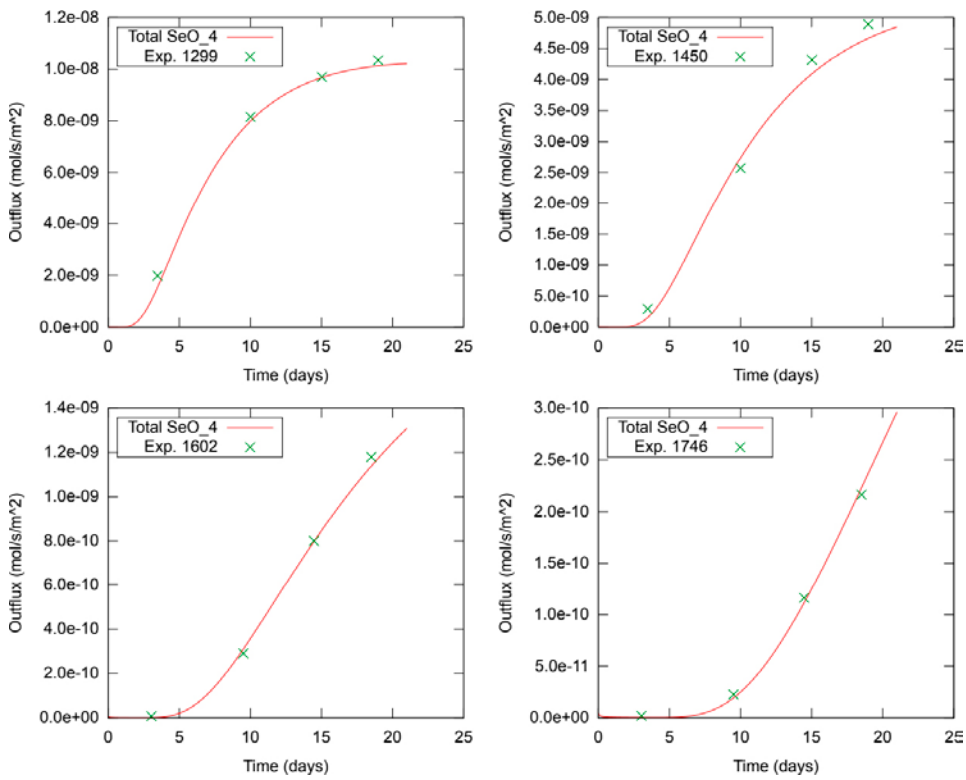


Figure 6-1. Total selenate outflux.

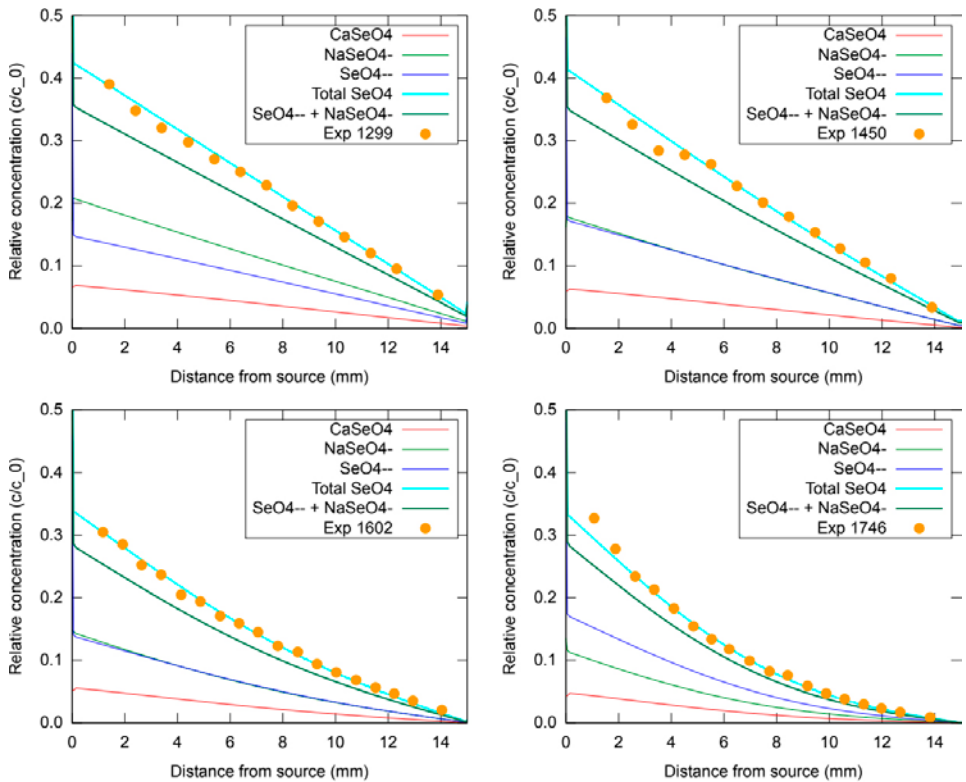


Figure 6-2. Selenate profiles at termination.

Table 6-1 shows the species concentrations at the end of each simulation at the interface between filter and clay at the source side, as well as the adopted values of activity coefficients and diffusion coefficients. The fitted values of the interlayer activity for SeO_4^{2-} are in the range 0.034–0.0075. Such very small values are in qualitative agreement with the behavior of sulfate in montmorillonite, as explored in Chapter 3 (and also in agreement with the expected behavior of sulfate in bulk solutions).

The fitted diffusion coefficients – in the range 7.0×10^{-11} – $1.2 \times 10^{-11} \text{ m}^2/\text{s}$ – are very reasonable and show a (reasonable) clear trend in decreasing with increasing density. Note that the diffusion coefficient for the system with highest density is more than five times smaller than that for the lowest density. Since the lowest density system merely reached steady-state during the 21 days of testing, it is thus expected that the high density system would have required more than 100 days to reach steady-state.

Regardless of mechanism, it is evident from the experimental data that the equilibrium concentration of selenate in the clay is substantial – in particular, it is evident that the selenate content is significantly higher than e.g. iodide, as will be discussed further in the next section. Within the homogeneous mixture model, this behavior is explained by very low values of the activity coefficients in an interlayer environment (high ionic strength).

It should, however, be noted that the exact value of the selenate activity coefficients in the present modeling is quite uncertain. As discussed above, the adopted fitting procedure assigns rather arbitrary, constant, values to the activity coefficients for CaSeO_4^0 and NaSeO_4^- , while any variation is accounted for solely in the activity coefficient for SeO_4^{2-} . It is not possible to completely determine the partition of selenate between these species given only the information contained in the benchmark data.

Since also the relative amount of di- vs. monovalent cations within the clay is quite uncertain, there is a corresponding uncertainty in the value of the Donnan potential (the Donnan potential depends strongly on this ratio, especially for low external ionic strength (Birgersson (2017))). This uncertainty, in turn, propagates to an additional uncertainty in the fitted activity coefficients. A test case with relative amount calcium/sodium of 67/33 rather than 50/50 at dry density 1 600 kg/m³, gave $\gamma_{\text{SeO}_4^{2-}} = 0.018$, i.e double the fitted value presented in Table 6-1. At the same time the Donnan factor increased from $f_D = 0.086$ to $f_D = 0.107$.

Table 6-1. Speciation in the external solution (ext.) and the clay (int.) at the filter/clay interface in the selenate/B75 system after 21 days of simulation. Concentration unit is mol/m³, unit for D_c is m²/s, and density unit is kg/m³.

ρ_d	1299		1450		1602		1746	
	ext.	int.	ext.	int.	ext.	int.	ext.	int.
[Na ⁺]	107.2	767.0	108.8	923.9	110.3	1128.2	111.7	1376.6
[Ca ²⁺]	4.1	289.2	3.7	362.2	3.2	451.2	2.7	556.1
[Cl ⁻]	99.5	18.39	99.5	15.1	99.6	11.9	99.7	9.2
[SeO ₄ ²⁻]	7.3	1.5	7.6	1.7	7.8	1.4	7.9	1.7
[NaSeO ₄ ⁻]	1.4	2.1	1.4	1.8	1.5	1.5	1.6	1.2
[CaSeO ₄ ⁰]	0.7	0.7	0.6	0.6	0.5	0.5	0.4	0.4
γ_{Na^+}	0.764	0.754	0.764	0.780	0.764	0.832	0.764	0.897
$\gamma_{\text{Ca}^{2+}}$	0.373	0.267	0.373	0.284	0.373	0.324	0.373	0.377
γ_{Cl^-}	0.767	0.578	0.755	0.573	0.755	0.568	0.755	0.568
$\gamma_{\text{SeO}_4^{2-}}$	0.347	0.034	0.347	0.02	0.347	0.0155	0.347	0.0075
$\gamma_{\text{NaSeO}_4^-}$	0.755	0.070	0.755	0.070	0.755	0.070	0.755	0.070
$\gamma_{\text{CaSeO}_4^0}$	1.000	1.000	1.000	1.000	1.000	1.000	1.000	1.000
f_D	0.142		0.115		0.090		0.069	
$\Xi_{\text{SeO}_4 \text{ TOT}}$	0.454		0.430		0.339		0.338	
D_c	7.0×10^{-11}		4.0×10^{-11}		2.1×10^{-11}		1.2×10^{-11}	

In spite of the uncertainty of the fitted activity coefficients, the main results of the simulations are very satisfying. In particular, the model naturally explains the high amount of selenate in the bentonite as an effect of low values of the activity coefficients in the interlayer pores. The same observation was made when modeling gypsum dissolution in sodium montmorillonite. It should be emphasized that these low values of the activity coefficients are expected from simple considerations of bulk solutions.

6.1.2 Iodide

The data for diffusion of (sodium) iodide consists of results from three tests performed at dry densities 1 390, 1 523, and 1 678 kg/m³, for 31, 54, and 36 days, respectively. In contrast to the selenate diffusion tests, the source reservoir was not exchanged during the course of the test, leading to a slight drop in iodide concentration with time in this reservoir. However, as the reservoir volume was large (210 ml) this only have minor effect on the diffusion process, which for all practical purposes still can be considered having a constant source.

The tests were modeled using the species Na⁺, Ca²⁺, Cl⁻, and I⁻. As for the case for selenate diffusion, the fitting strategy was to adjust the diffusion coefficient and the interlayer activity coefficient for the diffusing anion (γ_{I^-}). The activity coefficients for sodium, calcium, and chloride were set equal to their mean salt values. In contrast to the selenate case, these models contain no arbitrarily set parameters.

The modeled concentration profiles at termination are compared with measurements in Figure 6-3. The linear shape of these profiles reveals that all three systems were in (quasi-)steady-state when they were terminated. This is reasonable, as they were run for longer times as compared with the selenate diffusion tests, while the diffusion coefficients are considerably larger (in the range $2.6 \times 10^{-10} - 1.14 \times 10^{-10}$ m²/s). Moreover, the profiles of the lower density samples are seen to reach a non-zero value at the target side. This behavior indicates that the transfer resistance at the interface is not negligible in comparison with the transfer resistance of the clay samples themselves (the influence of filters is treated in detail in Birgersson and Karnland (2009)). In the models, the transfer resistance of the filters was therefore adjusted (by adjusting the filter porosity) to fit the model to data. The strategy here was to set the filter resistance once and for all in the low density sample, and then to use the same value in the other models. The adopted effective diffusivity of the filters is 3×10^{-11} m²/s.

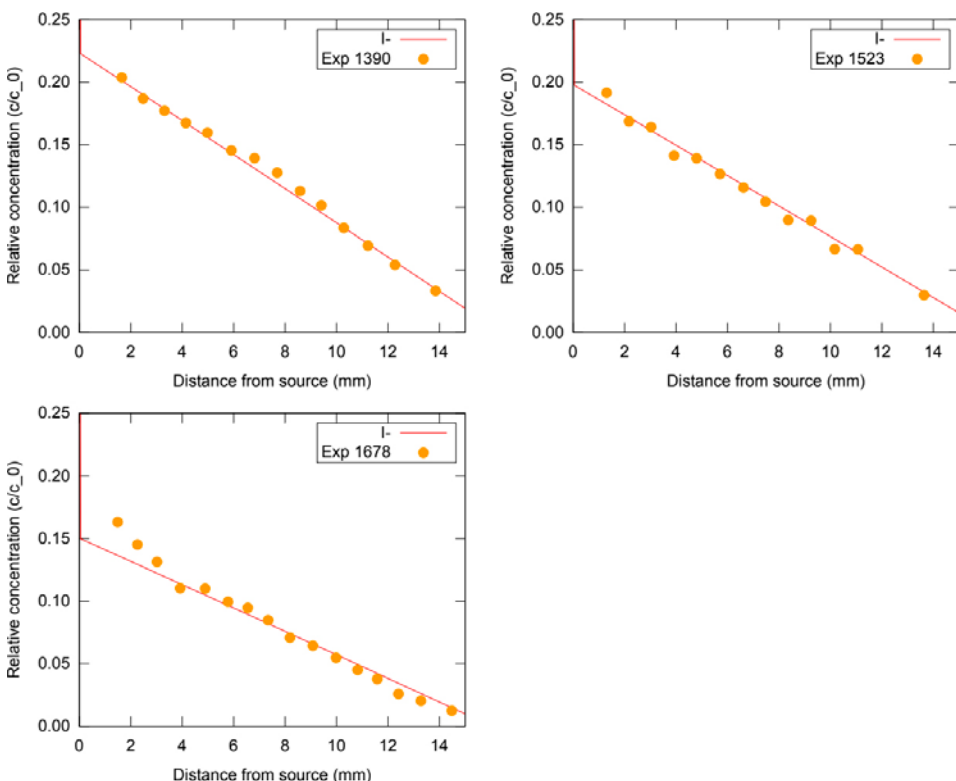


Figure 6-3. Iodide profiles at termination.

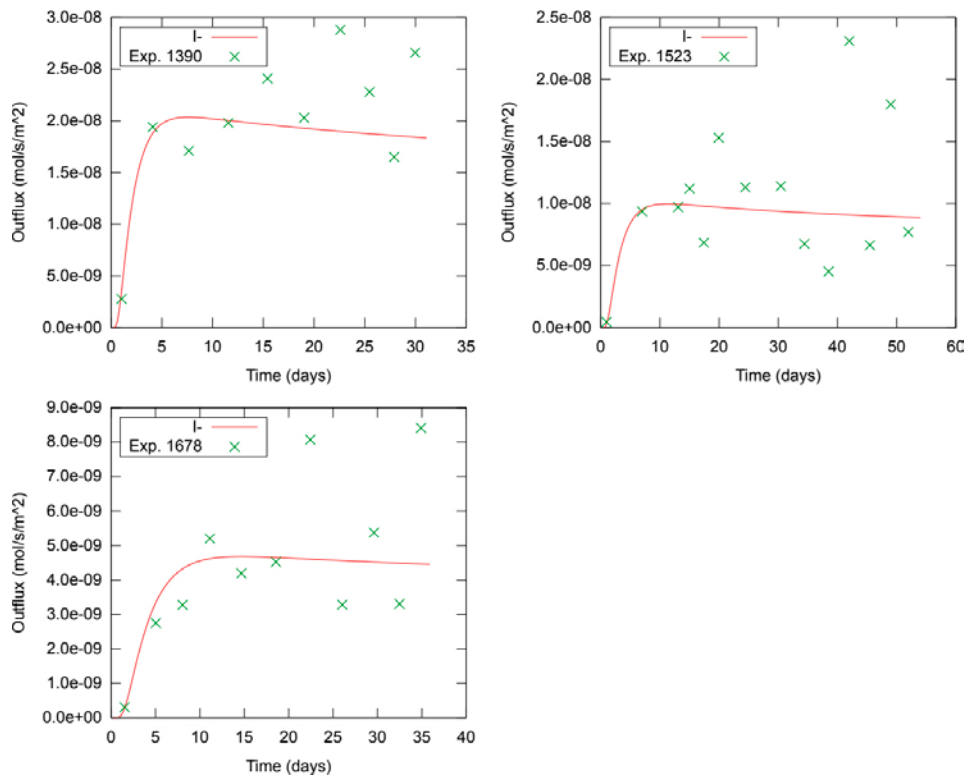


Figure 6-4. Iodide flux.

The modeled flux evolution is compared with experiment in Figure 6-4 for all three experiments. These figures confirm that all the systems were in (quasi-)steady-state at the time of termination; in fact, they all reached this state after less than 10 days. As a consequence, there is not much data in the transient phase that can be used for fitting. Thus, the diffusion coefficients are mainly fitted to the steady-state flux. Since this flux data is rather noisy, there is a corresponding uncertainty in the value for the diffusion coefficients.

Table 6-2 lists the concentrations at the filter/clay interface on the source side at termination, as well as the adopted values of activity and diffusion coefficients.

Table 6-2. Speciation in the external solution (ext.) and the clay (int.) at the filter/clay interface in the iodide/"B75" system. The system at density 1390 kg/m^3 was run for 31 days, the system at 1523 kg/m^3 for 54 days, and the system at 1678 kg/m^3 for 36 days. Concentration unit is mol/m³, unit for D_c is m²/s, and density unit is kg/m³.

ρ_d	1390		1523		1678	
	ext.	int.	ext.	int.	ext.	int.
[Na ⁺]	103.5	916.9	104.9	1117.5	105.1	1299.8
[Ca ²⁺]	2.7	298.5	2.2	351.4	2.3	480.2
[Cl ⁻]	99.6	14.8	99.7	11.7	99.8	9.3
[I ⁻]	9.4	2.2	9.6	2.0	9.8	1.5
γ_{Na^+}	0.773	0.780	0.773	0.832	0.773	0.897
$\gamma_{\text{Ca}^{2+}}$	0.387	0.284	0.387	0.324	0.387	0.377
γ_{Cl^-}	0.764	0.573	0.764	0.568	0.764	0.568
γ_{I^-}	0.764	0.36	0.764	0.325	0.764	0.350
f_D	0.112		0.087		0.070	
Ξ_{I^-}	0.237		0.205		0.152	
D_c	2.6×10^{-10}		1.55×10^{-10}		1.14×10^{-10}	

The fitted interlayer activity coefficients for iodide are very similar in all three tests, with a value around 0.35 kgw/mol. From a chemical point of view, iodide is expected to behave similar to chloride, whose mean salt value for the interlayer activity coefficient rather is ~0.57 kgw/mol at typical interlayer ionic strengths (Birgersson 2017). This apparent discrepancy may not, however, indicate that chloride and iodide behave significantly different in an interlayer environment. Instead, the low value of the evaluated iodide activity coefficient may reflect the uncertainty of the actual ratio between di- and monovalent cations in the clay (as discussed in the previous section).

Moreover, the value of an individual anion activity coefficient is correlated with the values of the cation activity coefficients (due to the requirement of charge neutrality). Thus, the rather low value of the fitted iodide coefficient may reflect that the activity coefficients for calcium or sodium deviate somewhat from the mean salt values in this system.

Disregarding the details of the exact values of the activity coefficients, the homogeneous mixture model gives a satisfying explanation for the striking experimental fact that the “B75” bentonite contains significantly more selenate than it does iodide, under basically chemically identical conditions. This finding is discussed in more detail in the following section.

6.1.3 Comparison with selenate

Even though the exact chemical state under which these tests were conducted is unknown (e.g due to lack of control of the exact cation population), it is safe to say that all the Benchmark 5 data was obtained under more or less identical conditions: both the selenate and iodide tests were conducted in a background of 0.1 M NaCl on the same type of bentonite. These experiments therefore show unambiguously that bentonite under the right conditions takes up *more* of a substance dominated by a divalent anion (selenate) as compared to a monovalent anion (iodide).

From e.g. an “effective porosity” view, which assumes anions to reside in a bulk water phase within the clay (Section 2.1.2), it is expected that the clay contains similar amounts of anions (due to identical chemical conditions, the presumed amount of bulk water must be the same in both the iodide and the selenate tests).

From the selenate diffusion tests, an “effective porosity” (ϵ_{Se}) can be evaluated using the following relation

$$\frac{\epsilon_{Se}}{\phi} \cdot ([SeO_4^{2-}]_{ext} + [NaSeO_4^-]_{ext}) + [CaSeO_4^0]_{ext} = [SeO_4]_{TOT,int} \quad (6-1)$$

where ϕ is the real porosity, the index “ext” denotes concentrations in the external solution at the clay interface on the source side, and $[SeO_4]_{TOT,int}$ is the total concentration of selenate in the clay at the same interface. Note that although Equation 6-1 requires the aqueous speciation for selenate in the external compartment, it is not dependent on the speciation within the clay, since the total concentration is obtainable directly from measurements. The evaluation of an “effective porosity” parameter using Equation 6-1 is therefore much more robust than e.g. the evaluation of individual interlayer activity coefficients.

Rearranging Equation 6-1 gives

$$\frac{\epsilon_{Se}}{\phi} = \frac{[SeO_4]_{TOT,int} - [CaSeO_4^0]_{ext}}{[SeO_4^{2-}]_{ext} + [NaSeO_4^-]_{ext}} \quad (6-2)$$

For the iodide data, the “effective porosity” parameter is simply evaluated from the external and internal concentrations at the source interface as

$$\frac{\epsilon_I}{\phi} = \frac{[I^-]_{int}}{[I^-]_{ext}} \quad (6-3)$$

which has the same numerical value as Ξ_I (Table 6-2).

The “effective porosities” evaluated from Equations 6-2 and 6-3, and data from Tables 6-1 and 6-2, are plotted in Figure 6-5. The “effective porosity” parameters are seen to differ roughly by a factor of two in *chemically identical systems*, depending on whether they are evaluated from the selenate or the iodide data. This behavior clearly demonstrates that an “effective porosity” parameter does not quantify what its name suggests. Moreover, since the “effective porosity” is larger in the case of selenate, this observation also disqualifies the argument sometimes raised that “anion exclusion” is larger for divalent as compared to monovalent ions. (Note also that a species specific “exclusion” is in itself incompatible with the “effective porosity” view, since the anions in this view are assumed to reside in bulk water).

It is consequently clear that the Benchmark 5 data for iodide and selenate diffusion together constitute a solid rebuttal to the ideas that salt diffusion through bentonite occurs in a bulk water phase, and that the extension of this phase varies with the chemical conditions (Equation 2-10).

The assumptions underlying the homogeneous mixture model are, on the other hand, compatible with the observation that bentonite takes up more divalent than monovalent ions. The ion equilibrium coefficient for an individual aqueous species *i* depends on the Donnan factor, f_D , as (Birgersson 2017).

$$\Xi_i \equiv \frac{C_{i,int}}{C_{i,ext}} = \frac{\gamma_{i,ext}}{\gamma_{i,int}} \cdot f_D^{-z_i} \quad (6-4)$$

where z_i is the species valency. Thus, from a pure Donnan potential perspective, bentonite is expected to contain more of monovalent than divalent ions under similar external conditions, since f_D is always less than unity (and often significantly smaller than unity). However, the ion equilibrium coefficient is also inversely proportional to the interlayer activity coefficient ($\gamma_{i,int}$). Thus, it is possible to have more selenate than iodide in the clay, if the interlayer activity for selenate is significantly smaller than that for iodide. This condition – a much smaller selenate activity coefficient – is also precisely what is expected from considering bulk solutions at very high ionic strength. Thus, although the precise values of individual interlayer activities are quite uncertain, applying the homogeneous mixture model to the Benchmark 5 data provides a very satisfactory principal explanation to the observed behavior.

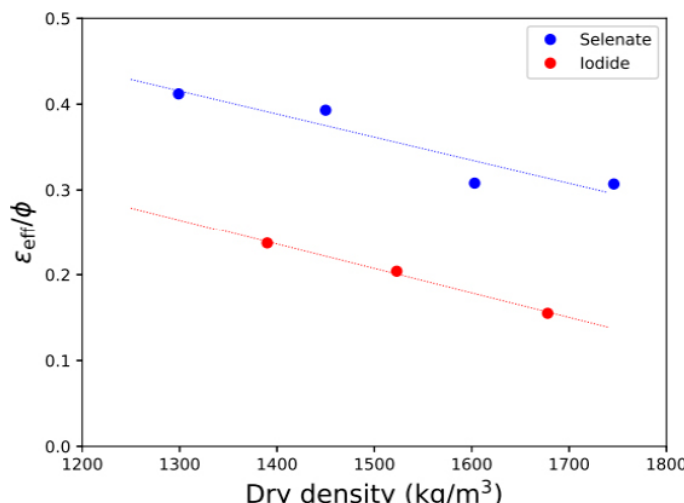


Figure 6-5. “Effective porosity” as a function of dry density. The parameter has been evaluated using Equation 6-2 for the selenate case, and Equation 6-3 for the iodide case. Also shown are separate linear regression lines for the selenate and iodide points.

6.1.4 Perchlorate

The data consists of results from diffusion of NaClO_4 in three samples of dry density 1 300, 1 431, 1 589 kg/m^3 . The provided data also contained results from replicates at each density, but, since the results are very similar, only the first set of results is used here. In contrast to the iodide and selenate diffusion tests, the background concentration used here was NaNO_3 , as a chlorine species were to be detected. All three tests were run for 21 days, using 60 ml source reservoirs, which were exchanged once a week.

The systems were modeled using basically the same approach as for iodide: the adopted species in this case were Na^+ , Ca^{2+} , NO_3^- , and ClO_4^- , and the diffusion coefficient and the interlayer activity coefficient for perchlorate were adjusted to fit the model to data, while the remaining activity coefficients were set equal to their mean salt values. As in the case of selenate, the model uses three times larger source and target reservoirs (180 ml), which are not exchanged during the simulation time.

The concentration profiles at termination are compared in Figure 6-6. These profiles clearly demonstrate that the filters constituted a significant transfer resistance, at least in the samples of lowest density. The transport capacity of the filter in the 1 300 kg/m^3 -test was therefore adjusted (by means of the filter porosity) to fit this profile to the experimental data. The obtained filter transport capacity was then used in the other models. The fitted effective diffusivity for the filters was $9 \times 10^{-12} \text{ m}^2/\text{s}$. It is difficult to understand why the filters (or, more generally, the interface regions) had such a significant resistance in these tests, but it is clear from the concentration profile data that this is the case. As a consequence of the high interface resistance, the fitted diffusion coefficient for the clay – especially for the 1 300 kg/m^3 -system – is quite uncertain.

The modeled outfluxes are compared with experiments in Figure 6-7. The outflux data is quite noisy, contributing to uncertainty of the fitted diffusion coefficients. The models were therefore fitted mainly to the steady-state flux data collected in the middle of the test duration, while points near the beginnings and ends of the time intervals, which appear as outliers, were disregarded (see Figure 6-7).

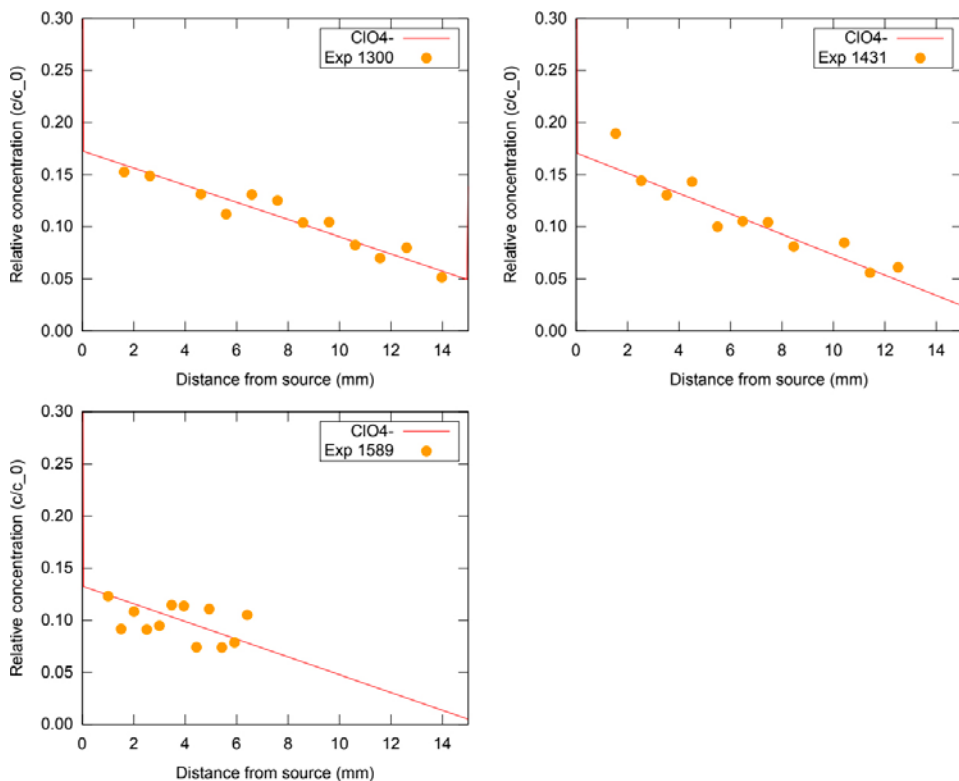


Figure 6-6. Perchlorate profiles at termination.

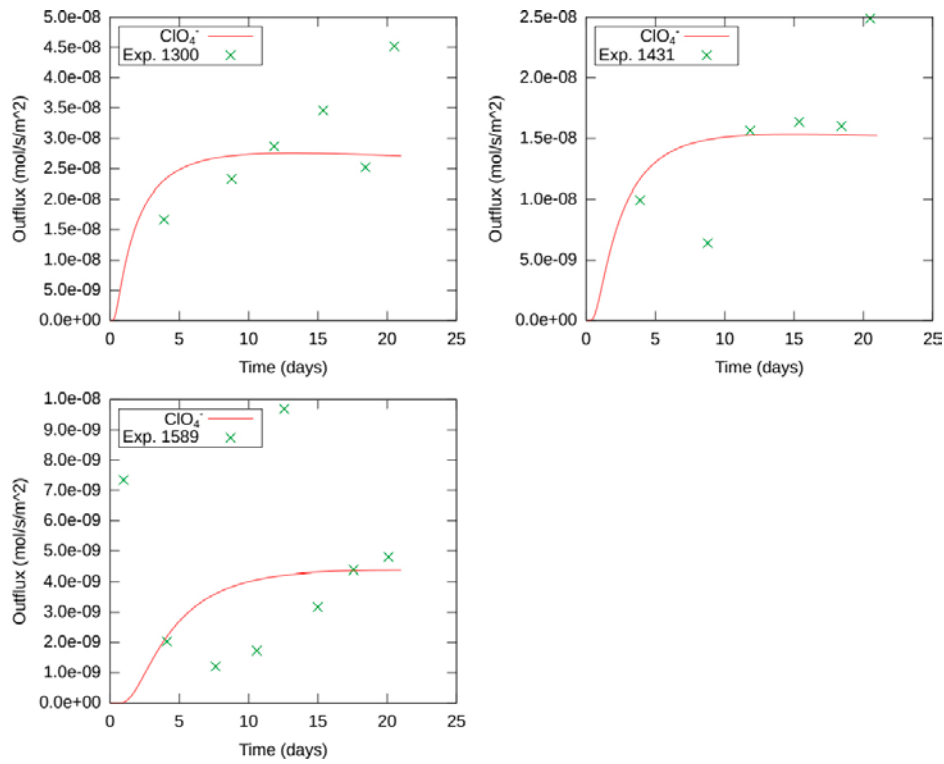


Figure 6-7. Perchlorate flux.

Table 6-3 shows that the fitted activity coefficients are rather narrowly collected in the range 0.44–0.49 kg/mol. These values are considerably larger as compared with the values evaluated for iodide. This difference reflects the experimental observation that the clay contains less amounts of perchlorate as compared to iodide, although the chemical conditions are basically identical. This is another indication that an “effective porosity” view is not fruitful; not only is there – again – much more selenate as compared to perchlorate in the clay at similar conditions, there is also a difference between the amount of iodide and perchlorate. Such behavior is unexpected if the anions are residing in a bulk water phase within the clay, but is easily understood as reflecting a difference in interlayer activity coefficients within the homogeneous mixture model.

Table 6-3: Speciation in the external solution (ext.) and the clay (int.) at the filter/clay interface in the perchlorate/“B75” system after 21 days of simulation. Concentration unit is mol/m³, unit for D_c is m²/s, and density unit is kg/m³.

ρ_d	1300		1431		1589	
	ext.	int.	ext.	int.	ext.	int.
$[\text{Na}^+]$	98.5	747.7	100.2	879.3	102.2	1075.8
$[\text{Ca}^{2+}]$	3.9	310.5	3.5	377.7	3.1	475.2
$[\text{NO}_3^-]$	98.6	45.6	98.5	44.0	98.7	42.9
$[\text{ClO}_4^-]$	7.7	1.7	8.7	1.7	9.6	1.3
γ_{Na^+}	0.773	0.754	0.773	0.780	0.773	0.832
$\gamma_{\text{Ca}^{2+}}$	0.387	0.267	0.387	0.284	0.387	0.324
$\gamma_{\text{NO}_3^-}$	0.764	0.223	0.764	0.193	0.764	0.155
$\gamma_{\text{ClO}_4^-}$	0.764	0.460	0.764	0.440	0.764	0.490
f_D	0.135		0.113		0.088	
$\Xi_{\text{ClO}_4^-}$	0.224		0.196		0.138	
D_c	6.0×10^{-10}		3.1×10^{-10}		1.15×10^{-10}	

6.1.5 Pertechnetate

The data consists of results from diffusion of the radioactive tracer $^{99}\text{TcO}_4^-$ in four samples of dry density 1 305, 1 453, 1 599, and 1 707 kg/m³. As these tests involve “real” tracer levels (negligible concentration contribution) in a background of 0.1 M NaCl, there is a slight – but insignificant – difference in chemical conditions as compared to the previously discussed systems (the ionic strength of the source reservoir is here 0.1 M, while it is 0.11 M in the perchlorate and iodide diffusion tests). All test were run for 21 days using reservoirs of volume 180 ml (which were not exchanged during the course of the tests).

The systems were modeled using basically the same approach as for iodide: the adopted species in this case were Na^+ , Ca^{2+} , Cl^- , and TcO_4^- , and the diffusion coefficient and the interlayer activity coefficient for pertechnetate were adjusted to fit the model to data while the remaining activity coefficients were set equal to their mean salt values.

The concentration profiles at termination are compared in Figure 6-8. At the lowest density, a slight influence of the filter transport capacity is seen, and the effective filter diffusivity was adjusted to 3×10^{-11} m²/s to fit this profile. This value of filter diffusivity was used in the rest of the other simulations (the filter influence is, however, seen to be insignificant in these cases, because the diffusion coefficient in the clay is lower for pertechnetate than for e.g. iodide and perchlorate).

The modeled outfluxes are compared with experiments in Figure 6-9. Since the absolute value of the trace level was not provided, these plots show the relative concentration evolution in the target reservoir, rather than the actual outflux (the tracer concentration in the source reservoir was arbitrarily put equal to 1×10^{-4} M in the models). It may be noted that the experimental data is of high quality (little noise) and that the fitting is basically perfect, giving minor uncertainty of the diffusion coefficients.

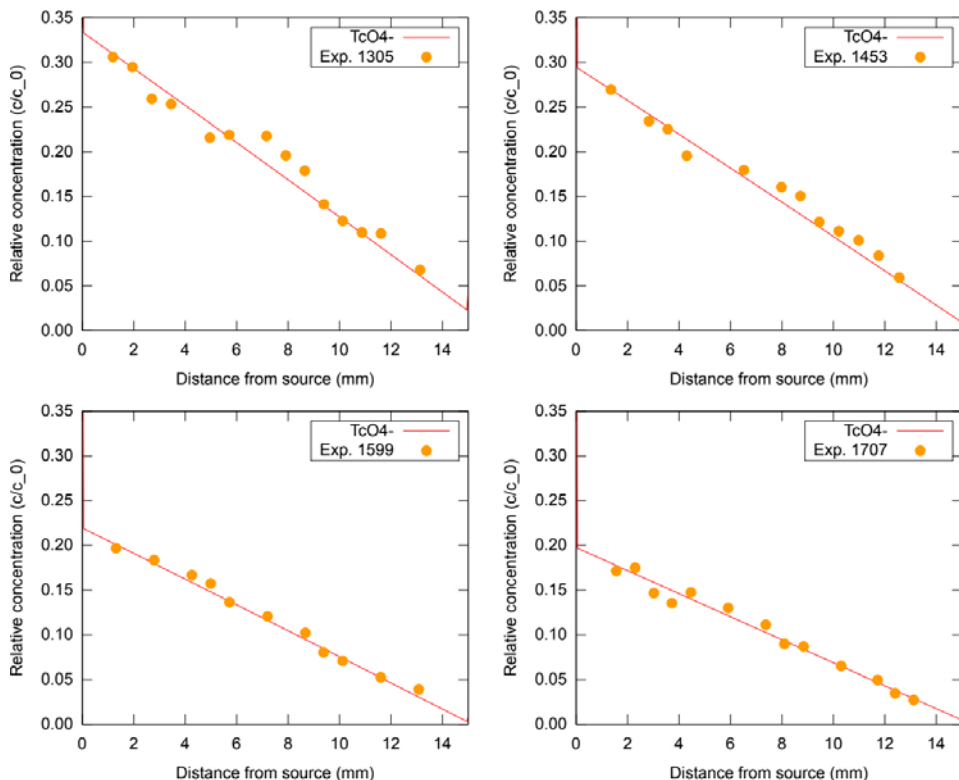


Figure 6-8. Pertechnetate profiles at termination.

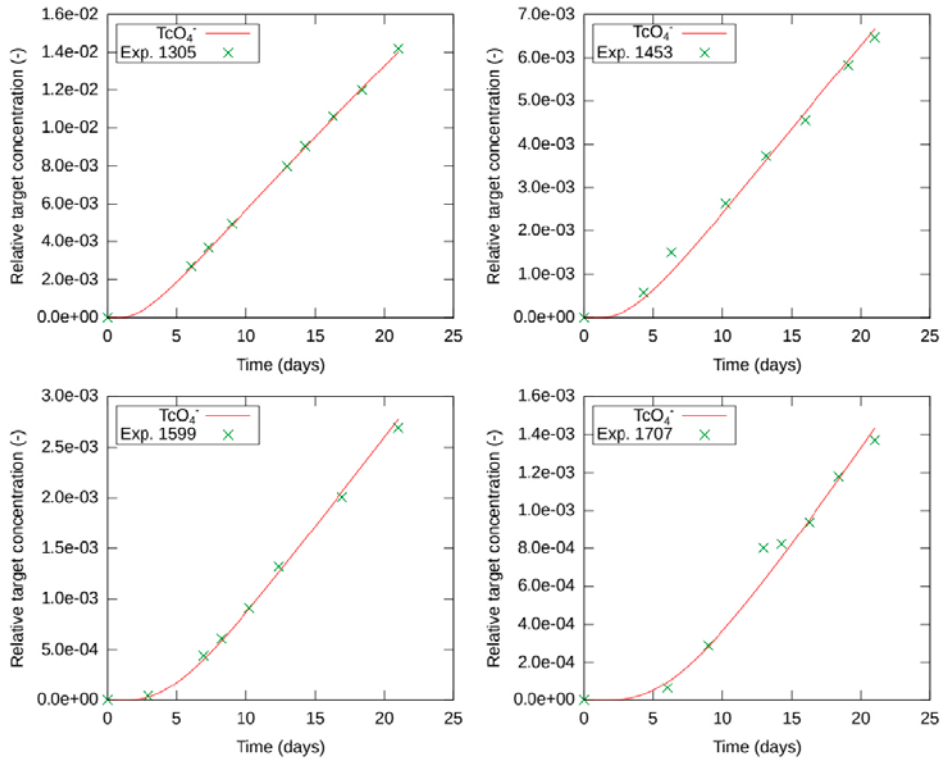


Figure 6-9. Pertechnetate flux.

Table 6-4 displays all adopted activity and diffusion coefficients, as well as the external and internal concentrations at the clay interface on the source side. The diffusion coefficient is significantly lower as compared to those evaluated for the other monovalent species (in the range 2×10^{-10} – 0.6×10^{-10}). At the same time, the fitted interlayer activity coefficients for TcO_4^- are lower than for the other monovalent species. This reflects the experimental fact that the “B75” clay contains more pertechnetate as compared to e.g. iodide and perchlorate, at basically identical chemical conditions. Note that the source reservoir ionic strength is slightly lower in this case, which might suggest that the pertechnetate level should be lower (due to a slightly lower Donnan potential). Instead, however, the pertechnetate level is higher, as a consequence of different interlayer activity coefficient. Again, this behavior is incompatible with the “effective porosity” view.

Table 6-4. Speciation in the external solution (ext.) and the clay (int.) at the filter/clay interface in the pertechnetate/“B75” system after 21 days of simulation. Concentration unit is mol/m³, unit for D_c is m²/s, and density unit is kg/m³.

ρ_d	1300		1450		1600		1750	
	ext.	int.	ext.	int.	ext.	int.	ext.	int.
[Na ⁺]	94.3	794.3	94.8	942.5	95.4	1126.6	95.8	1293.5
[Ca ²⁺]	2.8	277.0	2.6	352.6	2.3	445.2	2.1	529.7
[Cl ⁻]	99.8	16.0	99.8	13.3	99.9	10.6	99.9	8.6
[TcO ₄ ⁻]	0.093	0.033	0.096	0.029	0.098	0.022	0.099	0.020
γ_{Na^+}	0.773	0.754	0.773	0.780	0.773	0.832	0.773	0.897
$\gamma_{\text{Ca}^{2+}}$	0.387	0.267	0.387	0.284	0.387	0.324	0.387	0.377
γ_{Cl^-}	0.764	0.578	0.764	0.573	0.764	0.568	0.764	0.568
$\gamma_{\text{TcO}_4^-}$	0.764	0.260	0.764	0.250	0.764	0.270	0.764	0.245
f_D	0.122		0.100		0.079		0.064	
$\Xi_{\text{TcO}_4^-}$	0.357		0.305		0.223		0.199	
D_c	1.9×10^{-10}		1.18×10^{-10}		8.0×10^{-11}		5.9×10^{-11}	

6.1.6 Chloride

The data consists of results from diffusion of the radioactive tracer $^{36}\text{Cl}^-$ in three samples of dry density 1 302, 1 442, and 1 577 kg/m³. As for the pertechnetate case, the ionic strength is slightly lower in these tests as compared to the cases where the diffusive substance was of concentration 0.01 M. Also, as for the case of perchlorate diffusion, the background solution is here 0.1 M NaNO₃, as a chlorine species is to be detected. In practice, however, the conditions in these tests are very similar to the other tests in Benchmark 5. The chloride diffusion test were run for 15, 29, and 21 days, respectively, using reservoirs of volume 180 ml (which were not exchanged during the course of the tests).

The systems were modeled using Na⁺, Ca²⁺, Cl⁻, and NO₃⁻, and the diffusion coefficient and the interlayer activity coefficient for chloride were adjusted to fit the model to data while the remaining activity coefficients were set equal to their mean salt values.

The modeled and measured outfluxes are compared in Figure 6-10. As for the pertechnetate case, since the actual tracer concentration is unknown, these results are presented in terms of the evolution of the relative concentration in the target reservoir (the tracer level used in the models is 1×10^{-4} M). It is noted that the experimental data in this case has a certain level of noise. Also, the diffusion coefficients are so large in this case that not much of the transient phase is captured in the data. Both of these factors contribute to a certain uncertainty of the evaluated diffusion coefficients. Nevertheless, the model is satisfactory fitted to data.

Figure 6-11 shows the corresponding concentration profiles at termination. As seen in several other cases, there is a certain influence of the filter transfer resistance at lower density, and the effective filter diffusivity has been adjusted to 3×10^{-11} in all models.

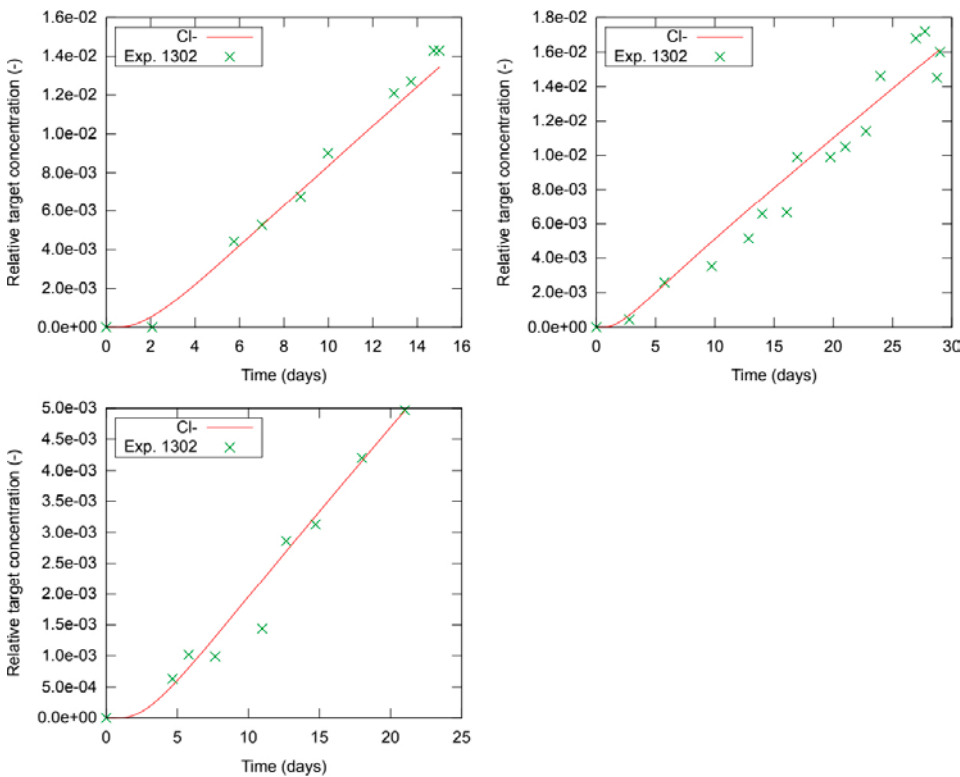


Figure 6-10. Chloride flux.

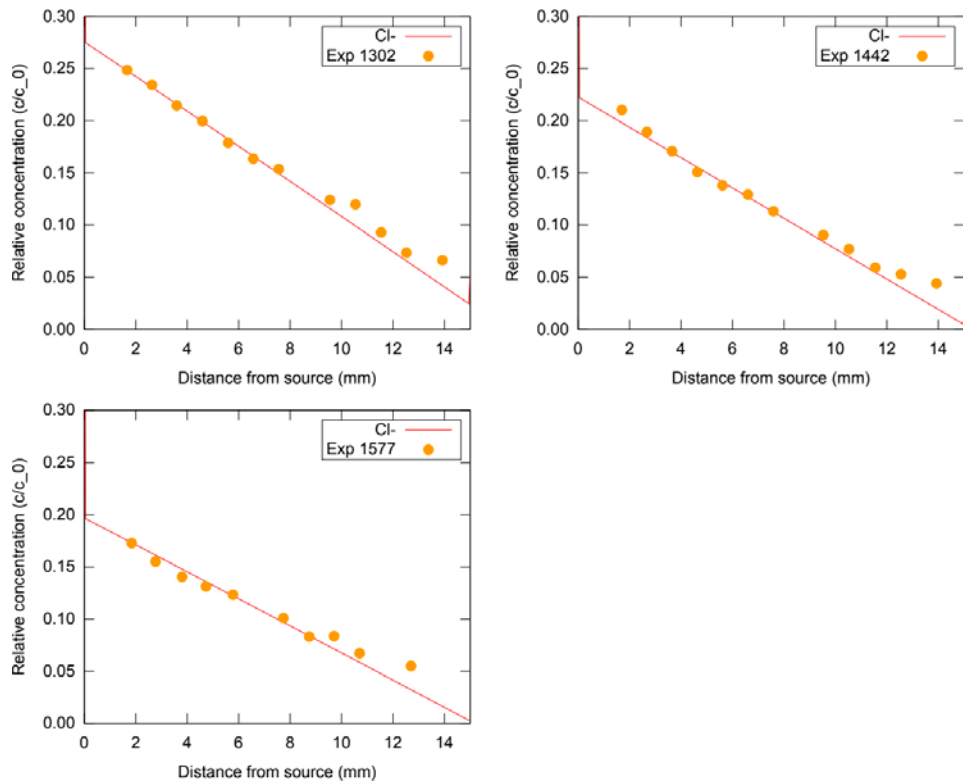


Figure 6-11. Chloride profiles at termination.

Table 6-5 summarizes all adopted activity and diffusion coefficients, and lists the concentrations at the clay interface at the source at the time of termination for each model. The fitted values of interlayer activity coefficients for chloride are in the range 0.28–0.31, which is considerably lower than the mean salt value, which is around 0.57 for typical interlayer ionic strengths. Relatively low evaluated interlayer activity coefficients were also noted in the case of iodide diffusion, but, as pointed out in that section, this cannot directly be concluded as demonstrating a deviation from the mean salt values of these ions. The evaluation of individual activity coefficients is quite uncertain due to the lack of information on e.g. the cation population in this specific system. It may rather be noted that the activity coefficients evaluated here for chloride is quite similar to the ones evaluated for iodide. This relative similarity indicates that chloride and iodide actually behave similar in an interlayer environment.

Table 6-5. Speciation in the external solution (ext.) and the clay (int.) at the filter/clay interface in the chloride/"B75" system after 21 days of simulation. Concentration unit is mol/m³, unit for D_c is m²/s, and density unit is kg/m³.

ρ_d	1302		1442		1577	
	ext.	int.	ext.	int.	ext.	int.
[Na ⁺]	93.6	786.7	95.2	1 063.1	96.3	1 231.3
[Ca ²⁺]	3.0	290.9	1.7	290.1	1.7	377.2
[Cl ⁻]	0.091	0.027	0.097	0.022	0.099	0.019
[NO ₃ ⁻]	99.5	41.6	99.5	35.4	99.5	35.6
γ_{Na^+}	0.773	0.754	0.773	0.780	0.773	0.832
$\gamma_{\text{Ca}^{2+}}$	0.387	0.267	0.387	0.284	0.387	0.324
γ_{Cl^-}	0.764	0.310	0.764	0.300	0.764	0.280
$\gamma_{\text{NO}_3^-}$	0.764	0.223	0.764	0.193	0.764	0.155
f_D	0.122		0.090		0.073	
Ξ_{Cl^-}	0.301		0.228		0.198	
D _c	3.2×10^{-10}		2.3×10^{-10}		1.35×10^{-10}	

6.1.7 Summary

A comparison between all the treated cases of Benchmark 5 is given in Figure 6-12. This figure shows the fitted diffusion coefficients and interlayer activity coefficients for all systems plotted as a function of dry density. Also plotted are the ion equilibrium coefficient for the total amount of diffusing substance, as well as the Donnan factor.

Looking first at the Donnan factor – which quantifies the electrostatic potential difference over the clay interface – in all the systems as a function of dry density, it is seen that they all follow basically the same line; a drop of the Donnan factor with dry density is expected at constant external concentration, since the interlayer cation concentrations increase with dry density (while the external concentrations remain constant). The similarities of the Donnan factor for all systems illustrates that Benchmark 5 consists of tests performed at basically identical chemical conditions – which makes the data very suitable for making relative comparisons e.g. of how much different species are taken up by the bentonite. The values of Donnan factor evaluated here can be contrasted with the values evaluated for the Benchmark 1 tests, which all were performed at very different chemical conditions: f_D varies there between 0.037 (0.1 M NaCl) and 0.413 (0.4 M CaCl₂).

The small variations in Donnan factor seen between the different systems in the present case reflect the small variations in the chemistry, which still exists. The selenate diffusion tests, for instance, have an ionic strength in the source reservoir of 0.13 M due to the presence of 0.01 M Na₂SeO₄, the iodide and perchlorate tests have a corresponding ionic strength of 0.11 M, while it is 0.1 M in the “real” tracer diffusion tests (pertechnetate and chloride). Moreover, the Donnan factor is not strictly a constant in these systems because there is an ongoing cation exchange process, as the Ca/Mg/Na bentonite is contacted with a (initially) pure Na solution. The values plotted in Figure 6-12 are at the end of each simulation, and since some of them are run longer than others, and also because the transport coefficients differ between simulations, the Donnan factor drifts unequal amounts. Still, the main impression of this plot is that *all* tests in Benchmark 5 can be considered to be performed at equal chemical conditions (with the only relevant variation of f_D being due to variations of dry density).

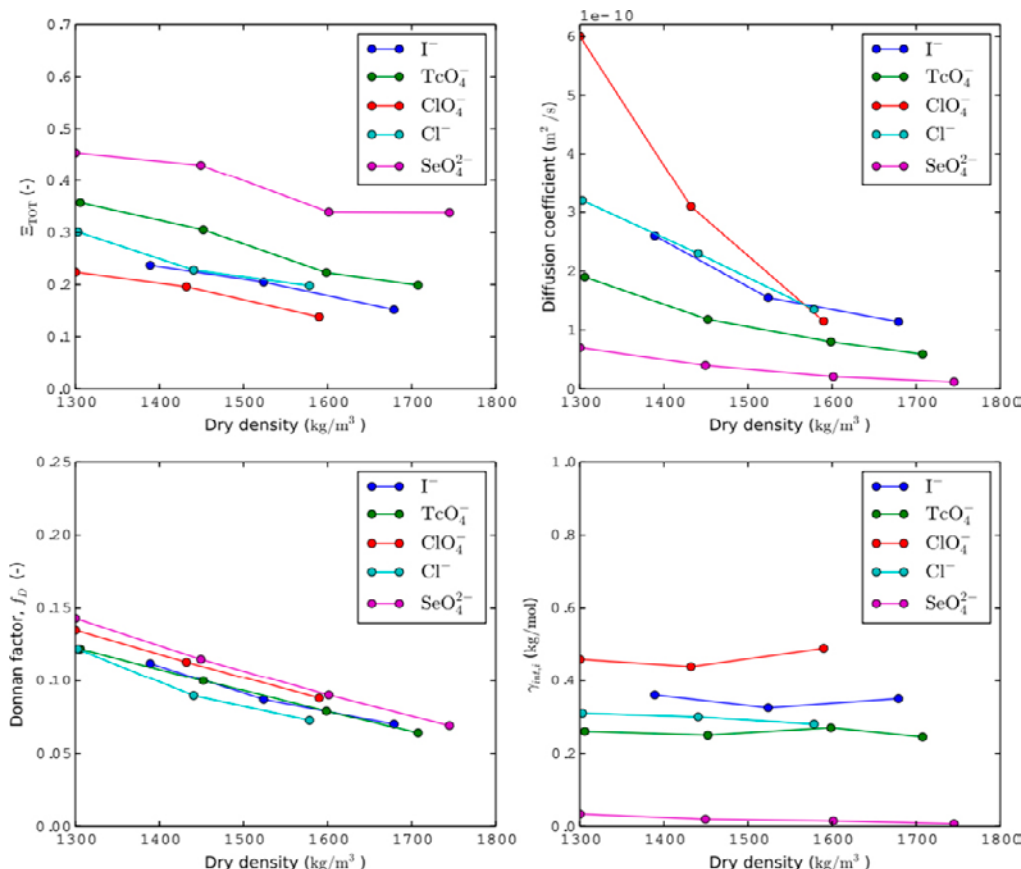


Figure 6-12. Ion equilibrium coefficients (for total diffusing substance), diffusion coefficients, Donnan factors and interlayer activity coefficients in all models of Benchmark 5.

The plot of ion equilibrium coefficients for the total amount of diffusing species (Ξ_{TOT}) as evaluated at the clay interface on the source side at the end of simulation demonstrates the intricate behavior caused by Donnan equilibrium between an external solution and the interlayer pores of the bentonite. As already discussed, selenate is by far the most preferable substance in the clay, even though it is dominated by a divalent anion in the external solution. Moreover, the plot (and even more the experimental data itself!) suggests that the clay contains significantly more TcO_4^- as compared to the other monovalent anions at similar chemical conditions. The amount of ions taken up by bentonite can consequently not be associated with a bulk water phase presiding in the clay, but rather reflects the difference in how these species interact within the interlayer pores, as quantified by their activity coefficients.

The fitted interlayer activity coefficients for the monovalent anions are seen to differ slightly for the different types of ions, and to have negligible variation with interlayer ionic strength (dry density). This lack of variation at high ionic strength is precisely what is observed for the mean salt activity coefficient for chloride in bulk water solutions (Birgersson 2017). The interlayer activity coefficient for SeO_4^{2-} differs significantly from the coefficients for the monovalent anions. Activity coefficients approaching zero at high ionic strength is also precisely what is expected for SO_4^{2-} in bulk solutions, as discussed in Chapter 3. Thus, to the extent that selenate behaves similarly to sulfate, all the inferred behavior of the interlayer activity coefficients complies with expectations from bulk water chemistry.

Finally, the diffusion coefficients are, unsurprisingly, seen to decrease with increasing density. The behavior of perchlorate stands out in that its seeming dependence on density is much stronger than for the other ions. However, since the data for this particular ion was the noisiest, this evaluated behavior is the most uncertain. It may also be noted that there is a negative correlation between diffusion coefficient and ion equilibrium coefficient; the slower the ion, the more it tends to be taken up by the clay. Such behavior could point to a common mechanism which influences both interlayer mobility and interlayer activity coefficient for a given specie.

In order to reduce uncertainty in evaluating the Donnan equilibrium for given ions and chemical environment, the present analysis suggests making measurements in pure systems, involving only one or two (controlled) cations, in order to better be able to separate effects from the Donnan potential and the actual interlayer activity coefficients. Note that diffusion experiments are not necessary for this type of evaluation. Rather, simpler equilibration experiments are to prefer, as they do not depend on any transport quantities, leading to more robust assessments of the quantities of interest.

References

SKB's (Svensk Kärnbränslehantering AB) publications can be found at www.skb.com/publications.

- Bhatnagar O N, Campbell A N, 1981.** Osmotic and activity coefficients of sodium sulphate in water from 50 to 150 °C. Canadian Journal of Chemistry 59, 123–126.
- Birgersson M, 2017.** A general framework for ion equilibrium calculations in compacted bentonite. Geochimica et Cosmochimica Acta 200, 186–200.
- Birgersson M, Karnland O, 2009.** Ion equilibrium between montmorillonite interlayer space and an external solution – Consequences for diffusional transport. Geochimica et Cosmochimica Acta 73, 1908–1923.
- Birgersson M, Karnland O, 2010.** On the concept of effective diffusion coefficients in compacted bentonite. In Proceedings of the 4. International meeting on clays in natural and engineered barriers for radioactive waste confinement, Nantes, France, 29 March – 1 April 2010. Chatenay-Malabry, France: Andra, 779–780.
- Birgersson M, Karnland O, 2015.** Flow and pressure response in compacted bentonite due to external fluid pressure. SKB TR-14-28, Svensk Kärnbränslehantering AB.
- Birgersson M, Åkesson M, Hökmark H, 2008.** Gas intrusion in saturated bentonite – A thermodynamic approach. Physics and Chemistry of the Earth, Parts A/B/C 33, Supplement 1, S248–S251.
- Birgersson M, Börgesson L, Hedström M, Karnland O, Nilsson U, 2009.** Bentonite erosion. Final report. SKB TR-09-34, Svensk Kärnbränslehantering AB.
- Birgersson M, Hedström M, Karnland O, Sjöland A, 2017.** Bentonite buffer: macroscopic performance from nanoscale properties. In Apted M J, Ahm J (eds). Geological repository systems for safe disposal of spent nuclear fuels and radioactive waste. 2nd ed. Woodhead Publishing, 319–364.
- Bourg I C, Tournassat C, 2015.** Self-diffusion of water and ions in clay barriers. In Tournassat C, Steefel C I, Bourg I C, Bergaya F (eds). Natural and engineered clay barriers. Amsterdam: Elsevier. (Developments in Clay Science 6), 189–226.
- Bradbury M H, Baeyens B, 2002.** Porewater chemistry in compacted re-saturated MX-80 bentonite: Physico-chemical characterisation and geochemical modelling. PSI Bericht Nr 02–10, Paul Scherrer Institut, Switzerland.
- Crank J, 1975.** The mathematics of diffusion. 2nd ed. Oxford: Oxford University Press.
- Fernández R, Mäder U, Jenni A, 2011.** Multi-component advective-diffusive transport experiment in MX-80 compacted bentonite: Method and results of 1st phase of experiment. Nagra Arbeitsbericht NAB 11-02, Nagra, Switzerland.
- Fritz S J, 1986.** Ideality of clay membranes in osmotic processes: a review. Clays and Clay Minerals 34, 214–223.
- Glaus M A, Baeyens B, Bradbury M H, Jakob A, Van Loon L R, Yaroshchuk A, 2007.** Diffusion of ^{22}Na and ^{85}Sr in montmorillonite: evidence of interlayer diffusion being the dominant pathway at high compaction. Environmental Science & Technology 41, 478–485.
- Glaus M A, Frick S, Rossé R, Van Loon L R, 2010.** Comparative study of tracer diffusion of HTO, $^{22}\text{Na}^+$ and $^{36}\text{Cl}^-$ in compacted kaolinite, illite and montmorillonite. Geochimica et Cosmochimica Acta 74, 1999–2010.
- Glaus M A, Birgersson M, Karnland O, Van Loon L R, 2013.** Seeming steady-state uphill diffusion of $^{22}\text{Na}^+$ in compacted montmorillonite. Environmental Science & Technology 47, 11522–11527.
- Hedström M, Karnland O, 2012.** Donnan equilibrium in Na-montmorillonite from a molecular dynamics perspective. Geochimica et Cosmochimica Acta 77, 266–274.
- Holmboe M, Wold S, Jonsson M, 2012.** Porosity investigation of compacted bentonite using XRD profile modeling. Journal of Contaminant Hydrology 128, 19–32.

- Hsiao Y-W, Hedström M, 2015.** Molecular dynamics simulations of NaCl permeation in bihydrated montmorillonite interlayer nanopores. *The Journal of Physical Chemistry C* 119, 17352–17361.
- Jaskula M, Hotłoś J, 1992.** Mean thermodynamic activity coefficient of CuSO₄ in the ternary system CuSO₄–H₂SO₄–H₂O at 60 °C. *Hydrometallurgy* 31, 233–242.
- Karnland O, Olsson S, Dueck A, Birgersson M, Nilsson U, Hernan-Håkansson T, Pedersen K, Nilsson S, Eriksen T E, Rosborg B, 2009.** Long term test of buffer material at the Äspö Hard Rock Laboratory, LOT project. Final report on the A2 test parcel. SKB TR-09-29, Svensk Kärnbränslehantering AB.
- Karnland O, Birgersson M, Hedström M, 2011.** Selectivity coefficient for Ca/Na ion exchange in highly compacted bentonite. *Physics and Chemistry of the Earth, Parts A/B/C* 36, 1554–1558.
- Molera M, Eriksen T, Jansson M, 2003.** Anion diffusion pathways in bentonite clay compacted to different dry densities. *Applied Clay Science* 23, 69–76.
- Muurinen A, Penttilä-Hiltunen P, Uusheimo K, 1988.** Diffusion of chloride and uranium in compacted sodium bentonite. *MRS Online Proceedings Library* 127. doi:10.1557/PROC-127-743
- Parkhurst D L, Appelo C A J, 2013.** Description of input and examples for PHREEQC version 3 – A computer program for speciation, batch-reaction, one-dimensional transport, and inverse geochemical calculations, Techniques and Methods. Denver, CO: U.S. Geological Survey.
- Tachi Y, Yotsuji K, 2014.** Diffusion and sorption of Cs⁺, Na⁺, I⁻ and HTO in compacted sodium montmorillonite as a function of porewater salinity: Integrated sorption and diffusion model. *Geochimica et Cosmochimica Acta* 132, 75–93.
- Van Loon L R, Glaus M A, Müller W, 2007.** Anion exclusion effects in compacted bentonites: Towards a better understanding of anion diffusion. *Applied Geochemistry* 22, 2536–2552.

SKB is responsible for managing spent nuclear fuel and radioactive waste produced by the Swedish nuclear power plants such that man and the environment are protected in the near and distant future.

skb.se